Chem

CellPress
REVIEWS

Review

The Versatility of Squaramides: From Supramolecular Chemistry to Chemical Biology

Luke A. Marchetti,[1] Lokesh Kumar Kumawat,[1] Nan Mao,[1] John C. Stephens,[1] and Robert B.P. Elmes[1,*]

This review covers recent advances in the use of the squaramide moiety in chemical research. We focus on the varied applications of squaramides under the broad headings of self-assembly, organocatalysis, molecular recognition, medicinal chemistry, and bioconjugation and highlight several examples of each application.

INTRODUCTION

Squaramides, a family of conformationally rigid cyclobutene ring derivatives, are rapidly gaining research interest across diverse areas of the chemical and biological sciences.[1–3] Composed of two carbonyl hydrogen-bond acceptors in close proximity to two NH hydrogen-bond donors, this small molecular scaffold benefits from unique physical and chemical properties that render it extremely useful as a tool in areas as diverse as catalysis, molecular recognition, bioconjugation, and self-assembly. One of its most striking properties arises from the delocalization of a nitrogen lone pair into the cyclo-butenedione ring system conferring the four-membered ring with aromatic character (Hückel's rule: [4n + 2] π electrons, n = 0). In addition, the capacity of squaramides to form strong hydrogen bonds that simultaneously increase the aromatic character of the four-membered ring is highly advantageous where self-assembly and molecular recognition processes can benefit from favorable thermodynamic stability brought about by aromatic gain.[4,5] This fact, along with synthetic versatility, conformational rigidity, and relative stability, has stimulated a burgeoning research effort over the past number of years toward exploiting this most useful of scaffolds. Derived from squaric acid (diketocyclobutenediol), itself first synthesized by Cohen et al. in 1959 via the hydrolysis of dichlorotetrafluorocyclobutene,[6] it was West and colleagues who provided an explanation for the stability and aromaticity of the dianionic diketocyclobutene.[7] Although a large body of work on squarate derivatives has been theoretical in nature, establishing the relative aromaticity of $C_nO_n^{2-}$ systems,[8,9] it is the facile synthesis of alkyl squarates that has opened the door to the synthetic accessibility of the squaramide that we enjoy today.[10] One of their particularly useful characteristics is the ability to be sequentially substituted whereby increased aromatic stabilization afforded by the first substitution reaction relative to the parent alkyl squarate is thought to render the monosubstituted intermediate less reactive thus allowing facile synthetic access to unsymmetrical squaramides.[9] Indeed, the alkyl esters have become increasingly useful tools as bioconjugation moieties and as the key starting materials for the synthesis of both mono- and di-substituted squaramides[11] and squaraine dyes[12] and most recently for the facile synthesis of thiosquaramides.[13] With the increasing research interest in exploiting the squaramide moiety, the aim of this review article is to focus on some recent advances in the field and highlight some of the interdisciplinary applications of the squaramides. We will focus on the use of squaramides at the borders of materials

The Bigger Picture

Squaramides are an intriguing class of compounds that, as a result of numerous advantageous properties, have found use across a diverse array of the chemical sciences. With their inherent ability to partake in strong bidirectional hydrogen bonding, in recent years, an explosion of research interest has led to a number of potential applications at the borders of materials science and biology, where new materials, molecular sensors, synthetic methodologies, and new drug candidates toward a diverse set of diseases have all been reported. With such a wide range of potential applications coupled with facile and robust synthetic approaches, it is clear that interest in the squaramide motif is likely to increase rapidly in the coming years. This review aims to summarize the recent uses of squaramides from scientific fields as diverse as supramolecular chemistry and chemical biology and to highlight the Brobdingnagian potential that this small building block has to effect real change and solve some of the challenges facing the world today.

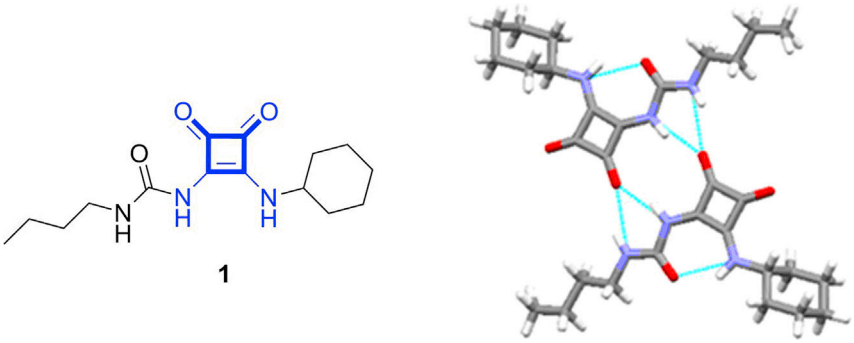

Figure 1. Chemical Structure of Compound 1 and Its X-Ray Crystal Structure Showing the Relationship between Adjacent Hydrogen-Bonded Molecules

science and biology under the broad headings of self-assembly, organocatalysis, molecular recognition, medicinal chemistry, and bioconjugation, where a number of recent elegant examples have been reported. Although non-exhaustive, this review aims to include a selection of recently published examples to highlight the utility, diversity, and future potential that this most useful of scaffolds holds.

SQUARAMIDES AS SUPRAMOLECULAR SELF-ASSEMBLY MOTIFS

Molecular self-assembly has emerged as a particularly useful approach for the bottom-up assembly of nanoscale materials where a wide variety of morphologies can be achieved either in bulk or in solution ranging from cylinders and spheres to micelles and vesicles.[14,15] The shape and size of self-organized morphologies can be accurately controlled both through judicious design and through a number of variables such as concentration, light, pH, temperature, etc.[16] As mentioned above, squaramides benefit from several characteristics that make them amenable for use in self-assembled materials, in particular their structural rigidity, aromaticity, and ability to form strong two-dimensional hydrogen bonds. This has led to a number of reports detailing the formation of non-covalent bonding networks, soft materials, and metal-organic frameworks.

One of the earliest examples of supramolecular self-assembly based on the squaramide motif was reported by Davis and co-workers who described the synthesis of compound **1** (Figure 1).[17] X-ray crystallography analysis of **1** revealed that the carbamoyl squaramide unit displayed planarity around the four-membered ring but importantly showed intramolecular hydrogen bonding. **1** was shown to exist as a centrosymmetric dimer in the solid state, sustained by four NH···O=C hydrogen bonds. The structure of the 1:1 dimer was confirmed by calculation of dimerization constants (K_d) (values range from 5×10^3 to 10^4 M^{-1} with chemical shift differences $d_{dimer} - d_{monomer} \cong 2.3–3$ ppm) with ^{1}H NMR dilution analysis in $CDCl_3$–CD_3CN (95:5).

Costa et al. subsequently reported further conformational analysis of secondary squaramide models **2–5** through NMR analysis in a range of different solvent systems (Figure 2).[18] The C–N bonds of several squaramide compounds were shown to be analogous to amide like structures whereby partially restricted rotation around the C–N bond gave rise to *syn*- and *anti*-conformations. The study showed that an energy barrier ≈ 63 kJ Mol^{-1} exists between the *syn*- and *anti*-modes of the various squaramide structures, allowing ready interconversion between the two conformers at room temperature (RT). In addition, mixtures of *syn*/*anti*- and *anti*/*anti*-conformations could be observed through molecular mechanics calculations and X-ray crystallographic analysis, thus supporting the earlier NMR evidence; however, the

[1]Department of Chemistry, Maynooth University, National University of Ireland, Maynooth, County Kildare, Ireland

*Correspondence: robert.elmes@mu.ie

https://doi.org/10.1016/j.chempr.2019.02.027

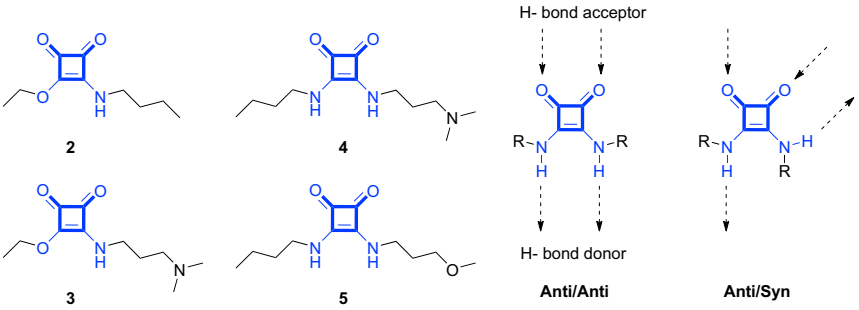

Figure 2. Chemical Structures of Compound 2–5 and Representations of the *anti/anti*- and *anti/syn*-Conformations of Bis-secondary Squaramides

syn/syn-conformation was not observed to be a result of a high energy barrier brought about by significant steric hindrance.

Prohens and co-workers have conducted several follow up conformational studies on a range of squaramides under variable conditions. In one report, three polymorphs of dibenzylsquaramide **6** were examined in different solvents and at varying temperatures (Figure 3).[19] Synthesized through reaction between diethylsquarate and benzylamine in ethanol, **6** was subjected to polymorphic screening in different combinations of DMF and DMSO with polar and non-polar solvents.

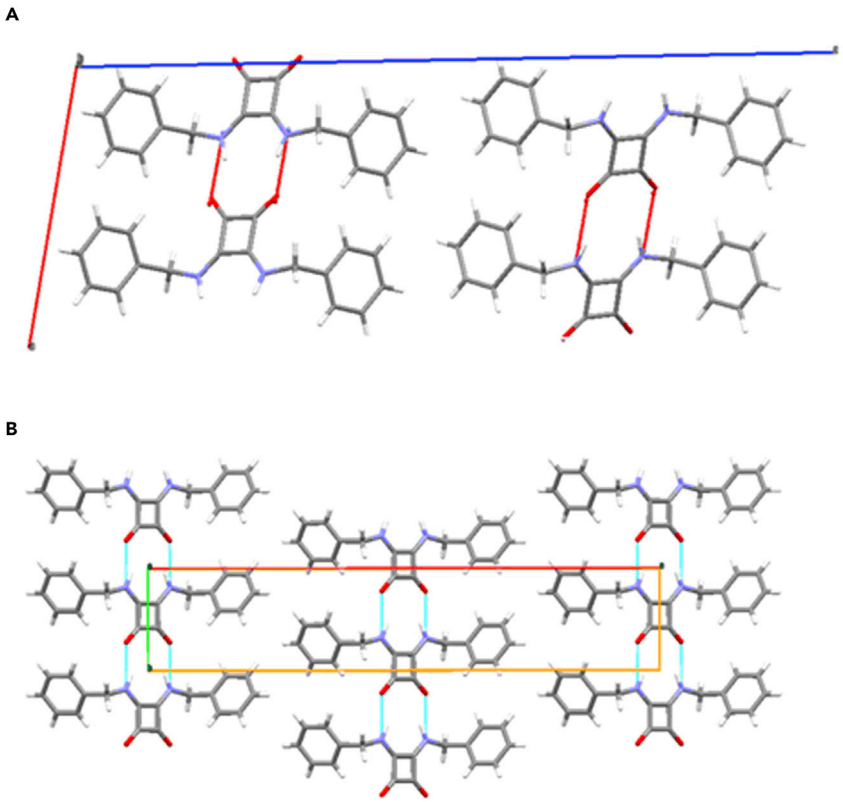

Figure 3. Single-Crystal X-Ray Structures of Forms 6A and 6C
(A) **Form 6A**.
(B) **Form 6C**.

DSC analysis revealed three distinct polymorphs and showed that **forms 6B** and **6C** transform into form **6A** at 257°C. Crystal structures of metastable **forms 6A** and **6C** were studied by single-crystal X-ray diffraction (XRD) and demonstrated well-defined head-to-tail hydrogen bonding (N–H···O 2.834 and 2.779 Å, respectively) between the intermolecular squaramide units with different packing directions. **Form 6A** showed parallel packing but formed an antiparallel chain, whereas **form 6C** exhibited an anti-parallel packing arrangement with parallel chains. This study confirmed earlier reports[18] of the favorable *anti*/*anti*-conformation in the solid structure of simple squaramides (Figure 3). Moreover, the inability to distinguish between these three polymorphs by differential scanning calorimetry (DSC) told a cautionary tale to those involved in pharmaceutical research about the limitations of DSC when characterizing crystalline solids. A follow-up study examined cooperativity in solid-state squaramides.[20] Here, polymorph preferences of a dipyridyl squaramide **7** were examined, and conformational equilibrium constants were calculated at different concentrations of $CHCl_3$. The results showed the existence of two dimers in solution, **forms 7A** and **7B** (Figure 4A), and revealed that **form 7B** dominates in supersaturated $CHCl_3$ solution.

The authors also performed a polymorphic screening under varying thermodynamic and kinetic conditions. Just two polymorphic forms, **forms 7I** and **7II**, directly related to the **form 7A** dimer (head-to-tail motif) were obtained, and there was no evidence of the existence of **form 7B**. However, DSC and thermomicroscopy analysis suggested an enantiotropic relationship between the two polymorphs whereby **form 7I** (melting point [m.p.] = 166°C) showed more stability below the transition temperature (<160°C), and polymorph **form 7II** (m.p. =188°C) was only observed when **form 7I** was heated to 175°C. The results suggested that both modes of interaction remain effective only in low-polarity solvents where cooperative hydrogen bonding favors the formation of the catemeric cluster. Although both polymorphs (**forms 7I** and **7II**) exhibited the same catemeric head to-tail motif, Hirshfeld surface plots for both polymorphs revealed that different secondary interactions led to the corresponding structural differences between the two polymorphs: π-π stacking interactions dominated in **form 7I**, whereas edge-to-face C–H-π interactions dominated in **form 7II** (Figure 4B).

Prohens, Portell, and Alcobé later investigated the preorganization effect on the polymorphism and co-crystallization of squaramide **8** and described new chain and ribbon synthons (Figure 5).[21] Bis-squaramide **8** with four predicted supramolecular synthons indeed produced four different solid-state structures through varying intramolecular hydrogen bonding. The structures of the different synthons were characterized by powder XRD, where two of the synthons showed a *trans*-configuration (a head-to-tail polymer and an intramolecular monomer) and the remaining two synthons showed a *cis*-configuration (a ribbon assembly and another intramolecular monomer). The head-to-tail polymer (**form 8A**) was obtained in pure form during the synthesis, whereas the ribbon assembly (**form 8B**) was obtained through slow-rate crystallization after **form 8A** melted at 160°C. As expected, **form 8A** presented the, by now well-known, head to-tail hydrogen-bonding motif associated with the squaramide structure and additionally demonstrated π-stacking interactions that resulted in the parallel layers observed in the polymorphic structure ($d_{centroids}$ 3.851 Å). **Form 8B** contained a pseudo six-membered ring structure perpendicular to the plane defined by the piperazine ring again brought about by the propensity of the squaramide to partake in intramolecular hydrogen bonding between the amidic NH and the piperazine nitrogen [N−H···N 2.843(8) Å] and resulted in a symmetric shortening of the assembly.

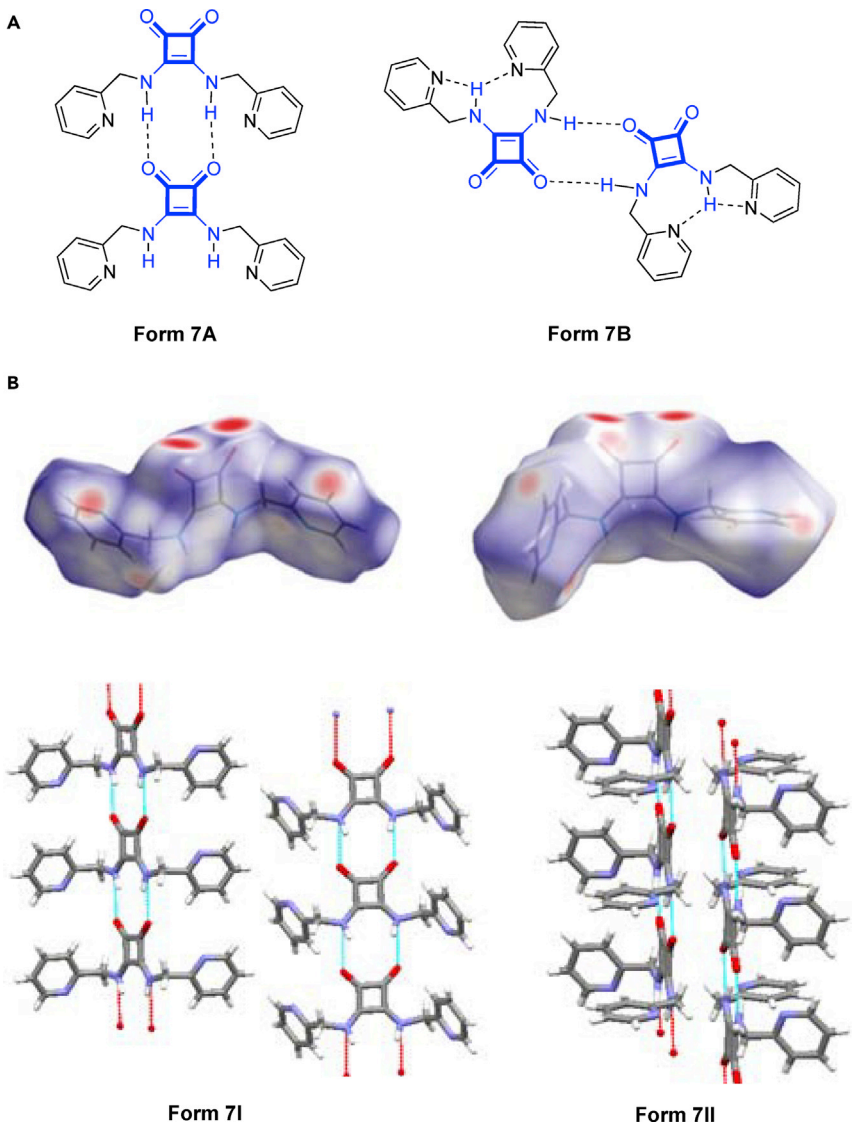

Figure 4. Polymorphic Behaviour of Dipyridyl Squaramide 7

(A) Potential catemeric dimers of bis-secondary squaramide **7** show **forms 7A** and **7B**.

(B) Crystal structures and Hirshfeld surfaces of **forms 7I** and **7II**.

Reproduced with permission from Prohens et al.[20] Copyright 2011 American Chemical Society.

Portel and Roffel continued to pursue the synthesis of supramolecular synthons based on the squaramide motif and reported the helical crystal structure of a disquaramide compound **9** through powder XRD (Figure 6).[22] The asymmetric compound **9** was synthesized by a condensation reaction between diethylsquarate and *N*,*N*-dimethylethylenediamine and tyramine. The result was an achiral compound capable of forming both clockwise and anti-clockwise rotating helical assemblies in a racemic crystal structure. Again, the self-assembly of **9** exhibited strong CO···HN hydrogen bonding within the squaramide portion of the molecule (the aforementioned head-to-tail motif) and provided a skeletal template for peripheral interactions to occur between a tertiary amine and a phenolic hydroxyl group. Additional weak CH···π interactions between the methylamino group and the aromatic phenol ring were also thought to contribute to the helical packing.

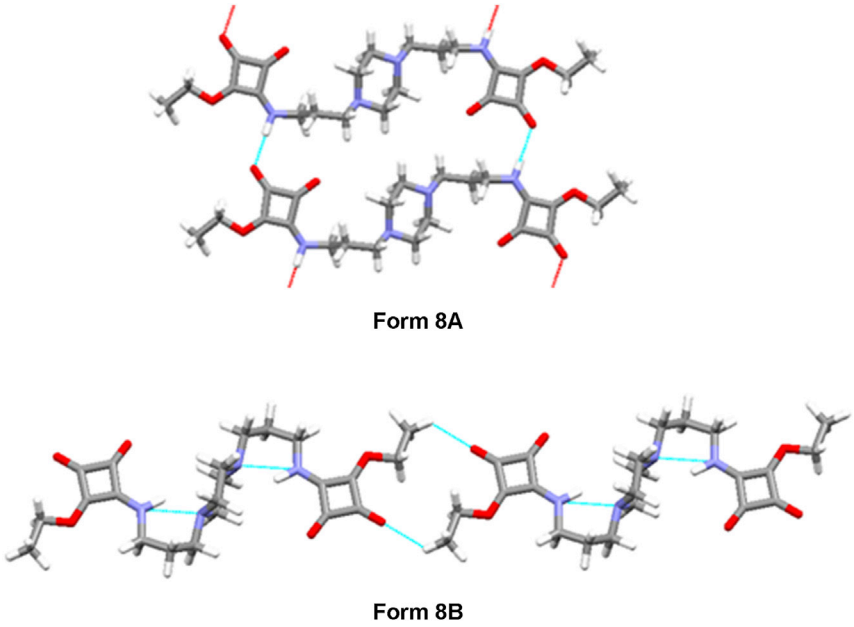

Figure 5. XRD Structure of Head-to-Tail Polymer Form 8A and Ribbon Assembly Form 8B

More recently, Portell, Bardia, and Prohens reported another supramolecular assembly based on the squaramide scaffold, this time with zwitterionic squaramide compound **10**.[23] The synthesis of **10** was achieved in a single step from squaric acid and *N*,*N*-dimethylethylendiamine in water and was expected to yield two distinct supramolecular synthons through charge-assisted hydrogen-bond formation and face-to-face π-stacking (Figure 7A). Indeed, through a polymorph screening, the structures of two anhydrate polymorphs (**forms 10I** and **10II**) and a hydrate (**form 10III**) were solved by single-crystal XRD. Both anhydrous crystals showed similar N−H···O interactions between adjacent dimers but with different centroids distances (3.47 and 3.70 Å, respectively). The most important difference between **forms 10I** and **10II** stems from the carbonylic oxygen involved in intermolecular hydrogen bonding. Whereas in **form 10I** the oxygen is *syn* with respect to the NH

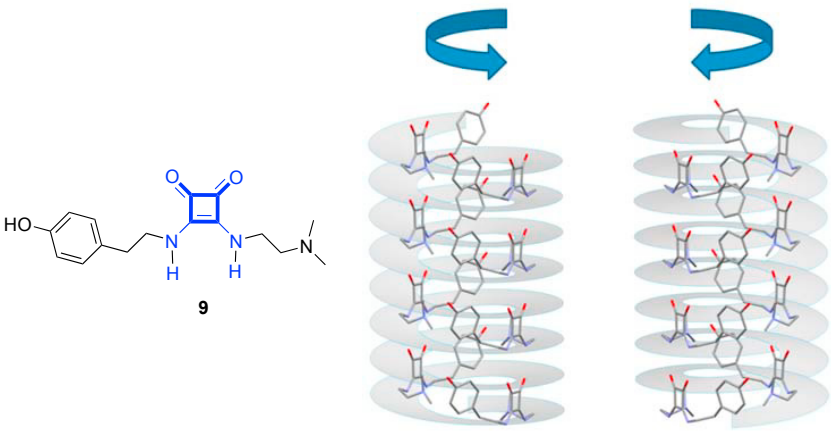

Figure 6. Chemical Structure of Compound 9 and the Resulting Clockwise and Anti-clockwise Rotating Supramolecular Helical Assemblies

Reproduced with permission from Portell and Prohens.[22] Copyright 2014 American Chemical Society.

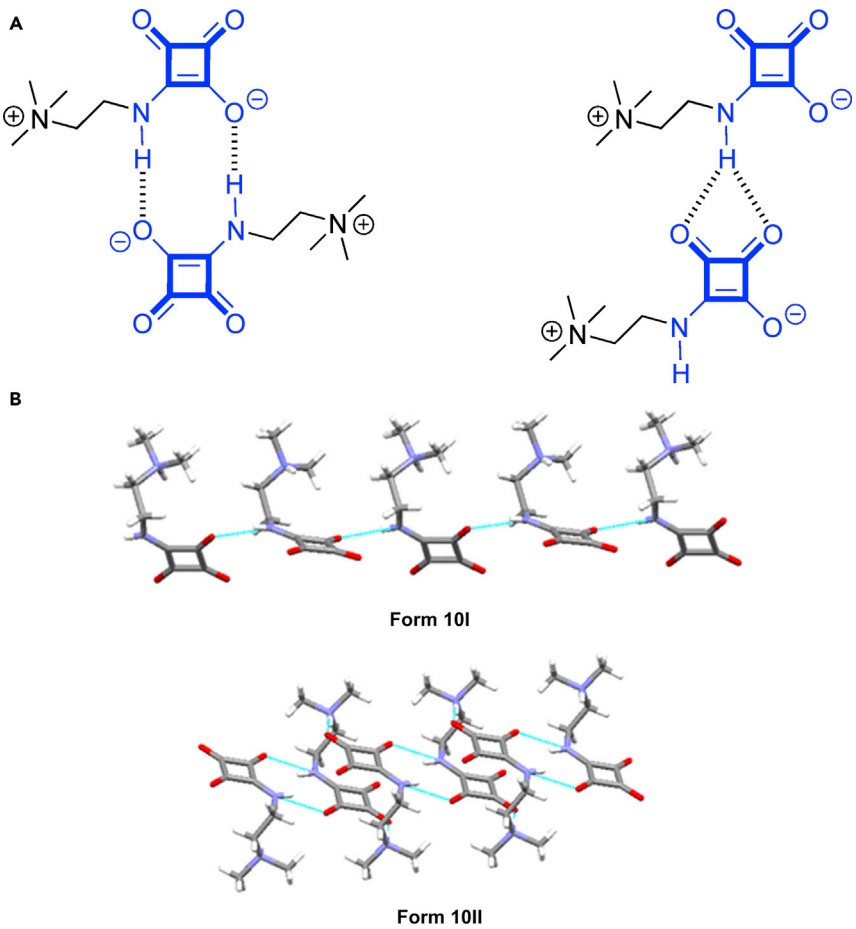

Figure 7. Supramolecular Assembly of Zwitterionicquaramide 10
(A) Different assembly motifs expected for **10** through charge assisted hydrogen bonding.
(B) Supramolecular synthons observed in **forms 10I** and **10II** show connected electrostatically compressed dimers.

with which it is forming the hydrogen bond, in **Form 10II** this interaction is *anti*. This minor difference in conformation leads to important consequences for the connection of the electrostatically compressed dimers, giving rise to completely different supramolecular synthons for both polymorphs: **form I** yields chains, whereas **form II** yields rings (Figure 7B). Interestingly, a dissimilar supramolecular synthon is obtained in the hydrate **form 10III**, where the addition of water molecules results in a stabilization of the entire structure through hydrogen-bonding interactions between the water molecules and the free carbonyls of a neighboring dimer.

Self-assembly of squaramides promoted by hydrogen-bonding interactions with a range of anions has also garnered significant research interest. One of the examples reported by Costa and co-workers in 2011 provided a combined crystallographic and computational study concerning the first example of a squaramide-nitrate salt crystal structure.[24] The study reported the synthesis of compound **11** and its subsequent crystallization from EtOH solution (Figure 8). The X-ray structure of **11** exhibited the familiar intermolecular head-to-tail arrangement by the formation of N–H···O hydrogen bonds between neighboring squaramide groups. The hydrogen-bonded network revealed additional stability promoted by the *syn* orientation of both the pyridine N atom and two additional C–H···N bonding interactions

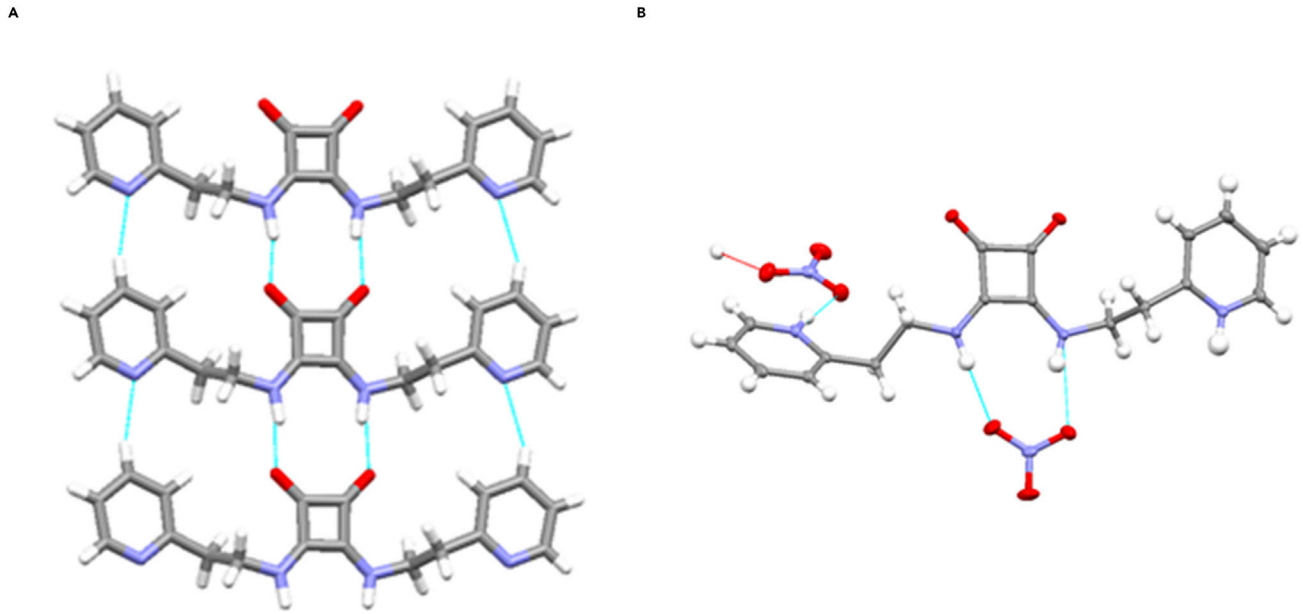

Figure 8. Single-Crystal X-Ray Structure of Dipydridyl Squaramide 11

(A) Head-to-tail hydrogen-bonded crystal structure of **11**.

(B) ORTEP drawing of **11** shows the pyridinium-nitrate and squaramide-nitrate units held together by a strong N–H···O and two N–H···O hydrogen bonds.

between neighboring molecules. The stability was further increased via two offset π-stacking interactions between the electron-rich squaramide and the electron-deficient pyridine rings at a centroid distance of 3.93 Å. The binding nature of **11** with nitrate was also revealed through X-ray crystallography and computational methods. Here, the crystal structure of **11** was bound to two nitrate anions in two distinct locations. The first nitrate was bound via coplanar N–H···O hydrogen bonds to the squaramide moiety, whereas the second was shown to be bound to the pyridinium ring via N–H···O hydrogen bonds. The simultaneous participation of the two squaramide N–H groups in a nitrate-squaramide motif prevents the formation of the head-to-tail packing observed in the crystal structure of **11** lacking nitrate; such an observation suggests the possibility of switchable supramolecular assemblies based on the addition of anion salts.

Recently, Prohens et al. discovered another example of an anion-promoted supramolecular assembly; they reported the synthesis of an anion-anion complex stabilized by hydrogen bonds to a secondary squaramide receptor 12 (Figure 9).[25] Using X-ray crystal-structure analysis, the authors were able to show the formation of a "H–G–G–H" (H = host, G = guest) system where hydrogen fumarate chains were shown to reside inside a channel formed by a series of hydrogen-bonded secondary squaramides (repeating units of **12**). The ability of **12** to form the hydrogen-bonding pattern shown in Figure 9 was thought to act as one of the driving forces behind the formation of the assembly. This combined with the presence of tertiary amine groups helped to facilitate the formation of the assembly. Moreover, *ab initio* calculations suggested that the anion-anion complex is thermodynamically unstable but kinetically stable relative to the isolated anions.

Costa and co-workers synthesized three structurally related squaramides, **13**–**15** (Figure 10); using a number of techniques such as elemental analysis,

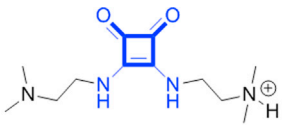

12

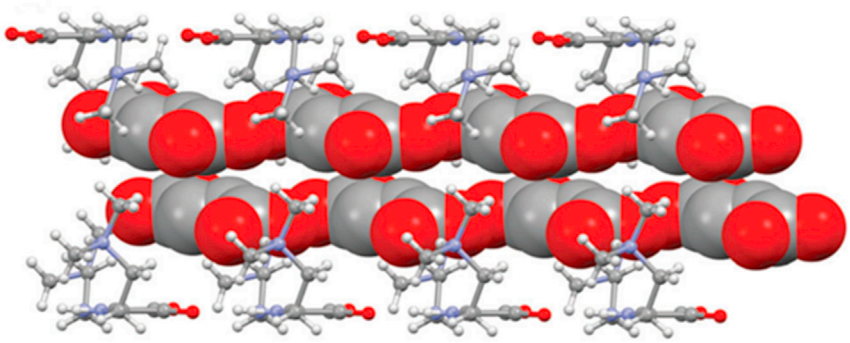

Figure 9. Chemical Structure of 12 and the Crystal Structure of "H–G–G–H" Supramolecular Assemblies Formed between 12 and Hydrogen Fumarate Showing the Hydrogen Fumarate Chains (in Spacefill Format) inside the Channel Formed by 12

Reproduced from Prohens et al.[25] with permission from the Royal Society of Chemistry.

thermogravimetric analysis (TGA), DSC, powder X-ray diffraction (PXRD), single-crystal XRD, solid-state ^{13}C NMR, and fourier-transform infrared spectroscopy-attenuated total reflection (FTIR-ATR), they studied changes in their self-assembly behavior brought about by N-methylation.[26] The authors showed that compounds **13–15** form dihydrates in the solid state and self-assemble into pillars of stacked squaramide units but with marked structural differences in the position of the water molecules, highlighting the influence of N-methylation in their self-assembly. *N*-Methyl groups appear to block the formation of N–H···O=C hydrogen bonding

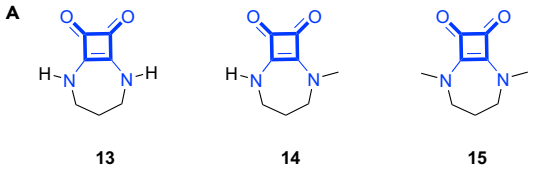

13 14 15

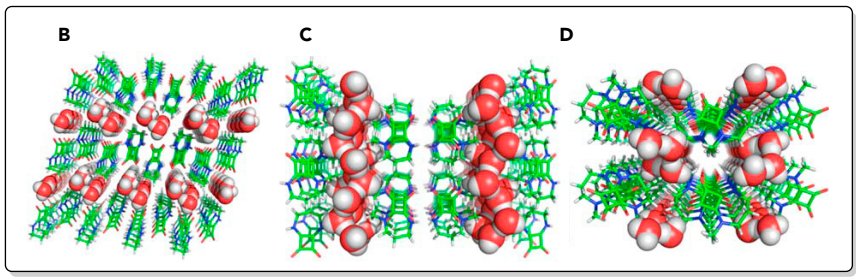

Figure 10. Self-Assembly of Squaramides 13–15

(A) Chemical structures of **13–15** and the crystal structure of supramolecular assemblies of **13–15**.
(B) Top view of the crystal structure of squaramide **13**·$2H_2O$ shows the 1D water tapes.
(C) Top view of the crystal structure of squaramide **14**·$2H_2O$ shows the 2D water layers.
(D) Top view of the crystal structure of squaramide **15**·$2H_2O$ shows the 1D water chains.
Reproduced with permission from Ximenis et al.[26] Copyright 2018 American Chemical Society.

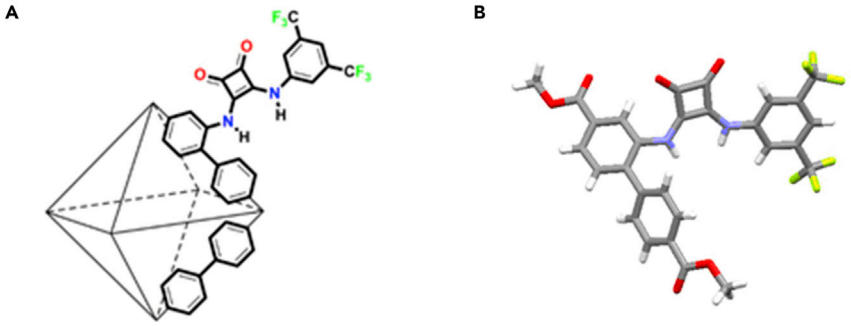

Figure 11. Squaramide-Based Zr-MOFs

(A) Schematic representation of the Zr-based MOF containing squaramide organocatalyst **16**.

(B) Solid-state X-ray crystal structure of **16**.

Reproduced with permission from McGuirk et al.[28] Copyright 2015 American Chemical Society.

that normally dominates the self-assembly of bis-secondary squaramides, thus favoring the appearance of dipolar stacking and weak C–H···O=C interactions. As a result, three distinct water clusters were observed: **13**·$2H_2O$ formed water tapes, = **14**·$2H_2O$ formed 2D hexagonal water layers, and **15**·$2H_2O$ formed 1D water chains. In all cases, the water molecules formed strong hydrogen bonds with the carbonyl oxygens of the squaramides, whereas weak CH···O=C interactions helped to maintain the columnar assemblies. The authors remarked that such results could provide future applications of cyclic squaramides toward artificial water confinement and transport systems.

Another recent application of squaramide containing compounds in self-assembly materials has been in the synthesis of metal-organic frameworks (MOFs). MOFs are an extensively studied class of porous materials made by linking inorganic and organic subunits. A vast array of metals and diverse organic linkers have been exploited for the synthesis of high-surface-area materials with large internal pore sizes in a 3D-ordered crystalline structure. Potential applications of MOFs are diverse and have already been investigated in areas such as chemical sensors, biomedicine, catalysis, and hydrogen storage to name just a few key areas.[27]

In 2015, McGuirk et al. incorporated the squaramide-based organocatalyst **16** into the framework of a Zr-based MOF (Figure 11).[28] The structure of the Zr-based cluster was probed by NMR spectroscopy and powder XRD techniques, which confirmed that the 3D architecture of the MOF was retained upon incorporation of **16**, and the surface area of the MOF was estimated at 1,700 m^2/g via the Brunauer-Emmett-Teller (BET) equation. The catalytic performance of the MOF was also evaluated in a model Friedel-Crafts reaction between indole and β-nitrostyrene; incorporation of **16** in the MOF was found to prevent the self-association of the active catalyst, known to be detrimental to its catalytic effect. This gave rise to a reaction yield of 78% in the presence of the MOF when conducted in DCM at RT over 24 h. When the same reaction was conducted in the presence of the free catalyst **16** under the same conditions, no product was isolated. Moreover, a direct comparison of the activity of the squaramide MOF catalyst with an identical urea MOF catalyst was also conducted and showed that the squaramide MOF was more than twice as active.

Cohen et al. subsequently reported a small family of Zr-based MOFs incorporating squaramides **17**–**19** (Figure 12).[29] Synthesized via a combination of the appropriate squaramide and $ZrCl_4$ under solvothermal conditions, PXRD structures of the

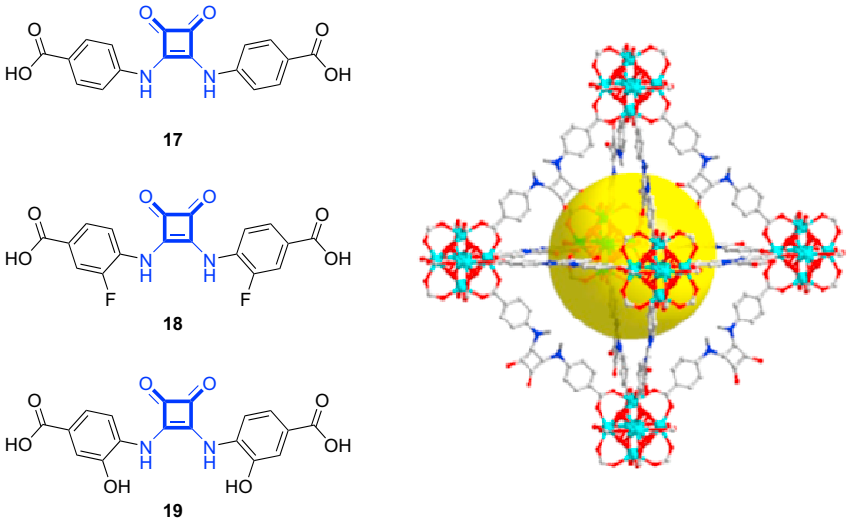

Figure 12. Chemical Structures of Compounds 17–19 and a Model of Zr-Based Squaramide-Containing MOF

Reproduced with permission from Cohen et al.[29] Copyright 2016 American Chemical Society.

squaramide MOFs exhibited a linear *anti*/*anti*-conformation with respect to the squaramide and allowed for highly effective pre-organization in favor of MOF formation. The carboxylate groups of the squaramides revealed intermolecular hydrogen bonds (O–H···O = 2.59 Å) that form 1D chains; however, hydrogen bonds (N–H···O = 2.82 Å) with the solvent NMP prevented the well-known head-to-tail self-assembly motif.

In another example, Cohen and co-workers developed squaramide-based Cu(II)-MOFs based around compound **20** (Figure 13), and these are also able to catalyze the Friedal-Crafts reaction of indole with β-nitrostyrenes.[30] Synthesized through a post synthetic exchange (PSE) reaction from its Zn(II) analog, the Cu(II) MOFs showed greater stability and catalytic activity than the parent Zn(II) derivative. Moreover, a catalytic study of a series of isostructural squaramide-based Cu(II)-MOFs showed that the catalytic performance increased as the amount of squaramide ligand increased, thus confirming the promise that squaramide MOFs show in the field of MOF-supported heterogeneous organocatalysis.

Macrocyclic compounds containing the squaramide moiety have also been exemplified in the literature. Although Costa and co-workers have previously demonstrated the self-templated formation of macrocycles containing both squaramides and a hydrogen-bond acceptor unit[18,31] and Elmes, Jolliffe, and co-workers have synthesized macrocyclic squaramides for anion recognition[32] (vide infra), a more recent report from Shimiziu and co-workers reports the self-assembly of squaramide macrocycles. A crystallographic comparison between squaramide **21** and its urea and thiourea analogs **22** and **23** (Figure 14) was conducted, and it was found that the macrocycles containing urea, thiourea, or squaramides each display a preference for *trans-trans* conformers in their crystal forms.[33] Moreover, squaramide **21** was found to assemble in the solid state in a "head-to-tail" hydrogen-bonding assembly where only one of the squaramide carbonyls participates in hydrogen bonding with a neighboring N–H (N···O distances ≈ 2.87 Å) and the second carbonyl exhibits just a close contact with an aromatic hydrogen. This behavior is rare for *trans-trans* squaramides, for which the usual arrangement is with both amide protons bonding to both

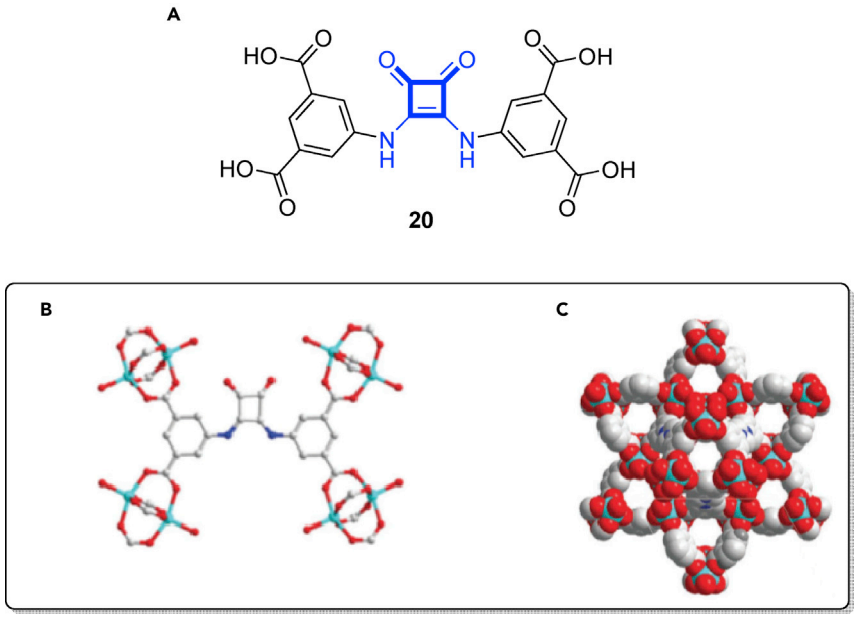

Figure 13. Squaramide-Based Cu(II)-MOFs
(A) Chemical structure of compound **20**.
(B) X-ray crystal structure of the Zn(II) MOF based on compound **20**.
(C) Observed packing of the squaramide-based Zn(II) MOF.
Reproduced from Zhang et al.[30] with permission from the Royal Society of Chemistry.

carbonyls in a ribbon-type structure. The DMSO solvate of **21** was also reported and exactly matched the previously reported crystal structure; again, the macrocycle displayed a *trans-trans* squaramide conformation with each of the NH groups hydrogen bonded to the DMSO oxygen.[32]

Another emerging use of the squaramide scaffold in supramolecular self-assembly has been toward the construction of polymers and gels. Early advances in this area focused on the development of traditional covalently linked biopolymers based on peptides and polysaccharides to develop materials for use in biomedical applications, such as MRI imaging.[34,35] In these examples, the squaramide was utilized for its ability to crosslink two amines; however, in recent times, the self-assembly properties of squaramides have been exploited for use in supramolecular polymers. These materials, crosslinked by various reversible supramolecular interactions, give rise to bulk materials that display unique properties such as self-healing, stimuli-responsiveness, and adaptability and have been investigated for use in a vast array of potential applications.[36] With their strong hydrogen-bond donor and acceptor behavior, squaramides are ideal candidates for building such materials, and early examples in the field have been reported in recent years.

Kieltyka et al. have taken advantage of the "head-to-tail" hydrogen-bonding pattern in bis-squaramide **24** to form a supramolecular polymer that gains additional stability through aromatic gain (Figure 15).[4] Consisting of two oligo(ethylene glycol) methyl ether chains on either side of a central hydrophobic core containing two squaramide units, **24** was shown to self-assemble into stiff micrometer-long fibers with a uniform diameter in water by a combination of cryogenic transmission electron microscopy (cryo-TEM) and X-ray scattering analysis. The authors were able to show not only that the self-assembly process was dictated by hydrogen-bonding

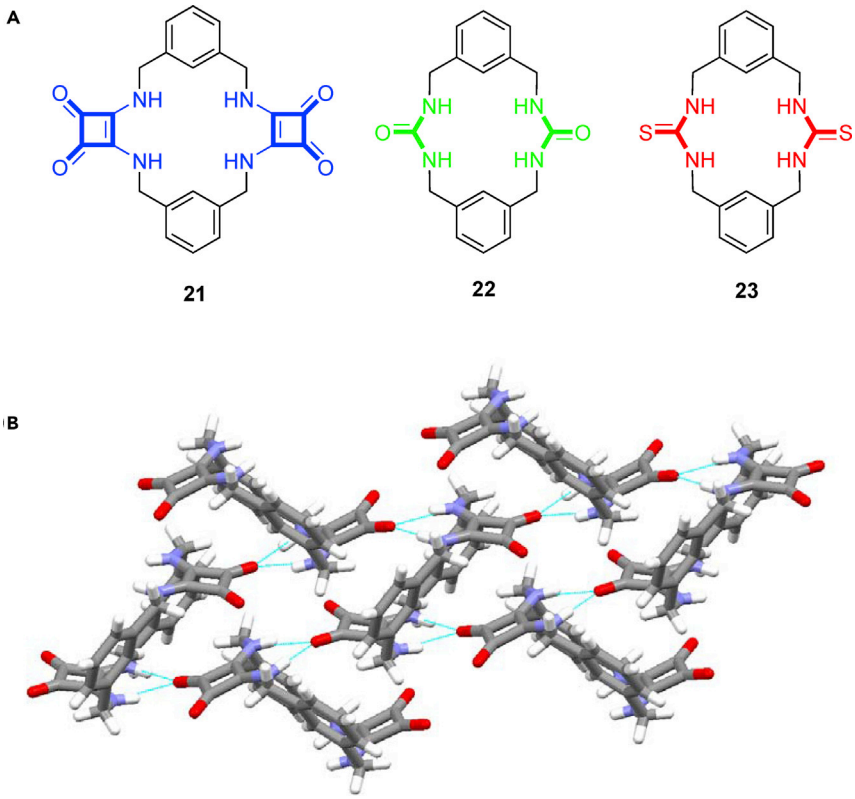

Figure 14. Macrocyclic Squaramides

(A) Chemical structures of macrocyclic compounds **21**–**23**.

(B) X-ray crystal structure of squaramide macrocycle **21** exhibiting the *trans-trans* conformation and demonstrating "head-to-tail" hydrogen-bonding assembly.

interactions between squaramide sub-units but that the self-assembly process itself promoted an increase in the aromatic character of the squaramides, thus providing an additional level of thermodynamic stability to the entire assembly. The gain in aromatic character upon assembly was demonstrated through a combination of experimental and computational techniques and is a key consideration for such applications because other analogous ditopic scaffolds, such as ureas and thioureas, cannot exhibit such behavior.

Kieltyka and co-workers have also synthesized a series of squaramides based around a flexible tripodal tris(2-aminoethyl)amine core, **25**–**28**, where **26** and **27** were shown to form transparent hydrogels in deionized water, and **25** and **28** were found to be ineffective as supramolecular hydrogelators (Figure 16).[37] Notably, for compound **29**, where the squaramide moieties of **26** are replaced with ureas, no hydrogelation occurred, demonstrating the importance of the squaramide motif. The properties of gels formed from **26** and **27** were studied by various techniques, including oscillatory rheology, cryo-TEM, and small-angle X-ray scattering experiments (SAXS); the gels were found to be self-recovering and formed from a network of entangled fibrils on the nanometer scale in width and micrometers in length. Spectroscopic measurements such as UV-vis absorption and infrared spectroscopy showed that monomer aggregation is mainly driven by a combination of both hydrogen bonding and hydrophobicity. The hydrogels formed from **26** and **27** were further examined for their ability to encapsulate mammalian cells in 3D. Fluorescence-activated cell sorting (FACS) and confocal laser scanning microscopy (CLSM) revealed that the

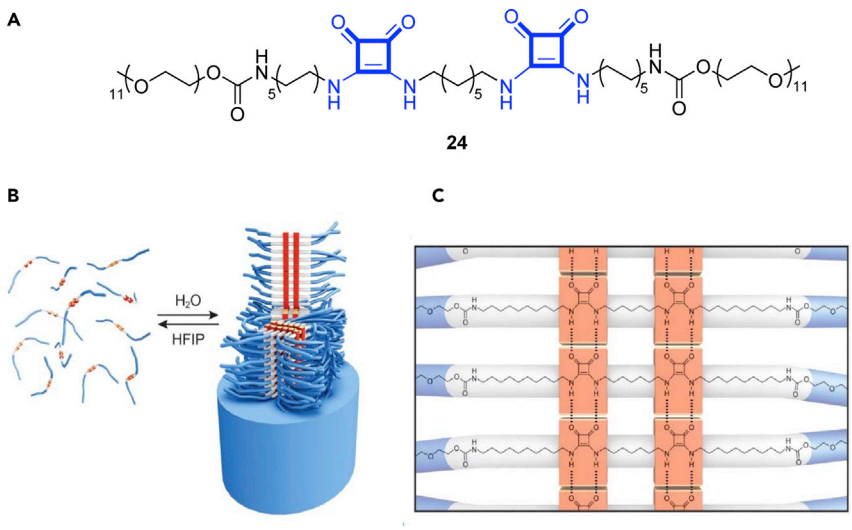

Figure 15. Squaramide-Based Supramolecular Polymers
(A) Chemical structure of squaramide **24**.
(B) Schematic representation of the self-assembly of **24** into fibrillar structures and disassembly promoted by hexafluoroisopropanol (HFIP).
(C) Proposed "head-to-tail" hydrogen-bonding interactions between monomers of **24**.
Reproduced with permission from Saez Talens et al.[4] Copyright 2011 Wiley-VCH Verlag GmbH & Co. KGaA.

squaramide-based supramolecular hydrogels were cytocompatible toward the NIH-3T3 cell line and the more sensitive human-induced pluripotent stem cells (hiPSCs). Moreover, hydrogel materials allowed the formation of 3D spheroids from single cells, and the hiPSCs retained their pluripotent state while under culture and upon release. The results suggest that such squaramide-based hydrogels could find biological application as a new 3D cell-culture medium and as cell delivery vehicles.

Another example of a squaramide-based low-molecular-weight gelator (LMWG) was recently described by Schiller et al., who described the synthesis of compound **30** and showed its ability to undergo self-assembly in a variety of alcohols to form alcogels (Figure 17).[38] Compound **30** was assembled by sequential reactions of *N*-((1*R*,2*R*)-2-aminocyclohexyl)-4-methylbenzenesulfonamide and 4-tertbutylaniline with 3,4-dimethoxy cyclobut-3-ene-1,2-dione in methanol before being evaluated as a LMWG in various solvents. **30** was found to be capable of forming gels in a number of alcoholic solvents, including primary, secondary, tertiary, lineal, and branched alcohols; critical gelation concentration (CGC) values ranged from 3 to 21 g L^{-1}.

Quantum-mechanical calculations of **30** and comparison with a range of structurally similar analogs revealed that dimers calculated for **30** show a large and complex network of inter- and intramolecular interactions that grow a stable gel network. Inspection of the lowest-energy dimer for **30** (Figure 18) showed that the squaramide moiety of each molecule was effectively stabilized through intramolecular π—π stacking, and NH—π and CH—π intermolecular interactions with multiple phenyl—phenyl and squaramide—phenyl stacking interactions provided extra stability to the assembly. Field emission scanning electron microscopy (FESEM), transmission electron microscopy, and atomic force microscopy (AFM) demonstrated the effect of solvent on gel formation where the nature of the gelling solvent was shown to have a dramatic effect on the morphology of the aggregates formed. For example, straight laths of *ca.* 0.2–1.4 mm were formed in benzylalcohol, whereas

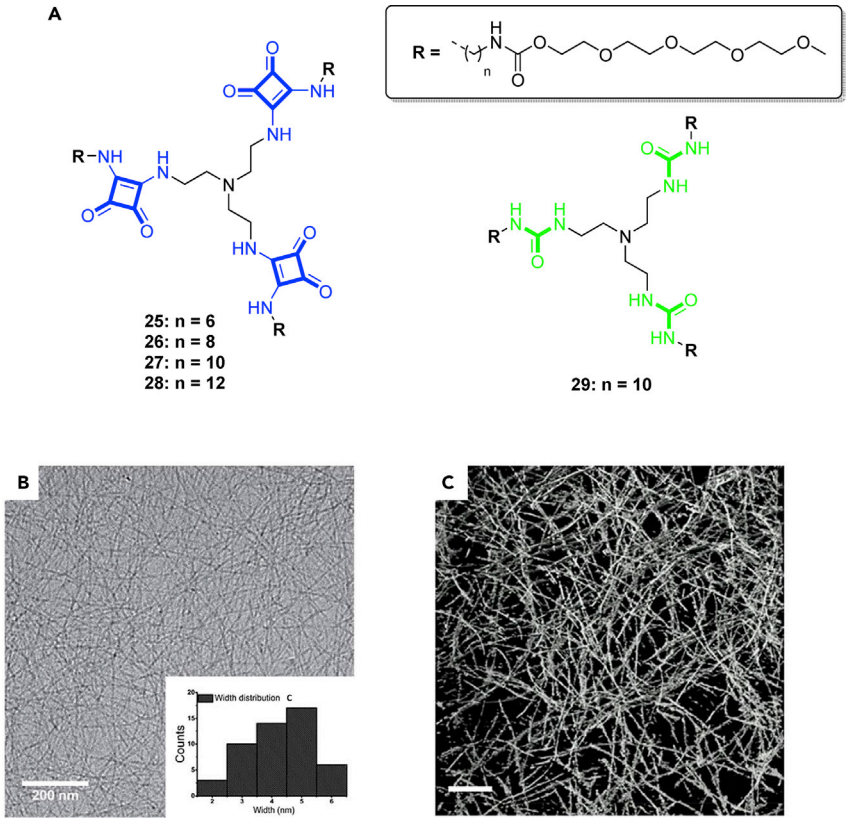

Figure 16. Supramolecular Hydrogels

(A) Chemical structures of tripodal squaramides **25**–**28** and tripodal urea **29**.

(B) Cryo-TEM image of hydrogel **27**. Inset: histograms of fiber width distribution for a sample size of n = 50.

(C) Cryo-electron tomography image of a hydrogel of **27** (scale bar: 200 nm).

Reproduced with permission from Tong et al.[37] Copyright 2018 American Chemical Society.

fibrillar networks of entangled fibers of ca. 10–20 nm in diameter were observed in hexan-1-ol and methanol.

Amphiphilic squaramide-squaramate conjugates have been designed by Costa and co-workers as potential hydrogelators (Figure 19).[39] Conjugates **31**–**33** were reported, and although **31** and **32** successfully formed, low-molecular-weight

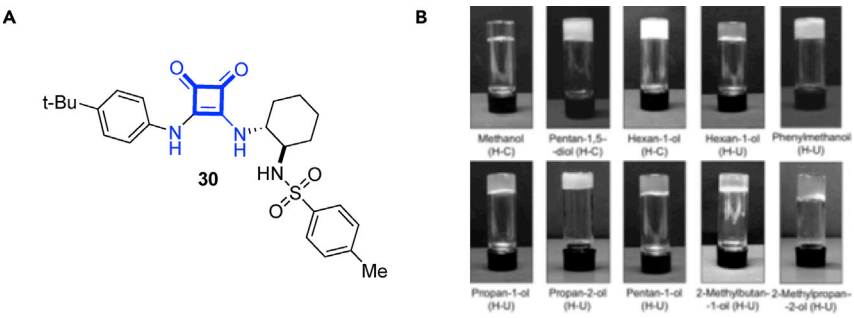

Figure 17. Squaramide-Based Low-Molecular-Weight Alcogels

(A) Chemical structure of **30**.

(B) Alcogels of **30** formed in a range of alcohol solvents.

Reproduced from Schiller et al.[38] with permission from the Royal Society of Chemistry.

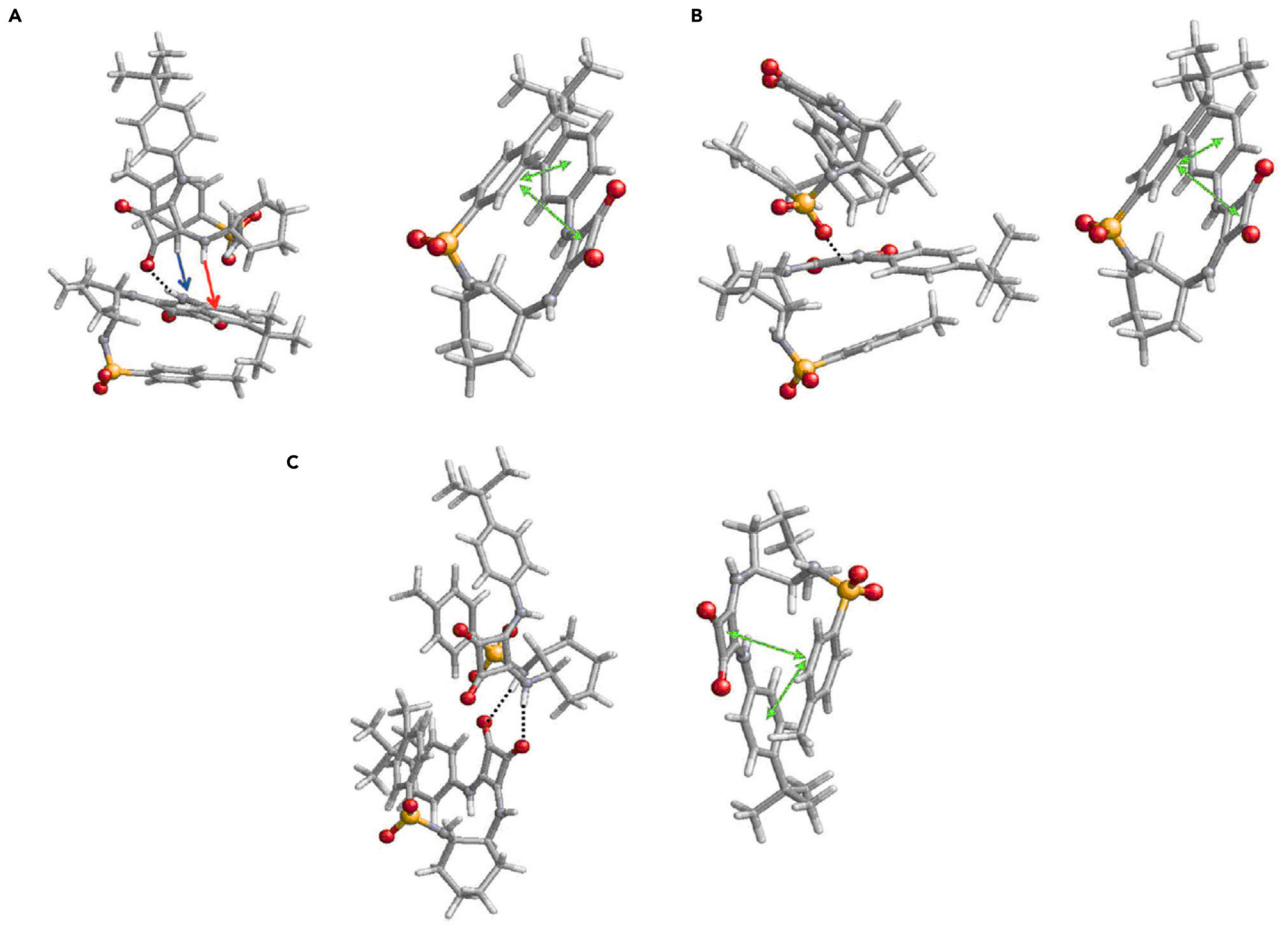

Figure 18. Alcogel Assembly

Graphical representation of the three most stable complexes (A–C) obtained for **30** through quantum-mechanical calculations. Hydrogen bonds are represented by black dashed lines, N–H···π and C–H···π interactions are represented by red and blue arrows, and intramolecular π···π stacking interactions are represented by green double arrows. Reproduced from Schiller et al.[38] with permission from the Royal Society of Chemistry.

supramolecular hydrogels **33** did not. Indeed, the authors found that the squaramide substituents had a profound effect on the gelation properties of the amphiphilic squaramide-squaramate conjugates whereby **31**, containing a *para*-nitrophenyl substituent, formed a hydrogel at relatively low concentration (0.1%–0.2% w/v), whereas **32**, containing a *para*-CF_3–phenyl substituent, exhibited a significantly higher critical gelation concentration (1.6% w/v). Moreover, AFM analysis of hydrogels formed from **31** and **32** revealed both similarities and marked morphological differences. Micrometer-sized disordered fibers were observed in both gels of **31** and **32**; however, **31** showed bundled fibrous assemblies composed of one or more strands with an apparent width of 42 nm, whereas **32** was composed of both right-and left-handed helical ribbons with an average diameter of 52 nm twisting around a central axis of the fiber (Figure 19). SEM and TEM images confirmed the formation of networks of bundled fibers. The authors suggested that these morphological differences were a consequence of varying the peripheral substituents on the self-assembly of the precursor hydrogelators **31** (*para*-nitrophenyl) and **32** (*para*-CF_3–phenyl). The self-assembly behavior was confirmed through various techniques, including NMR spectroscopy, mass spectrometry, UV-vis spectroscopy, and DSC. The biocompatibility of the hydrogels formed from

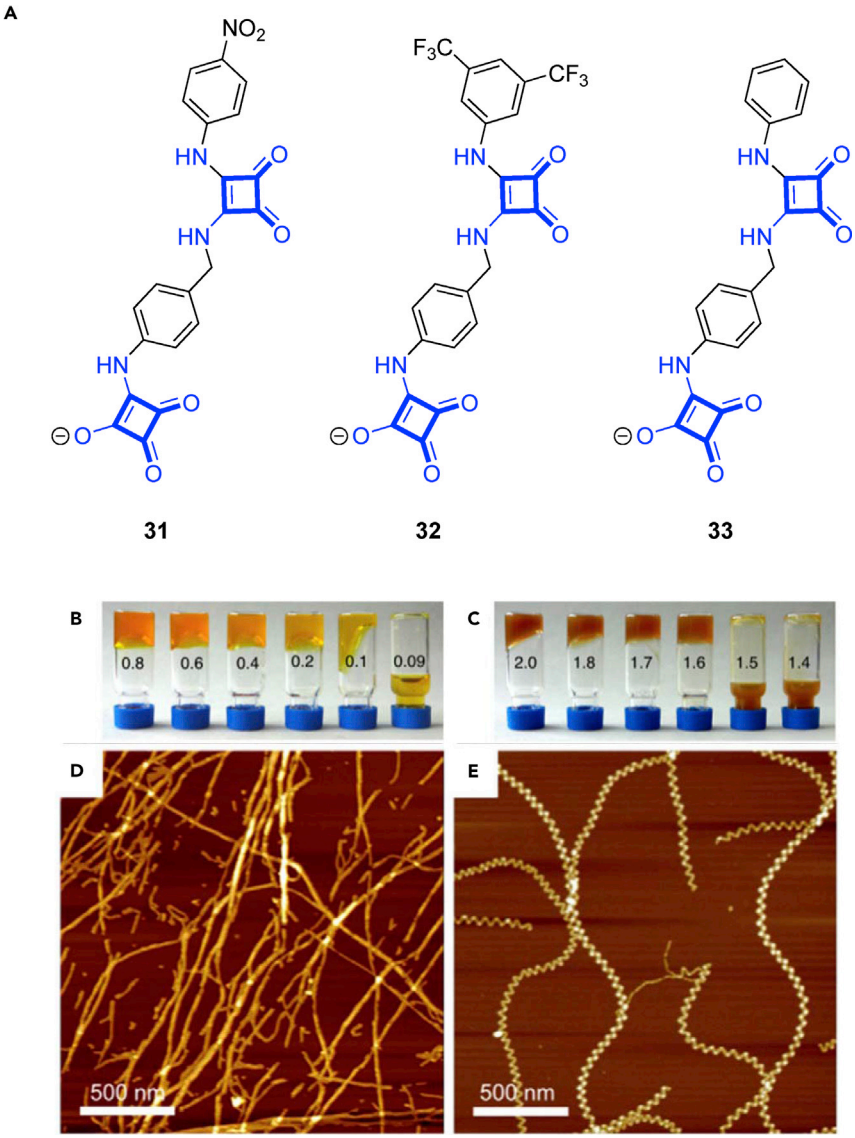

Figure 19. Amphiphilic Squaramide-Squaramate Hydrogelators
(A) Chemical structures of **31**–**33**.
(B and C) Vial inversion tests on samples of hydrogel **31** (B) and hydrogel **32** (C).
(D and E) AFM images of hydrogel **31** (D) and hydrogel **32** (E) obtained on mica show the morpholigcal differences between both hydrogels.
Reproduced with permission from López et al.[39] Copyright 2017 Wiley-VCH Verlag GmbH & Co. KGaA.

31 was also evaluated; U87 cells were grown in the presence of **31** at increasing concentrations, and no toxicity was observed up to 500 μM. Indeed, the hydrogel composed of **31** was also found to be thermoreversible, thixotropic (viscosity diminishes under compression), and injectable and could be loaded with zwitterionic biomolecules such as $_{L}$-carnitine,γ-aminobutyric acid (GABA) and $_{D,L}$-Ala-$_{D,L}$-Ala without disrupting the hydrogel structure. Finally, to demonstrate the applicability of **31** as a potential delivery vehicle, the authors showed that the loaded hydrogel could release its zwitterionic guest in a controlled manner upon treatment with either water or saline (for more rapid release).

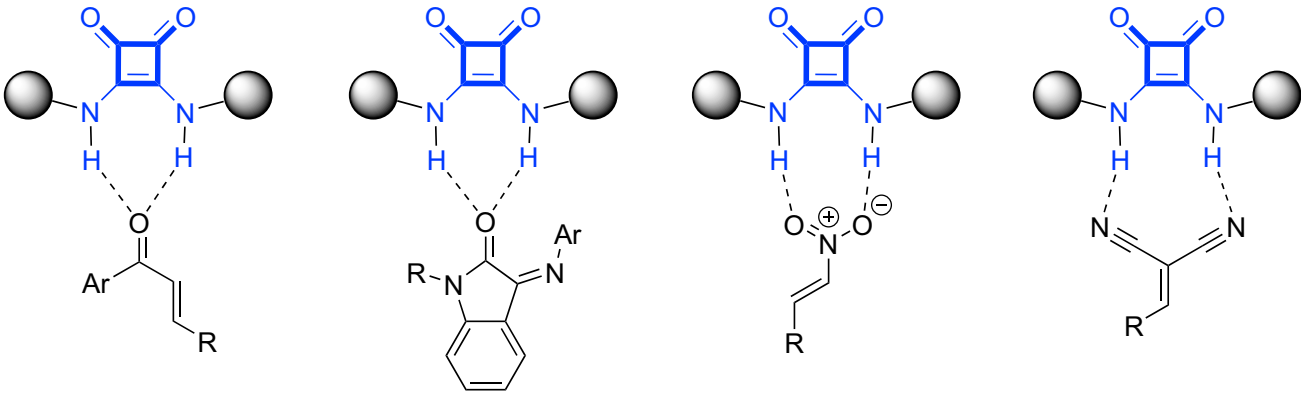

Figure 20. Substrate Activation by Squaramide Organocatalysts

From the above examples, it is clear that the squaramide moiety has the potential to be exploited across a broad spectrum of self-assembled materials and is only now beginning to be explored in greater detail. The strong hydrogen-bond donating and accepting ability of squaramides dominates their self-assembly characteristics; however, it is also clear that their aromatic nature and indeed ability to increase their aromatic character when partaking in non-covalent binding interactions that confers a great deal of additional stability to squaramide-based self-assembled aggregates and assemblies. Indeed, the very same characteristics have been exploited in the area of organocatalysis where, again, the strong hydrogen-bond-donating ability of the squaramide is key to its success as an excellent catalyst across a broad range of synthetic transformations.

SQUARAMIDES AS ORGANOCATALYSTS

Organocatalysis can be described as the use of relatively simple organic molecules as effective and often highly enantioselective catalysts for a variety of synthetic transformations.[40] The field of organocatalysis has, since its reawakening in 2000,[41] been established as a proven and highly robust and important tool in modern synthesis. Various research groups have made considerable efforts at developing new and improved organocatalysts, with several focused on establishing novel bifunctional hydrogen-bonding catalysts. Initial efforts using a thiourea hydrogen-bonding core proved highly successful and dominated the area of hydrogen-bonding organocatalysis for some time.[42,43] The related hydrogen-bonding squaramide motif first found use as an anion receptor as previously mentioned. It was not until the pioneering work of the Rawal group in 2008,[44] on the development of Cinchona-squaramide organocatalysts, that the potential and range of applications of squaramide organocatalysts became apparent.

The squaramide moiety is considered to be able to form strong hydrogen bonds with reaction substrates that bear hydrogen-bond-accepting functionalities, such as carbonyl, nitro, nitrile, and imino substrates (Figure 20).[40]

It is this hydrogen-bonding ability that makes squaramides such effective organocatalysts, as it can substantially increase the reactivity of a substrate. Often, the squaramide catalyst has a basic moiety, typically a tertiary amine, and a chiral scaffold incorporated. This strategy results in a chiral bifunctional organocatalyst that can simultaneously activate both the electrophile and nucleophile while controlling the stereochemistry of the transition state. The precise nature of the catalyst, electrophile, and nucleophile interaction is perhaps not easily defined and at least three closely related mechanisms can be considered (Figure 21).[45]

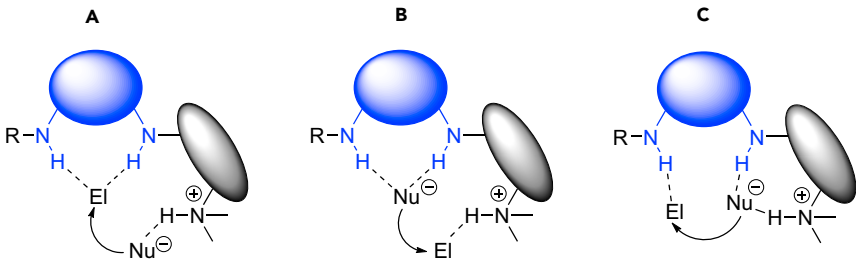

Figure 21. Bifunctional Organocatalyzed Transition-State Variants

A joint experimental-theoretical study was conducted by Soós and co-workers in 2014[45] and explored the mechanism of a bifunctional squaramide-amine-catalyzed Michael addition reaction between 1,3-dioxo nucleophiles and nitrostyrene (Scheme 1). The squaramide organocatalyst **34** was chosen and allowed computational analysis at a reasonably high level of theory. Catalyst **34** also performed well, with high yields and high stereoselectivity, in the experimental Michael addition of acetyl acetone and ethyl 2-oxo-cyclopentanecarboxylate to nitrostyrene. Subsequent density functional theory (DFT) calculations were conducted to investigate the potential pathways, A–C (Figure 21), operating in the rate-determining step. Here, Soós and co-workers suggested that reaction pathway B, corresponding to activation of the electrophile via the protonated amine, is the most plausible mechanism.[6] However, they also noted that some of the reaction channels described as pathway A were also accessible, implying that a single reactivity model may not always be able to sufficiently rationalize the stereoselectivity outcome and the precise role of the squaramide organocatalyst. The alternative path C could not be identified as a viable mechanism for the Michael addition reaction in their DFT study.

In the organocatalytic section of this review, we would like to highlight a selection of recently published synthetic transformations that have exploited the powerful catalytic and stereodirecting ability of squaramide organocatalysts. We recommend that readers consult the referenced articles in order to fully explore each citation and the examples not covered in this review. Finally, we regret the

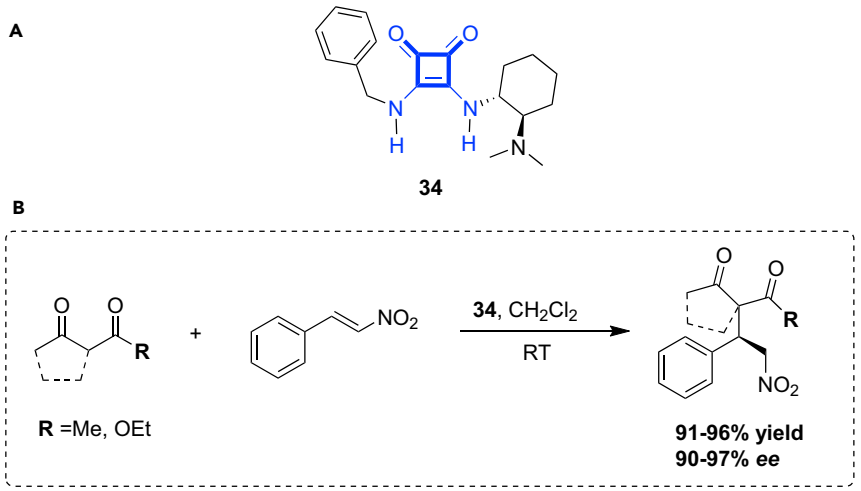

Scheme 1. Michael Addition of Acetyl Acetone and Ethyl 2-Oxo-cyclopentanecarboxylate to Nitrostyrene

(A) Chemical structure of squaramide catalyst **34**.

(B) General reaction for the stereoselective Michael addition to nitrostyrene.

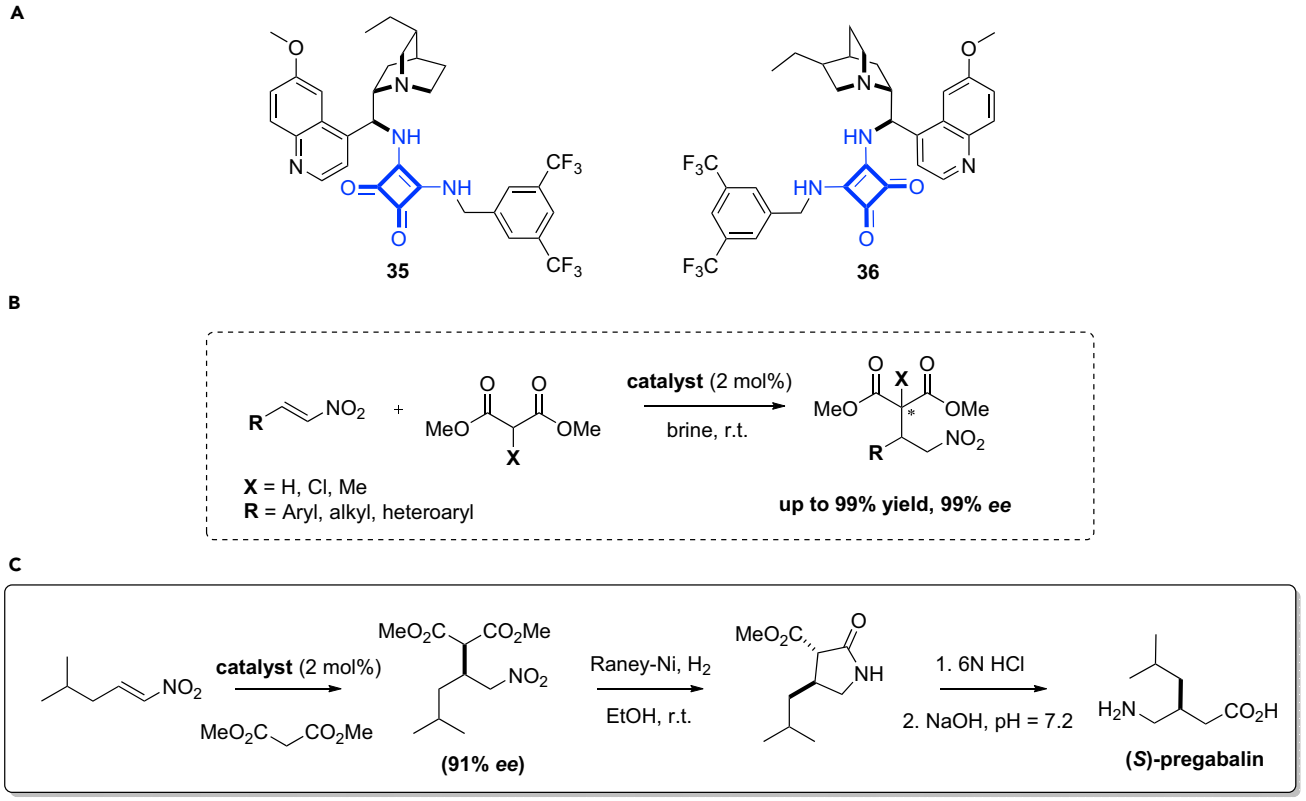

Scheme 2. Enantioselective Michael Addition of β-Dicarbonyl Compounds to Nitroolefins "on Water"

(A) Chemical structures of cinchona-based squaramide catalysts **35** and **36**.

(B) General reaction scheme for squaramide catalyzed Michael addition of malonates to nitroalkenes.

(C) Asymmetric synthesis of (*S*)-pregabalin.

omission of relevant work, as the field of squaramide organocatalysis is vast in terms of publications and contributors, which points to the significance of this area of research.

Squaramide-catalyzed conjugate addition reactions have garnered significant research attention in recent years. The hydrogen-bonding-promoted enantioselective Michael addition of β-dicarbonyl compounds to a diverse range of nitroolefins, with cinchona-based squaramide catalysts, was explored by Song and co-workers in 2015 (Scheme 2).[46] In this work, a significant increase in the rate of reaction was observed when the reaction was performed "on water." This rate acceleration under "on water" conditions allowed a reduction in catalyst loading, where 0.01 mol % of catalyst was sufficient to allow complete reaction at RT with high diastereo- and enantioselectivity of >99:1 and up to 99%, respectively. This enhanced reaction performance "on water," compared with that of conventional organic solvents, was attributed to the hydrophobic hydration effect. The hydrophobic amplification depended on the catalyst used, where catalysts with increased hydrophobicity (vinyl or ethyl C3 substituents) gave superior performance. A number of aryl-, alkyl-, and heteroaryl-substituted nitroolefins were explored with malonate pronucleophiles, and both the *R* and *S* enantiomers of the products were obtained for some examples when different pseudo enantiomers of the catalysts (**35** and **36**) were employed. β-Ketoesters and β-diketones were also utilized as pronucleophiles, and in all cases, high yields and stereoselectivity were reported (up to 99% yield, 99:1 diastereomeric ratio [d.r.], 99% enantiomeric excess [ee]). In order

A

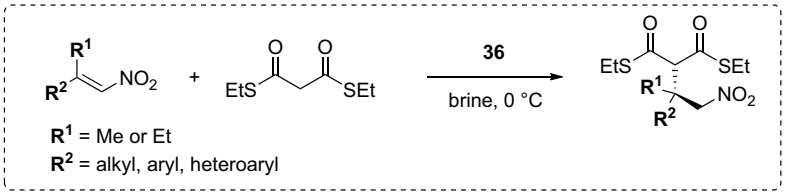

B

Scheme 3. Enantioselective Michael Addition Dithiomalonates to the β,β-Disubstituted Nitroalkenes "on Water"

(A) General reaction scheme for the Michael addition reaction of dithiomalonates to β,β-disubstituted nitroalkenes using catalyst **36**.

(B) Synthetic applications of catalyst **36** toward a one-pot synthesis of a chiral β-substituted GABA analog.

to demonstrate synthetic utility, the "on water" protocol was successfully applied for the scalable syntheses of an antidepressant (*S*)-rolipram and an anticonvulsant (*S*)-pregabalin (Scheme 2).

Subsequently, in 2017, Song and co-workers expanded their "on water" squaramide work and studied unreactive β,β-disubstituted nitroalkene substrates (Scheme 3).[47] Here, they found that the "on water" conditions enabled new catalytic reactions for otherwise unreactive substrate systems. The Michael addition reaction of dithiomalonates (DTMs) to the β,β-disubstituted nitroalkenes, using the chiral squaramide catalysts **35** and **36**, afforded both enantiomers of the Michael adducts with all-carbon-substituted quaternary centers. High yields and enantioselectivities were observed in most cases using β,β-disubstituted nitroalkenes with methyl as one of the β-substituents (up to 99% yield and 96% ee). A lower yield and ee were recorded when one of the β -substituents was an ethyl group (42% yield and 42% ee). To demonstrate the synthetic utility and potential large-scale applications, the reported "on water" protocol was applied to the gram-scale one-pot syntheses of chiral GABA analogs, with all carbon quaternary stereogenic centers at the β position (Scheme 3). In 2017, Palomo and co-workers employed a Brønsted base-squaramide bifunctional catalyst to promote the conjugate addition of either unsubstituted or α-monosubstituted β-tetralones to nitroalkenes (Scheme 4).[48] One of the difficulties in working with a nonsymmetric cycloalkanone such as a β-tetralone is that enolization may occur at either the α or α′ site. Paloma and team suggested that the fused aromatic ring in β-tetralones might induce preferential enolization at Cα rather than Cα′ and that the use of a Brønsted base would generate relatively high concentrations of the enolic form and drive the catalytic process forward. This regioselective question was accompanied by a second challenge, control of the stereochemistry during construction of the new quaternary carbon stereocenter. In this case, a solution lay in the use of a chiral squaramide bifunctional catalyst to control the stereochemistry of the transition state. A catalyst screen identified squaramide **37** as the preferred bifunctional catalyst, furnishing the product of the test reaction in a 93% yield and an ee of 80%. Exploration of substrate scope, with respect to the α-substituted β-tetralones

A

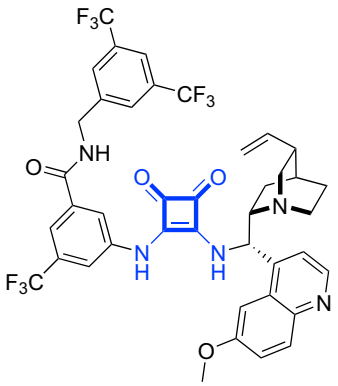

37

B

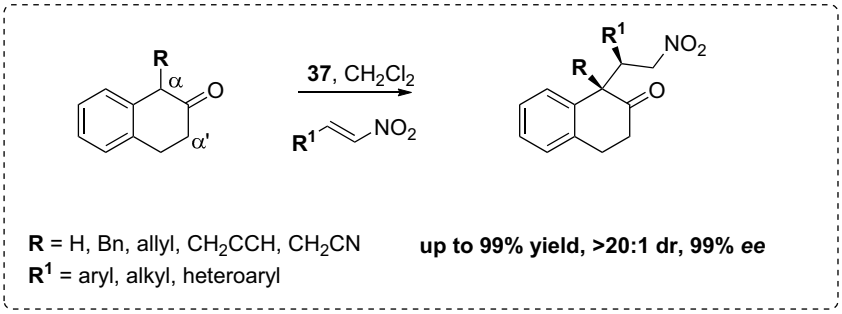

Scheme 4. Conjugate Addition of Unsubstituted and α-Monosubstituted β-Tetralones to Nitroalkenes

(A) Chemical structure of the squaramide bifunctional catalyst **37**.

(B) General reaction scheme for the catalytic addition of β-tetralones to nitroalkenes.

and a selection of nitroolefins, generated the expected products in high yields and enantioselectivities (up to 84% yield and 99% ee). The reaction of the unsubstituted β-tetralone, R = H, with a number of nitroalkenes was also investigated, resulting in the smooth conversion to the Cα-alkyled β-tetralone products in high yields and stereoselectivities (up to 88% yield, >20:1 d.r., and 99% ee). To demonstrate synthetic utility, the adducts were readily converted into diverse polycyclic compounds featuring up to six stereogenic centers.

Oiarbide, Palomo, and co-workers, also in 2017, reported their successful attempt at controlling the α/γ-reactivity of vinylogous ketone enolates in squaramide catalyzed Michael reactions (Scheme 5).[49] The majority of catalytic reactions that involve vinylogous enolate equivalents proceed with a nucleophilic attack from the γ-carbon atom, and not the α-site, of the unsaturated substrate. Switching the reactivity from the more typical γ- to the α-carbon atom is challenging. In this report, a regio-, diastereo-, and enantioselective direct Michael addition of β,γ-unsaturated ketones with nitro olefins is described, where a squaramide bifunctional catalyst enables the reaction of a range of β,γ-unsaturated ketones to proceed exclusively at the α-site. Different subsets of β,γ-unsaturated ketones, including those with aryl, alkyl, alkynyl, and hydroxyalkyl side chains, as well as a variety of nitroolefins, all participated well. This gave access to a variety of α-branched ketone products, generally with two vicinal tertiary carbon stereocenters and with high stereoselectivity. The enantioselectivity was typically >90% ee, with yields ranging from 68% to 98%.

A

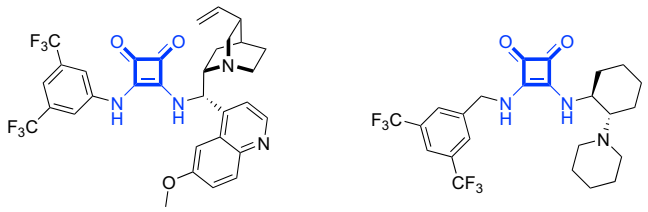

38 39

B

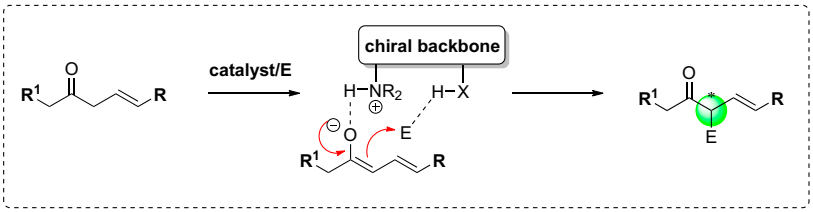

C

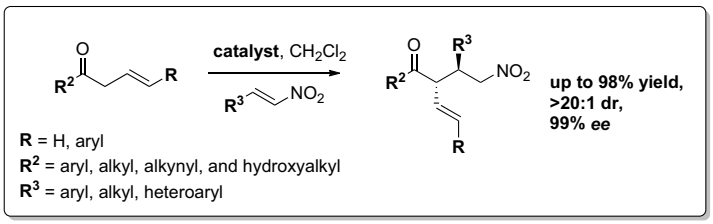

Scheme 5. Controlling the α/γ-Reactivity of Vinylogous Ketone Enolates in Squaramide-Catalyzed Michael Reactions to Nitroalkenes

(A) Chemical structures of squaramide-based catalysts **38** and **39**.

(B) Schematic representation of site selectivity in functionalization of vinylogous enolates.

(C) General reaction scheme for the Michael addition to nitroalkenes.

An intramolecular aza-Michael addition, also catalyzed by chiral cinchona-squaramide **38**, was developed by Ghorai and co-workers in 2018 and allowed the enantioselective synthesis of dihydroisoquinolines and tetrahydropyridines (Scheme 6).[50] A variety of Michael acceptors were employed, including α,β-unsaturated esters, thioesters, enones, and Weinreb amides, and showed generally good yields and high enantioselectivities (up to 90% yield and >99% ee). It is of note that in this work, Ghorai and co-workers were able to recover the catalyst almost quantitatively and that the ee value remained unchanged in additional reaction cycles. A possible mechanism and transition state were proposed (Scheme 6). Attempts to use ^{1}H NMR analysis to identify the imine or enamine intermediates was unsuccessful and may be due to a possible fast N cyclization step and consumption of the shorter-lived intermediates. The proposed transition state reflects the observed absolute stereochemical outcome of the reaction and is consistent with other reports suggesting electrophile activation by the squaramide catalyst. Subsequent reaction of the dihydroisoquinolines with meta-chloroperoxybenzoic acid allowed oxidation of both the keto and enamine functionalities. This led to the generation of an interesting tetracyclic core with fused tetrahydroisoquinoline, ketal, and amino-ketal moieties, as a single diastereomer and without loss of enantioselectivity.

Organocatalytic asymmetric Michael addition reactions (1,4-addition) are a powerful and atom-economic method for the formation of C–C and C–X bonds in a stereoselective manner. Recently, the related enantioselective 1,6-conjugate addition has gained

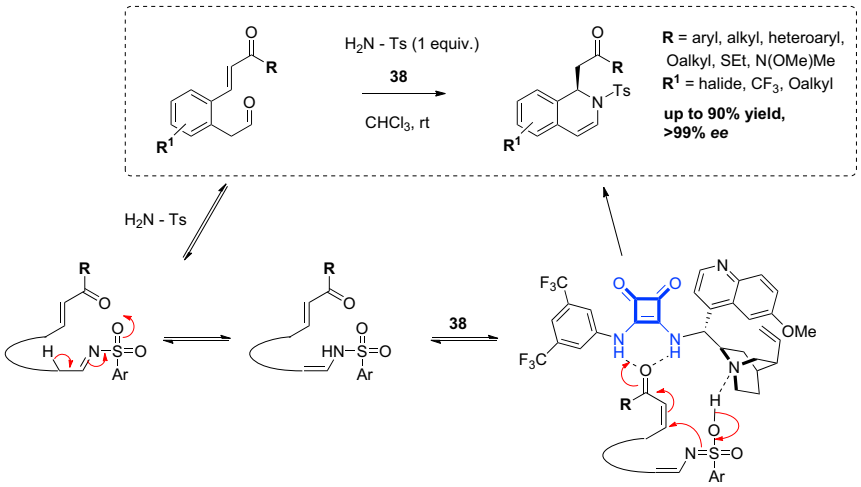

Scheme 6. General Reaction Scheme for the Intramolecular Aza-Michael Addition and the Proposed Mechanism and Transition States for the Transformation

significant attention in the organocatalysis field. Various catalytic systems have been explored; for example, Enders and co-workers reported the use of a chiral squaramide catalyst in 2016.[51] Here, a highly stereoselective organocatalytic 1,6-conjugate addition of 3-substituted oxindoles to *para*-quinone methides allowed the construction of all-carbon quaternary stereocenters (Scheme 7). A selection of cinchona, thiourea, and squaramide catalysts were employed in the catalyst screen, and squaramide catalyst **40** proved most effective. The scope of the *para*-quinone methide and the oxindole was investigated. A broad range of *p*-quinone methides could be used and furnished the

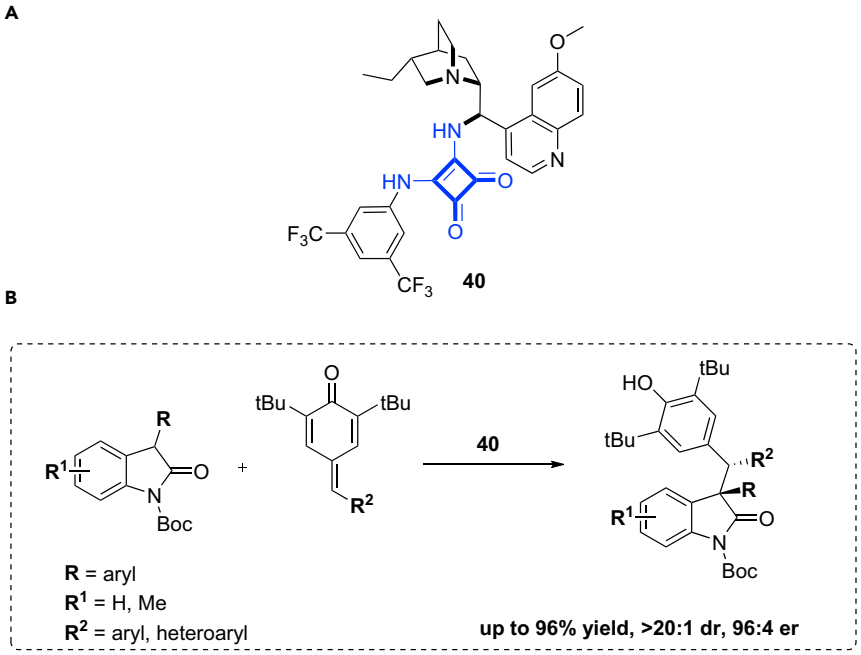

Scheme 7. 1,6-Conjugate Addition of 3-Substituted Oxindoles to *para*-Quinone Methides for the Construction of All-Carbon Quaternary Stereocenters

(A) Chemical structure of catalyst **40**.

(B) General reaction scheme for the asymmetric synthesis of 3-diarylmethine substituted oxindoles via 1,6-conjugate addition to *p*-quinone methides.

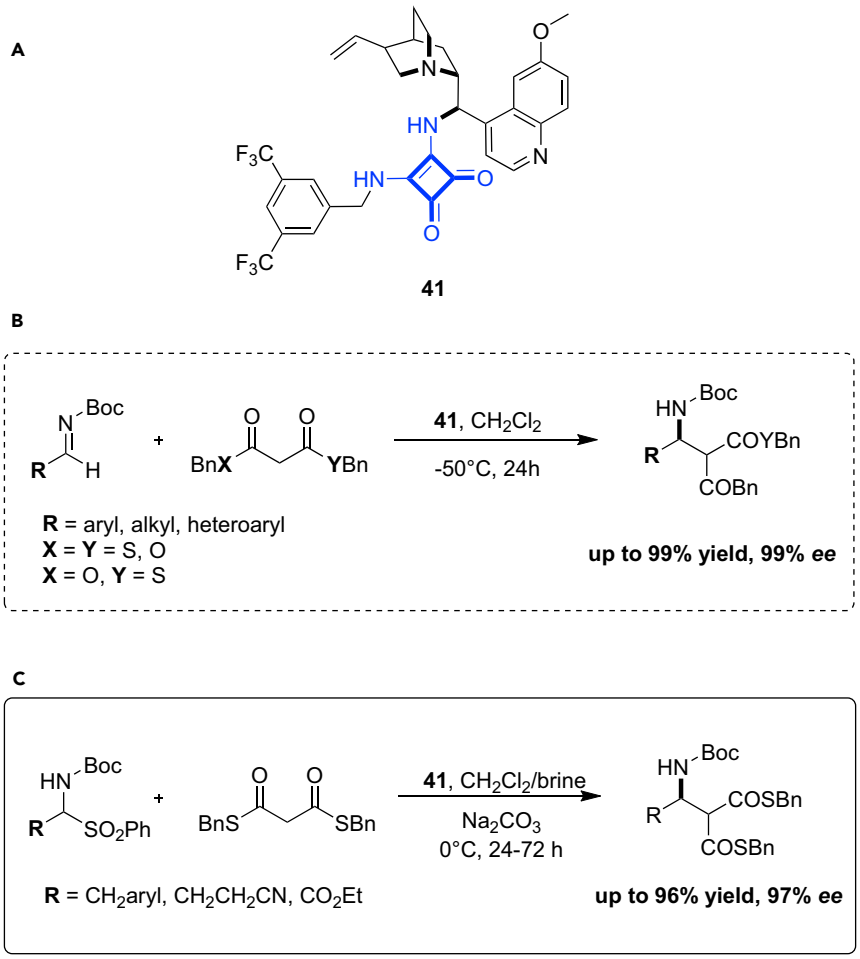

Scheme 8. Dithiomalonates as Efficient Mannich Donors in Squaramide-Catalyzed Enantioselective Mannich Reactions

(A) Chemical structure of catalyst **41**.

(B) General reaction scheme for the asymmetric Mannich reaction of malonates with N-Boc protected imines.

(C) General reaction scheme for the asymmetric reaction of dithiomalonates with α-amidosulfones.

expected products in 68%–96% yield with high diastereo- and enantioselectivities (up to >20:1 d.r. and 96:4 enantiomeric ratio [e.r.]). In addition, a number of 3-aryl oxindoles, bearing electron-withdrawing or electron-donating groups on the benzene ring or electron-donating groups on the aromatic ring of the oxindole moiety, could be converted into the desired products in 80%–89% yield with good to very good diastereo- and enantioselectivities (up to >20:1 d.r. and 97:3 e.r.).

Squaramide-catalyzed Mannich reactions have also been the subject of several research endeavors. In a 2016 study, Song and co-workers were able to show that DTMs are efficient Mannich donors, in terms of both reactivity and stereoselectivity, in cinchona-based-squaramide-catalyzed enantioselective Mannich reactions (Scheme 8).[52] Here, a diverse range of imines and α-amidosulfones acting as imine surrogates were employed. The DTMs displayed superior reactivity compared with that of conventional malonates, and this increased reactivity was attributed to the significantly higher acidity of its α-hydrogen atom than of monothiomalonate and malonate. Song and team utilized deuterium-exchange experiments with malonate derivatives to demonstrate this higher

A

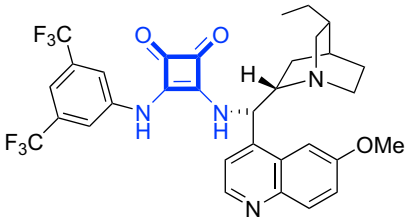

42

B

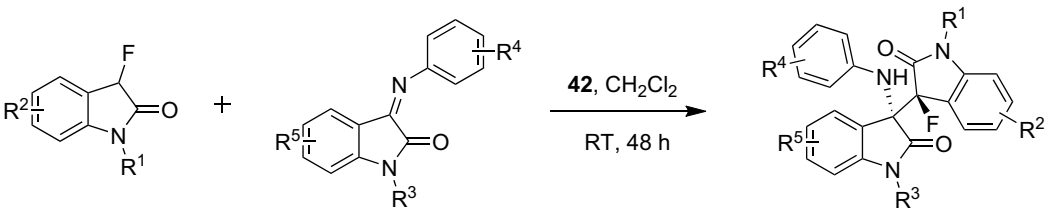

R^1 = H, Me, allyl
R^2 = H, Me, halogen
R^3 = alkyl, allyl, Bn
R^4 = H, Me, halogen, MeO, NO_2
R^5 = H, Me, halogen, MeO

up to 99% yield, >99:1 dr, 99% *ee*

C

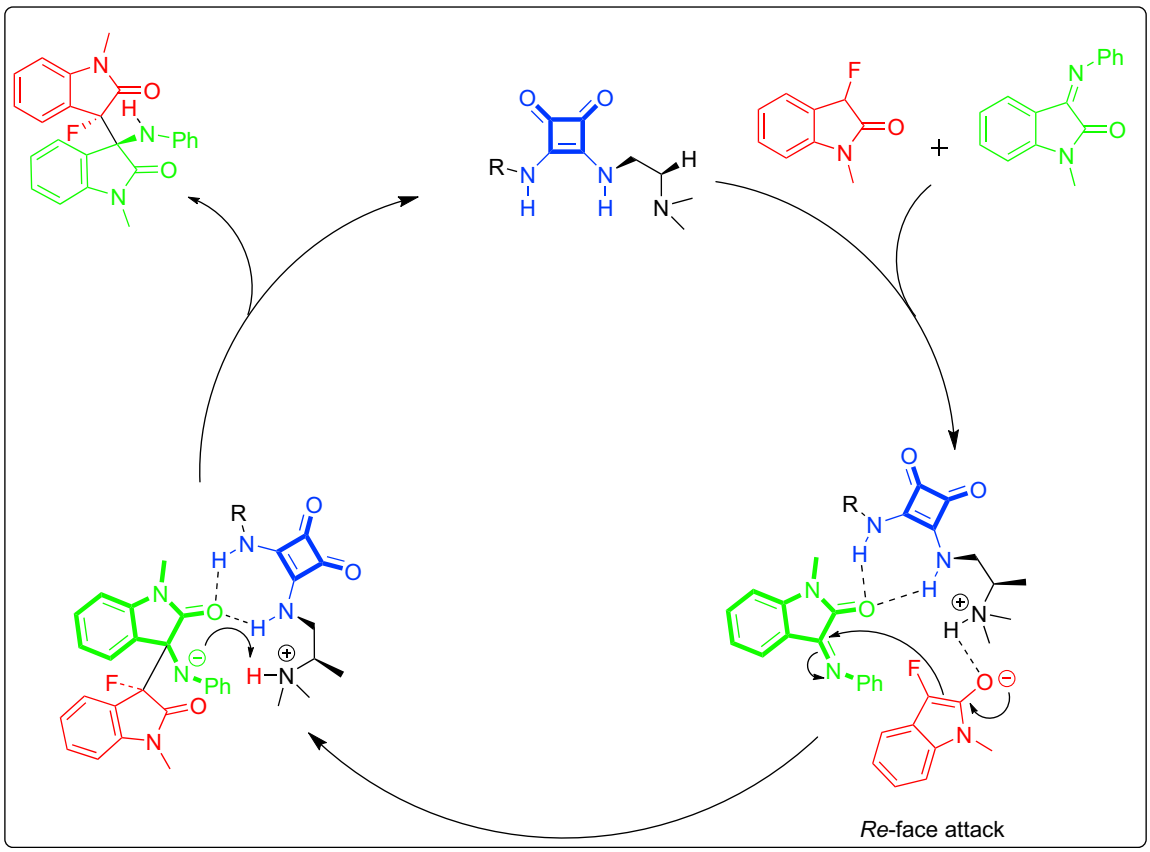

Scheme 9. Squaramide Catalyzed Asymmetric Mannich Reaction of 3-Fluorooxindoles to Isatin-Derived Imines
(A) Chemical structure of catalyst **42**.
(B) General reaction scheme for the asymmetric Mannich reaction of 3-fluorooxindoles to isatin-derived imines.
(C) Proposed mechanism and transition states for the transformation.

α-hydrogen acidity. The squaramide catalyst **41** was identified as the catalyst of choice and allowed the addition of DTMs to imines with Boc, Cbz, or CO_2Me protecting groups (97%–99% yield and 95%–99% ee). The benzyl-substituted DTM was the most suitable Mannich donor and was used in reaction with a variety of aromatic, heteroaryl, secondary alkyl, and primary alkyl aldimines. High yields and enantioselectivities were observed in all cases (85%–99% yield and 88%–99% ee). The reaction scope was expanded to include challenging primary alkyl substrates via a one-pot Mannich reaction of the alkyl-substituted α-amidosulfone imine surrogates. The same squaramide organocatalyst was employed, but this time under biphasic conditions, and showed high yields and enantioselectivities (up to 95% yield and 97% ee). Furthermore, the synthetic utility of the chiral Mannich adducts obtained from primary alkyl substrates was highlighted by the synthesis of the antidiabetic drug (−)-(*R*)-Sitagliptin.

More recently, in 2018, Du and co-workers reported the squaramide-catalyzed asymmetric Mannich reaction of 3-fluorooxindoles to isatin-derived imines (Scheme 9).[53] This methodology, using squaramide catalyst **42**, furnished fluorinated 3,3′-bisoxindoles with two contiguous stereocenters in high yields with high diastereo- and enantioselectivities (up to 99% yield, >99:1 d.r., and >99% ee). In order to account for the observed absolute configuration of the Mannich adduct (obtained via X-ray structure determination), possible transition states and a mechanistic path that included catalyst control of *Re*-face attack on the imine substrate were proposed. To demonstrate synthetic utility, the p-methoxy phenyl (PMP) group for one derivative was removed, using cerium ammonium nitrate, to generate the free amine product in 98% yield and without any loss of stereochemical purity. Furthermore, the scalability of this Mannich reaction was demonstrated, on a gram scale, where a bisoxindole was obtained in slightly lower yield (97%) but with the same excellent diastereoselectivity (>99:1 d.r.) and enantioselectivity (>99% ee).

Cycloaddition reactions are another class of synthetic transformations that have employed squaramide organocatalysis. Cycloaddition reactions involve the reaction of two π-systems, forming new ring structures, and are a versatile method for the stereoselective synthesis of a variety of cyclic compounds. Many cycloaddition reactions can be accelerated by Lewis acid catalysts, with chiral hydrogen bonding organocatalysts, such as squaramides, enjoying significant success. In 2014, Connon and Manoni employed a novel bifunctional tert-butyl-substituted squaramide-based catalyst **43** in a Tamura cycloaddition reaction of enolizable anhydrides with alkylidene oxindoles. The methodology furnished spirooxindole structures in excellent enantio- and diastereocontrol (Scheme 10).[54] Exploration of the substrate scope determined that a range of enolizable anhydrides could be utilized, and the expected products were generated in up to 98% yield and >99% ee. Employment of the less electrophilic benzylidene indole derivative, in reaction with a number of anhydrides, was also found to allow the formation of the corresponding spirooxindoles in good yields, albeit with marginally diminished enantioselectivities in some cases (65%–98% yield and 89%–>99% ee). An interesting observation was the unusual influence of temperature on diastereocontrol, where reactions performed at 30°C and −30°C delivered products epimeric at one stereocenter only.

In 2015, Vicario, Reyes and co-workers utilized *in-situ*-generated benzopyrylium ylides, in reaction with α,β-unsaturated aldehydes, to furnish 8-oxabicyclo[3.2.1]octane

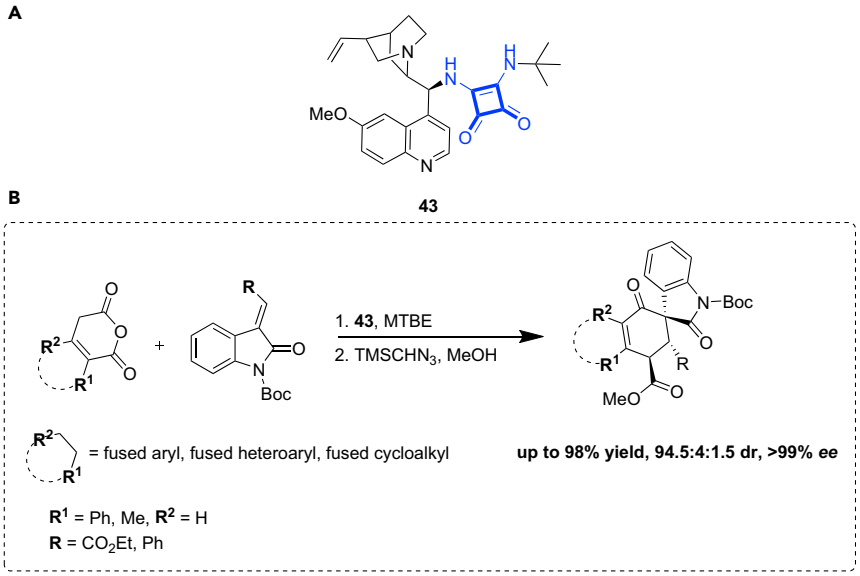

Scheme 10. Enantioselective Tamura Cycloaddition Reaction of Enolizable Anhydrides with Alkylidene Oxindoles

(A) Chemical structure of catalyst **43**.

(B) General reaction scheme for the asymmetric Tamura cycloaddition.

cycloadducts (Scheme 11).[55] The benzopyrylium ylides were generated *in situ* from 1-acetoxyisochroman-4-ones, and the use of a bifunctional secondary-amine-squaramide catalyst **44** allowed their smooth conversion to [5 + 2] cycloaddition products in good yield with high diastereo- and enantioselectivity (up to 92% yield, d.r. > 20:1, and 99% ee). Here, they suggested that the reaction exploited a HOMO-raising effect associated with dienamine activation and involved β,γ-functionalization of the enal. It was suggested that the ability of the bifunctional secondary-amine/squaramide catalyst to engage in hydrogen-bonding interactions with the yield made the methodology particularly effective in terms of yield and stereoselectivity.

Zhao and co-workers successfully applied a Cinchona alkaloid based squaramide organocatalyst in the [3 + 2] cycloaddition of isatin-derived azomethine ylides with maleimides (Scheme 12).[56] A number of Cinchona and hydrogen-bonding organocatalysts were screened, and the bifunctional squaramide catalyst **38** proved most effective. A screen of acid additives was also performed, and stearic acid in combination with molecular sieves gave the best results (81% yield, >20:1 d.r., and 90% ee). The scope of the methodology was explored with structural variation of all three starting materials. Here, the 1,3-dipolar cycloaddition proceeded smoothly in almost all cases, generating the desired pyrrolidine-fused spirooxindoles in 61%–89% yields with >20:1 d.r. and up to >99% ee. The absolute configuration of one of the products spirooxindoles was unambiguously determined by means of X-ray single crystal structure analysis and used to support a possible reaction mechanism that accounted for its enantioselective formation. A transition state TS1 was proposed, where the *Si* face of the 1,3-dipole attacked the 3*Si*-4*Re* face of the maleimide and delivered the final product in a stereocontrolled fashion.

A recent example of a squaramide catalyzed [3 + 2] cycloaddition can be found in the work reported by Weng, Lu, and co-workers.[57] Here, an asymmetric exo-selective [3 + 2] cycloaddition reaction of CF_3-containing isatin-derived azomethine ylides with methyleneindolinones is described (Scheme 13). The reaction leads to the formation

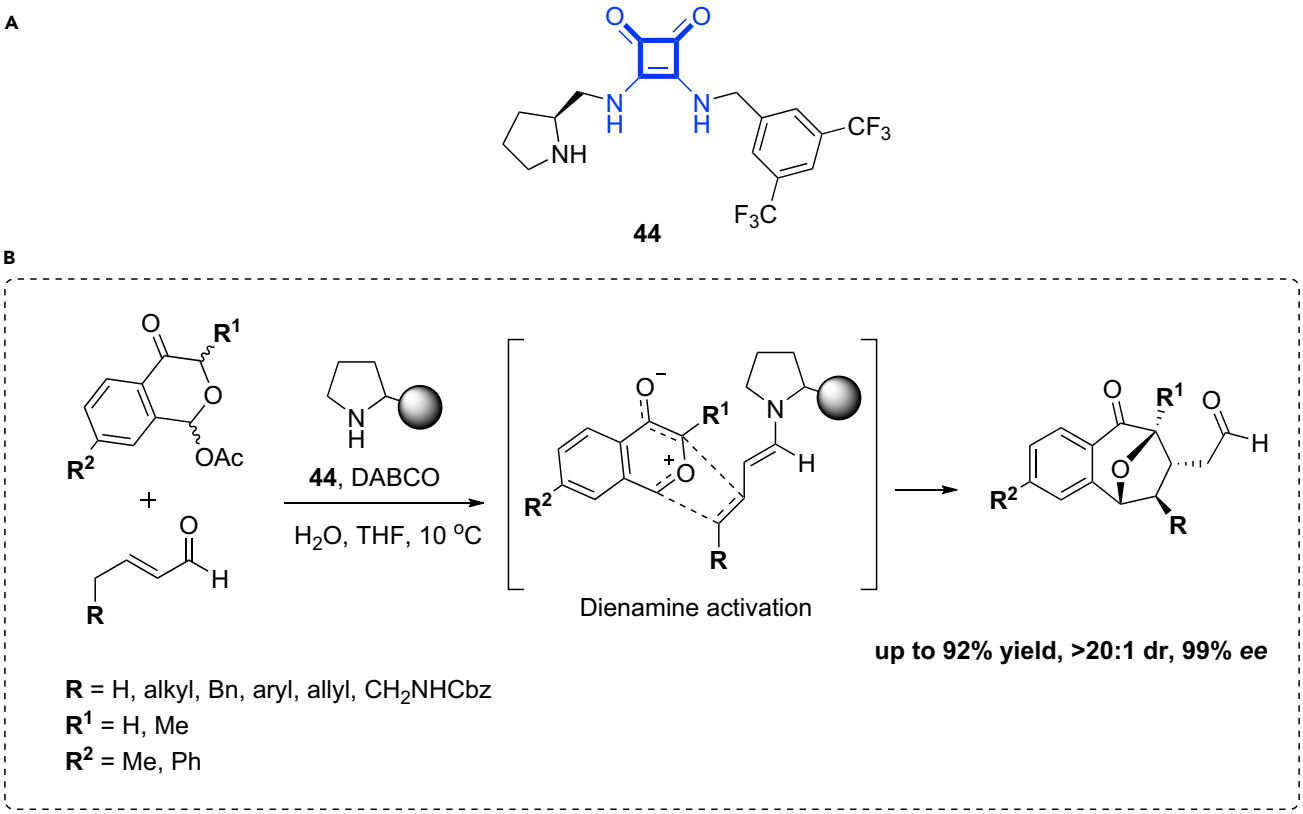

Scheme 11. Enantioselective Formation of 8-Oxabicyclo[3.2.1]octane Cycloadducts via *In-Situ*-Generated Benzopyrylium Ylides in Reaction with α,β-Unsaturated Aldehydes

(A) Chemical structure of catalyst **44**.

(B) General reaction scheme for the asymmetric cycloaddition.

of dispiro products bearing four contiguous chiral centers, including the two adjacent spiro quaternary stereocenters. Under bifunctional organocatalysis, by the cinchona-derived squaramide catalyst **45**, a series of interesting trifluoromethylated 3,3′-pyrrolidinyl-dispirooxindoles were generated with high stereoselectivity (84%–99% yields, up to >20:1 d.r., and >99% ee). A variety of ketimine and methyleneindolinone starting materials were tolerated, and the absolute configuration of one of the products was obtained by X-ray crystallographic analysis. The stereochemical outcome of this study revealed that the cyclization occurred in an exo-selective manner and not by the perhaps expected endo-selective reaction. This suggested that that the reaction was not a concerted 1,3-dipolar cycloaddition, and Weng, Lu, and team proposed a stepwise anti-selective Michael-Mannich mechanism. A possible transition state was suggested where the squaramide catalyst simultaneously activated both the azomethine ylide and the methyleneindolinone. It was postulated that this transition state could have induced the *Re* face anti-Michael addition and subsequent intramolecular *Re*-face Mannich reaction to furnish the 3,3′-pyrrolidinyl-dispirooxindole product in a stereoselective manner. The equilibration between the stereoisomers obtained in the cycloaddition was explored by treating the (*R*) isomer of one of the products (>20:1 d.r.) with a strong base. This resulted in a decrease in the ratio of (*R*)/(*S*), and equal amounts of the *R* and *S* isomers were generated after a prolonged reaction time (24 h). This epimerization took place at the quaternary C-2′ atom, which suggested that the proposed Mannich reaction was reversible, returning to the preceding intermediate, and then the intramolecular Mannich reaction of the intermediate afforded the (*R*) and (*S*) products via *Re*-face and

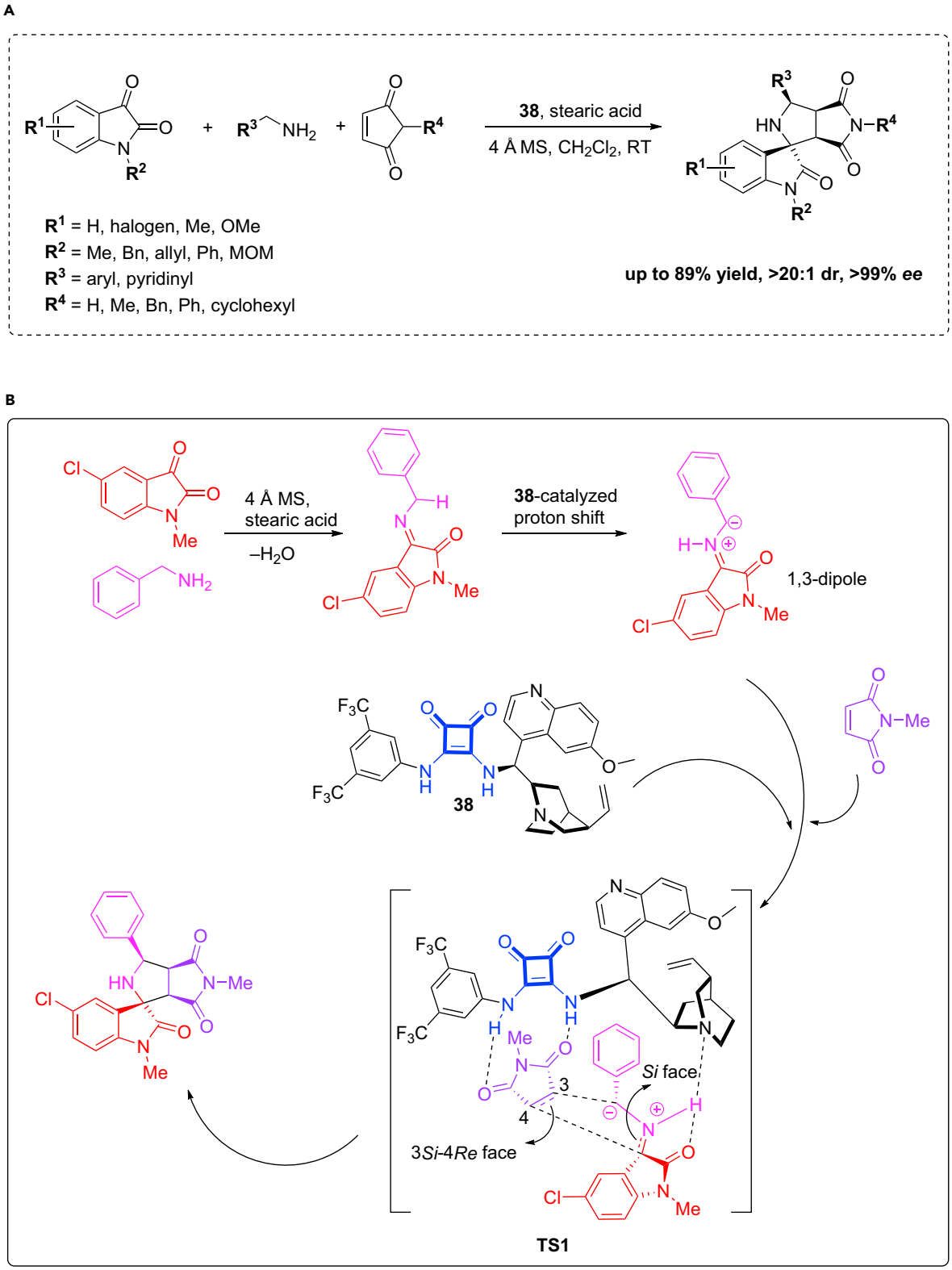

Scheme 12. Squaramide-Catalyzed [3 + 2] Cycloaddition of Isatin-Derived Azomethine Ylides with Maleimides

(A) General reaction scheme for the asymmetric 1,3-dipolar cycloaddition.

(B) Proposed mechanism and transition states for the transformation.

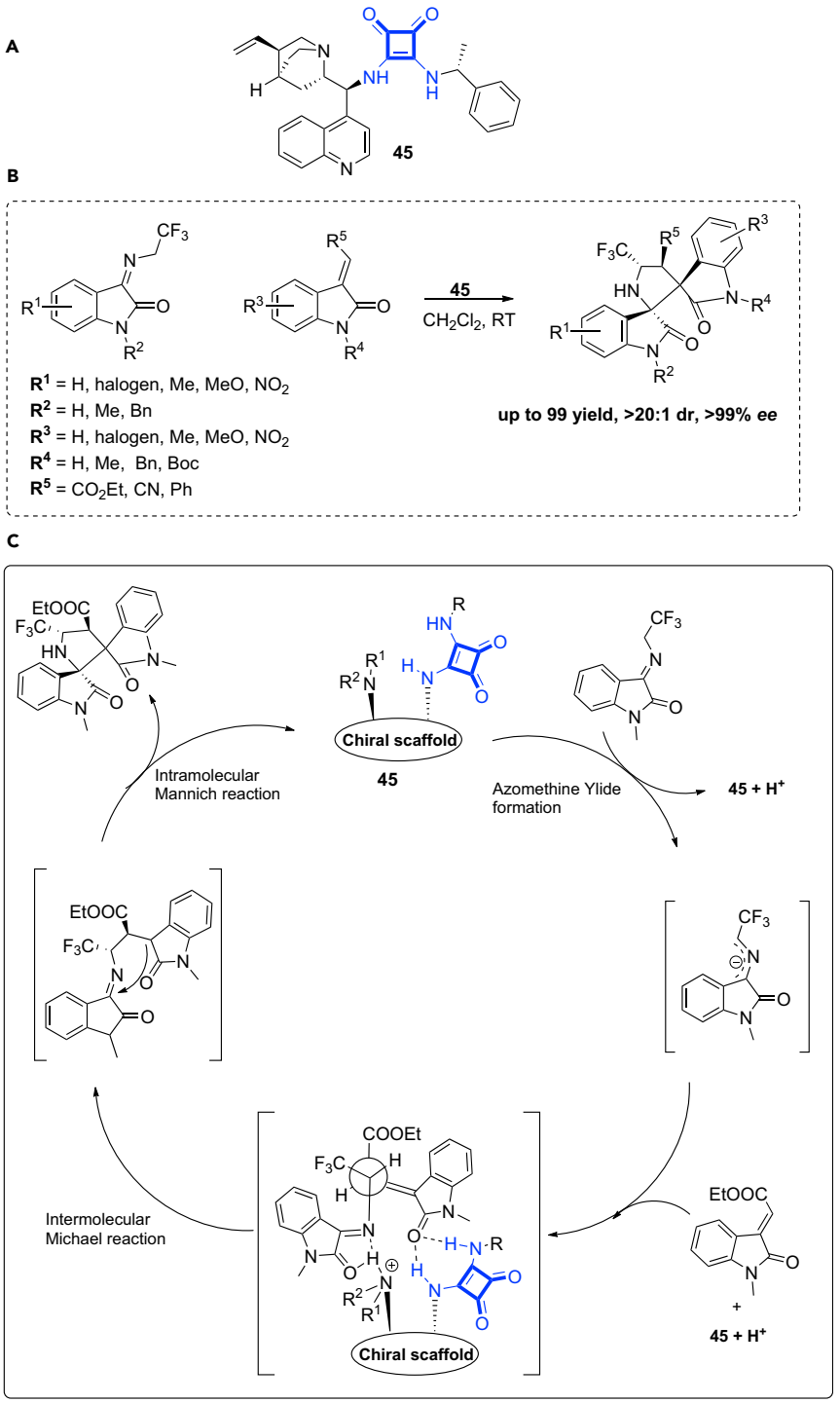

Scheme 13. Asymmetric Exo-selective [3 + 2] Cycloaddition Reaction of CF_3-Containing Isatin-Derived Azomethine Ylides with Methyleneindolinones

(A) Chemical structure of catalyst **45**.

(B) General reaction scheme for the asymmetric cycloaddition.

(C) Proposed mechanism and transition states for the transformation.

A

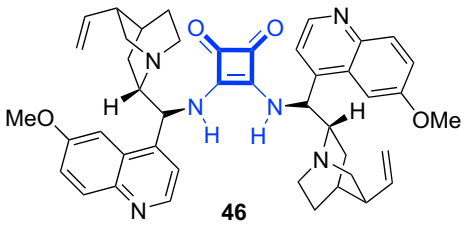
MeO
OMe
46

B

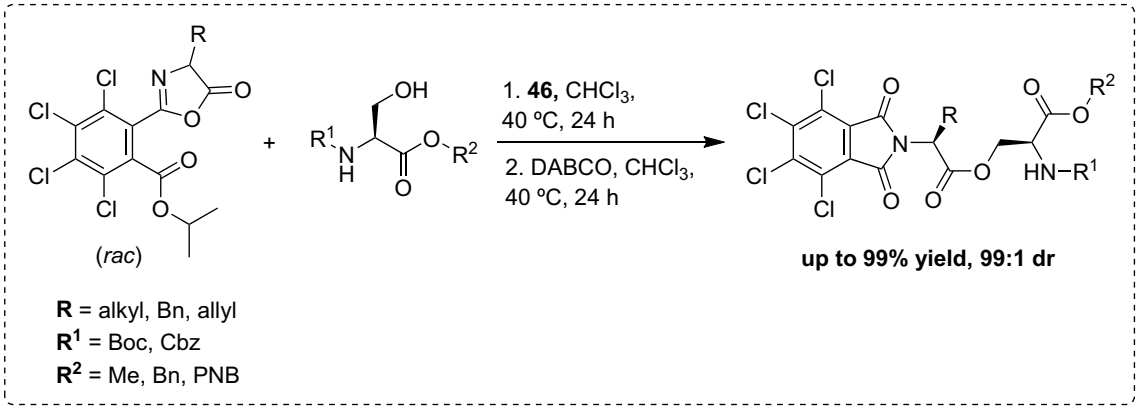
(rac)
1. 46, CHCl3, 40 °C, 24 h
2. DABCO, CHCl3, 40 °C, 24 h
up to 99% yield, 99:1 dr
R = alkyl, Bn, allyl
R1 = Boc, Cbz
R2 = Me, Bn, PNB

C

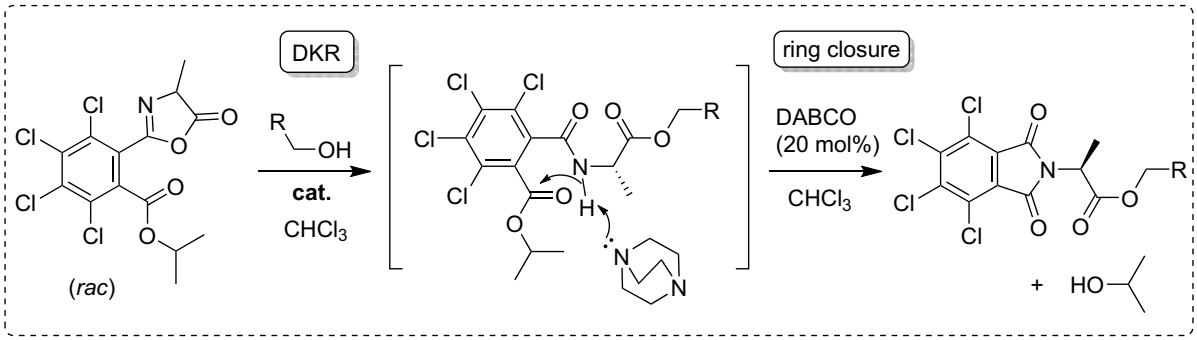
DKR
cat.
CHCl3
ring closure
DABCO
(20 mol%)
CHCl3
(rac)

D

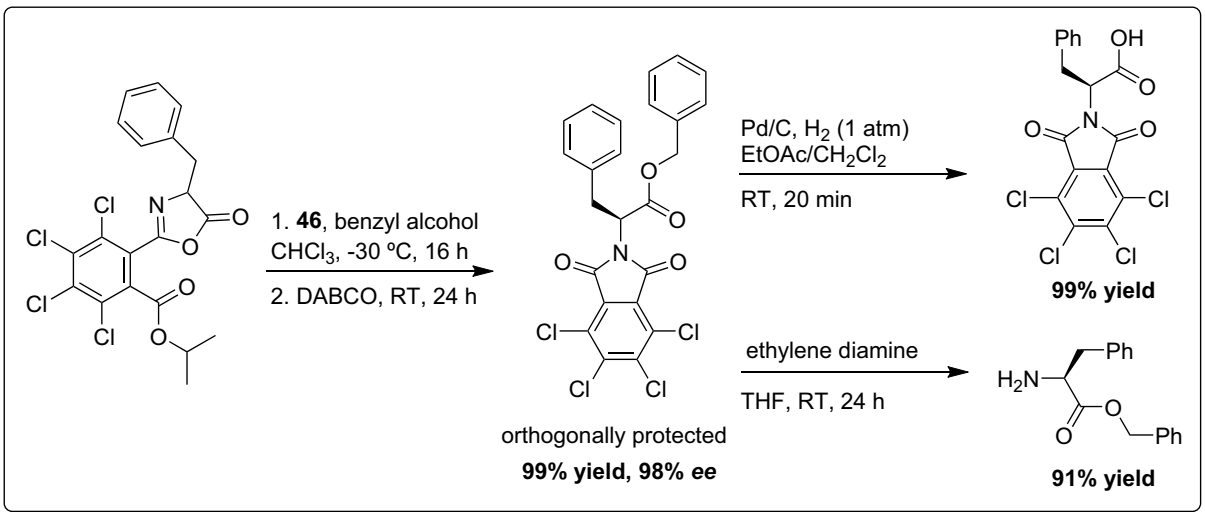
1. 46, benzyl alcohol
CHCl3, -30 °C, 16 h
2. DABCO, RT, 24 h
orthogonally protected
99% yield, 98% ee
Pd/C, H2 (1 atm)
EtOAc/CH2Cl2
RT, 20 min
99% yield
ethylene diamine
THF, RT, 24 h
91% yield

Scheme 14. Enantioselective Azlactone Dynamic Kinetic Resolution for the Generation of Orthogonally Protected Amino Acids
(A) Chemical structure of catalyst **46**.
(B) General reaction scheme for the dynamic kinetic resolution.
(C) Proposed mechanism and transition states for the resolution.
(D) Demonstration of the orthogonally masked amino acids.

Si-face attack, respectively. This result provided additional support for the proposed stepwise Michael-Mannich cyclization mechanism. A gram-scale experiment was performed and demonstrated that the reaction could be performed on a larger scale without obvious loss of diastereo- or enantioselectivity.

Squaramide organocatalysts have found use in the dynamic kinetic resolution (DKR) of a variety of substrates and have employed a number of catalytic methods, including bifunctional, Brønsted basic or nucleophilic, and Brønsted acidic systems. In 2014, Connon and co-workers described an enantioselective azlactone DKR that generated orthogonally protected amino acids.[58] A key finding was the successful reaction of the tetrachloroisopropoxycarbonyl (TCIC)-substituted alanine-derived azlactone (*rac*) with a range of C- and N-protected serines (Scheme 14). This generated the corresponding *N*-phthalimido amino acid esters in good to excellent yields and high diastereocontrol (up to 99% yield and 99:1 d.r.). The addition of catalytic DABCO, after DKR had taken place, allowed the efficient one-pot formation of the phthalimides. A mechanism was proposed, where the catalytic addition of the alcohol to (*rac*) azlactone resulted in the ring-opened adduct intermediate, which was identified by ^{1}H NMR spectroscopic analysis. The hindered isopropyl ester moiety of the starting azlactone is a structural requirement, as employing analogs of the starting azlactone that incorporated simpler methyl or ethyl esters in place of the isopropyl ester was unsuccessful. In these cases, the methanol or ethanol liberated during phthalimide formation competed effectively as nucleophiles with the protected serine starting material for the starting azlactone. This led to the formation of some undesired phthalimide methyl or ethyl ester products. The scope of the methodology was also explored with a range of amino-acid-derived TCIC-substituted azlactones. This sequence of reactions allowed the synthesis of the phenylalanine- and valine derived O-acyl serines in good yields and diastereocontrol (up to 99% yield and 99:1 d.r.). Finally, benzyl alcohol was reacted with the TCIC-substituted azlactones to generate the phthalimide products, which can act as masked amino acids. The phthalimides were orthogonally N and C protected and could be selectively deprotected through the use of ethylene diamine or hydrogenolysis. It was also demonstrated that the process could be utilized to bring about a highly stereoselective ligation-type coupling of protected serines with racemic TCIC-substituted azlactones.

In 2017, Berkessel and co-workers employed kinetic resolution and squaramide organocatalysts in the generation of N-protected β^2-amino acid esters from racemic 5-substituted oxazinones (Scheme 15).[59] A number of bifunctional chiral base-squaramide organocatalysts, **47–51**, were utilized and allowed the alcoholytic ring opening of the oxazinones to occur with selectivity factors up to 43. Oxazinones with *i*-Bu, *c*-hexyl, and aryl substituents at the 5 position were used, and squaramide **47** generated the best ee for the *i*-Bu- and *c*-hexyl-substituted N-protected β^2-amino acid esters (82% and 90%, respectively). Squaramide **49** proved the most selective for the aryl-substituted oxazinones, whereby an ee of 74% was obtained for the phenyl-substituted N-protected β^2-amino acid ester.

Organocatalytic cascade, tandem, and domino reactions provide a convenient method for the stereoselective construction of complex molecular structures with one or more stereocenters.[60] Such transformations can be considered to resemble natural

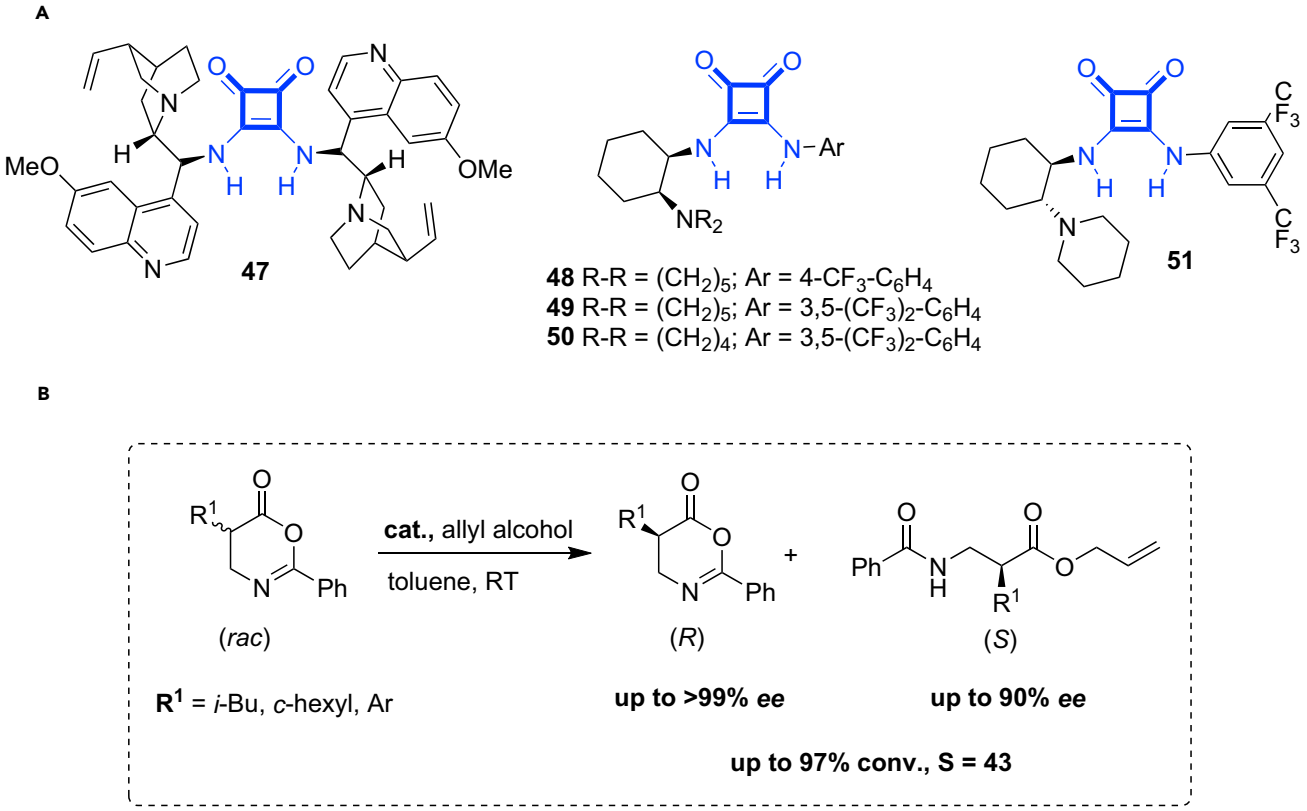

Scheme 15. Generation of N-Protected B^2-Amino Acid Esters from Racemic 5-Substituted Oxazinones Using a Squaramide Catalyzed Kinetic Resolution

(A) Chemical structure of catalysts **47**–**51**.

(B) General reaction scheme for the kinetic resolution.

biosynthetic processes, where an enzymatic active site can contain a set of different functionalities that can act either alternatively or contemporaneously in multiple catalytic cycles.[61] Many organocatalysts have been successfully applied in asymmetric organocascade sequences, and bifunctional squaramides have emerged as powerful hydrogen-bonding catalysts for the promotion of a wide variety of organocatalyzed cascades.[60,61]

In 2014, Du and co-workers reported an effective asymmetric sulfa-Michael-aldol cascade reaction between benzylidenechroman-4-ones and 1,4-dithiane-2,5-diol by using a bifunctional squaramide organocatalyst (Scheme 16).[62] They conducted a catalyst, solvent, temperature, and additive screen in order to identify the preferred reaction conditions. The resulting methodology, employing squaramide **52** in toluene at 55°C, allowed the stereoselective construction of chiral spirocyclic tetrahydrothiophene chromanone derivatives with three contiguous stereocenters in a single operation. The reaction proceeds in high isolated yield and with good diastereoselectivity and enantiocontrol (up to 99% yield, 92: 8 d.r., and 92% ee). A wide variety of substrates were utilized, giving access to a diverse range of spirocyclic tetrahydrothiophene chromanone derivatives. However, the desired products could not be obtained when (*E*)-3-alkylidenechroman-4-ones (R = alkyl) served as substrates. Additionally, an interesting temperature effect on reaction efficiency was observed, where either increasing or decreasing temperature led to a decrease in stereoselectivity. A gram-scale synthesis was also performed and found to proceed smoothly with the same efficiency as the smaller-scale reactions.

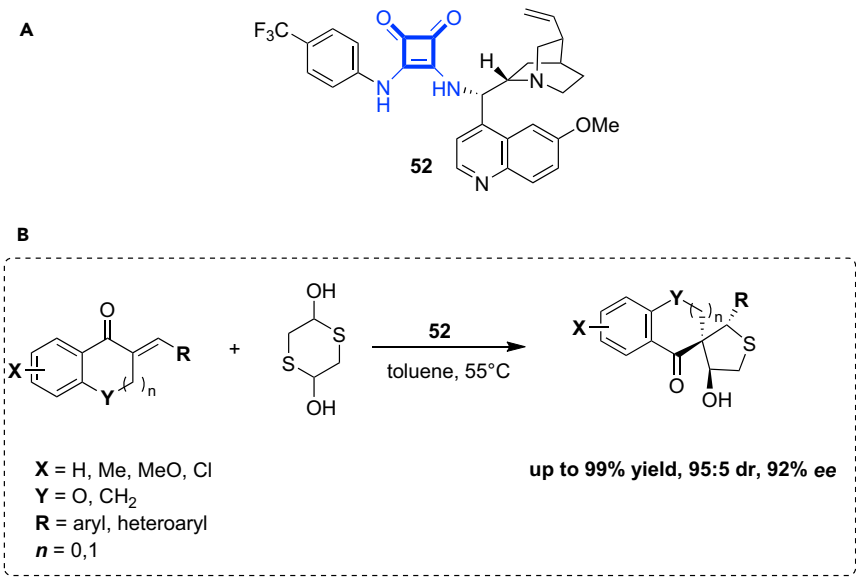

Scheme 16. Asymmetric Sulfa-Michael-Aldol Cascade Reaction between Benzylidenechroman-4-ones and 1,4-Dithiane-2,5-diol

(A) Chemical structure of catalyst **52**.

(B) General reaction scheme for the Michael-initiated cascade.

A method, exploiting a Michael-Mannich cascade reaction, for the construction of five-membered spirocyclic oxindoles was developed by Sun and co-workers in 2015.[63] Here, Sun and team generated a ketimine intermediate, which subsequently underwent reaction with a methyleneindolinone via a Michael-Mannich sequence. All steps were catalyzed by a single bifunctional quinine-derived squaramide **53** (Scheme 17). The substrate scope was explored with a variety of ketimine intermediates, generated from β-dicarbonyl compounds with different carbon chains and additional *p*-MeO and *p*-Br nitrosobenzenes, as well as a selection of methyleneindolinones. The desired products were obtained in excellent yields (up to 94%) and stereoselectivities (up to >20:1 d.r. and >99% ee). A mechanism was proposed, where enolization of acetylacetone, promoted by the amino group of the bifunctional catalyst, is followed by *N*-selective addition to nitrosobenzene. The resulting ketimine, an interesting multi-active synthon with two different electrophilic sites and nucleophilic carbons, is transformed into the corresponding enoate. The methyleneindolinone is activated by the same squaramide catalyst and subsequent intermolecular Michael addition with the ketimine enoate, followed by the final irreversible cyclization, furnished the enantioenriched product. The one-pot reaction was scaled up and performed in the presence of only 2 mol % of a bifunctional quinine-derived squaramide catalyst.

A method for the rapid generation of a series of spiro-pyrrolidine-pyrazolones via an aza-Michael-Michael-addition cascade was developed by Du and co-workers in 2016.[64] Here, Du targeted bifunctional hydrogen-bonding organocatalysis to promote the reaction of tosylaminomethyl enones or enoates with unsaturated pyrazolones (Scheme 18). A catalyst screen identified squaramide **54** as the preferred organocatalyst and, along with a solvent and temperature study, allowed the final reaction conditions to be established (5 mol % catalyst [cat.], $CHCl_3$, RT). A range of substrates were utilized, and variations in both the tosylaminomethyl enones and enoates and the pyrazolones were tolerated. The tandem reaction sequence proceeded well and afforded the desired products in high yields (up to 98%) with

A

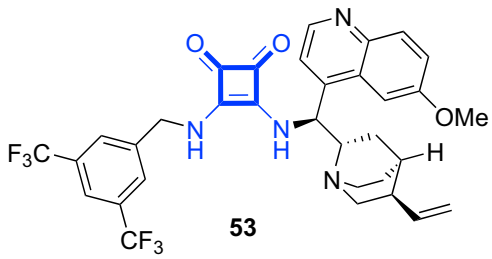

B

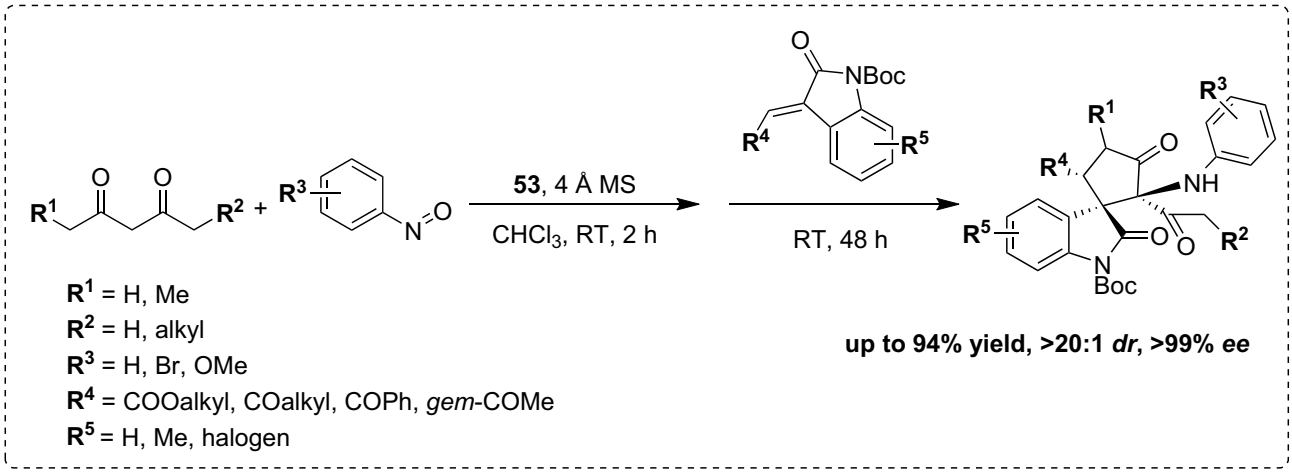

C

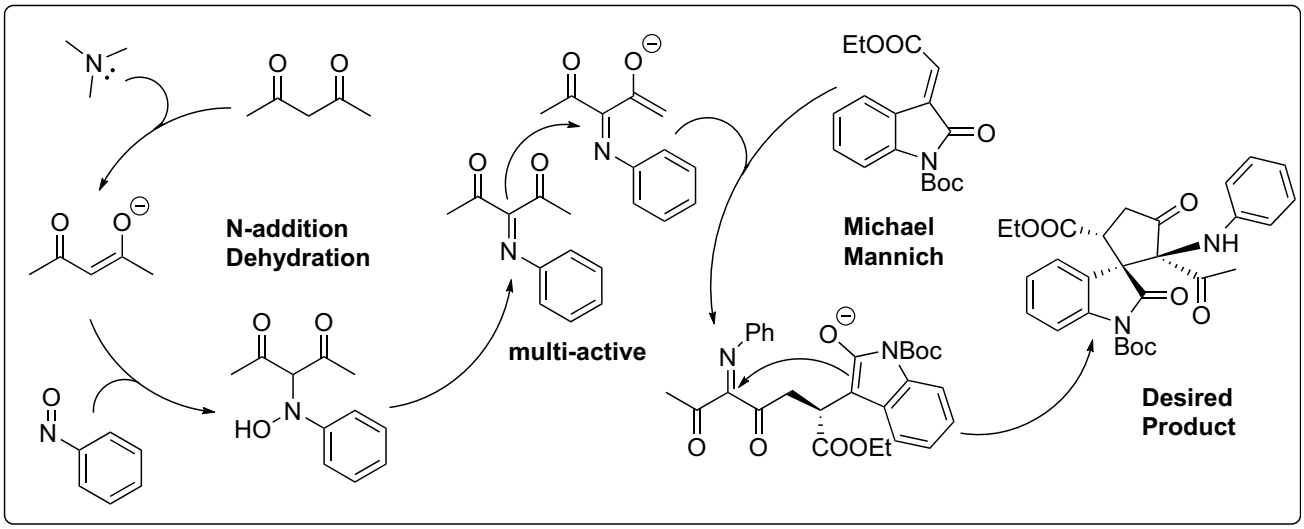

Scheme 17. Squaramide Michael-Mannich Cascade Reaction for the Construction of Five-Membered Spirocyclic Oxindoles

(A) Chemical structure of catalyst **53**.

(B) General reaction scheme for the Michael-Mannich cascade reaction.

(C) Proposed mechanism for the transformation.

A

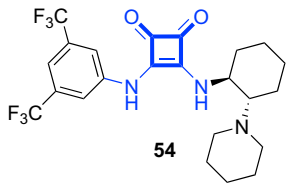
F3C
F3C
O
O
N
H
N
H
N
54

B

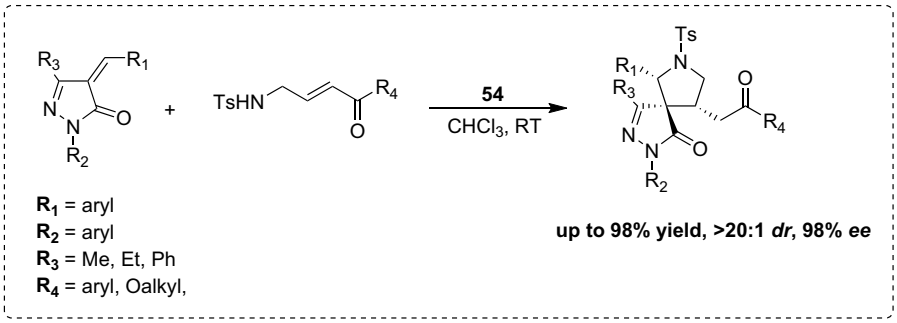
R3
R1
N
N
O
R2
+
TsHN
R4
O
54
CHCl3, RT
Ts
N
R1
R3
O
R4
N
N
O
R2
R1 = aryl
R2 = aryl
R3 = Me, Et, Ph
R4 = aryl, Oalkyl,
up to 98% yield, >20:1 dr, 98% ee

C

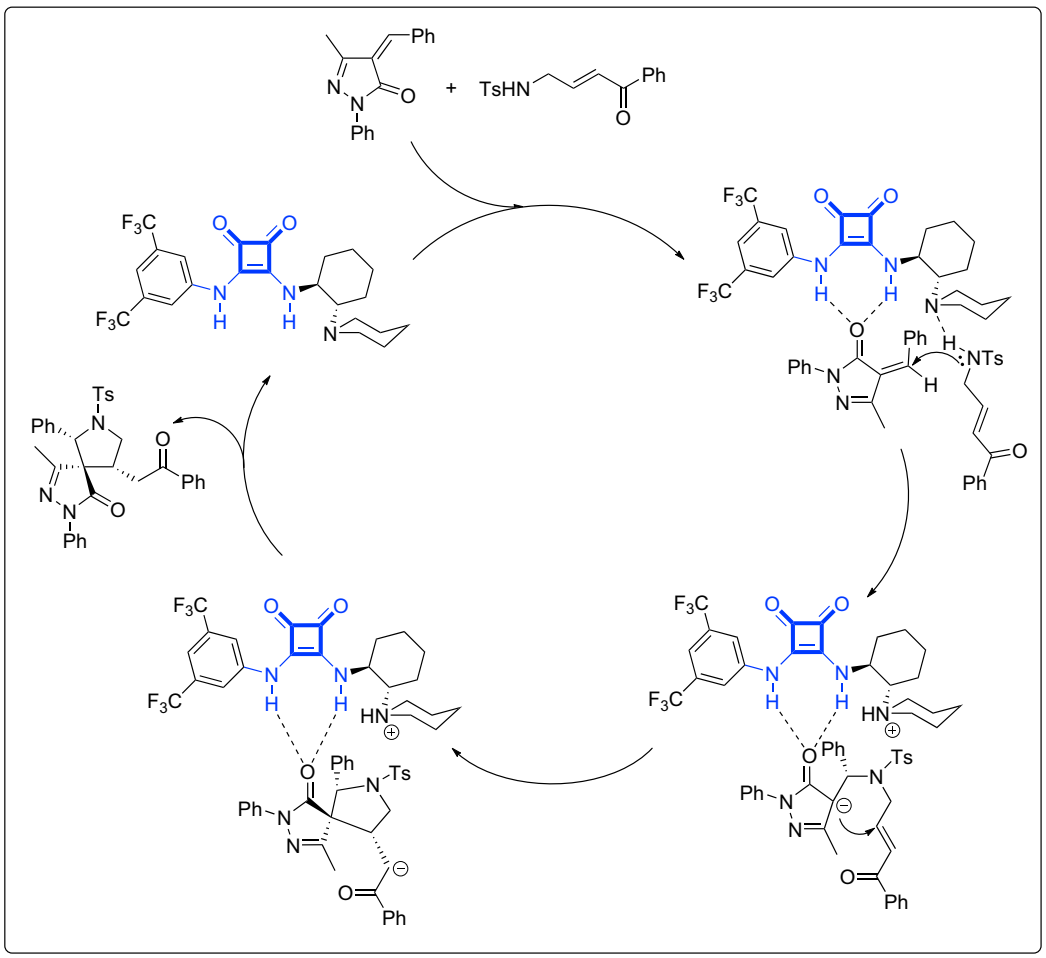
Ph
N
N
O
Ph
+
TsHN
Ph
O
F3C
F3C
O
O
N
H
N
H
N
Ts
Ph
N
O
N
N
O
Ph
Ph
F3C
F3C
O
O
N
H
N
H
N
O
Ph
Ph
N
H
NTs
H
Ph
O
F3C
F3C
O
O
N
H
N
H
HN
O
Ph
Ts
Ph
N
N
O
Ph
F3C
F3C
O
O
N
H
N
H
HN
O
Ph
Ts
Ph
N
N
O
Ph

Scheme 18. Generation of Spiro-Pyrrolidine-Pyrazolones via an Aza-Michael-Michael-Addition Cascade
(A) Chemical structure of catalyst **54**.
(B) General reaction scheme for the Michael-initiated cascade.
(C) Proposed mechanism for the transformation.

high diastereoselectivities (up to >20:1 d.r.) and high enantioselectivities (up to 98% ee). The absolute configuration of one of the spiro-pyrrolidine-pyrazolones was unambiguously established by single-crystal XRD analysis and formed the basis for a proposed mechanism. Here, Du and team suggested that chiral squaramide **54** acts as a bifunctional catalyst to deprotonate the tosylaminomethyl enone and activate the unsaturated pyrazolone by forming two hydrogen bonds. The deprotonated tosylaminomethyl enone then attacks the pyrazolone, and a subsequent intramolecular Michael addition by a *Si* face attack forms the (2′*S*,3′*R*,4′*R*)-configured product. To highlight the synthetic value of this method, a gram-scale preparation where the high yield was maintained without loss of enantioselectivity was performed.

Subsequently, in 2018, Du and co-workers reported another Michael-reaction-initiated organocatalyzed cascade.[65] In this report, a highly efficient method for the construction of oxindolepyrrolidone-thiazolidinone bispirocyclic heterocycles bearing three contiguous chiral centers was disclosed (Scheme 19). Here, a bifunctional cinchona-derived squaramide catalyst allowed the selective generation of the three stereocenters, including two quaternary centers via a Michael-cyclization cascade reaction between 3-isothiocyanato oxindoles and unsaturated thiazolidinones. The squaramide catalyst **42** was identified by a catalyst screen, and once more, a solvent and temperature study allowed the preferred reaction conditions to be determined (5 mol % cat., CH_2Cl_2, RT). Exploration of the substrate scope showed that a variety of isothiocyanato oxindoles and thiazolidinones could be employed with high yields (up to 99%) and high diastereo- and enantioselectivities (up to >99:1 d.r. and >99% ee). A single crystal of one of the products was obtained, which enabled its absolute configuration to be established. A plausible mechanism for this Michael/cyclization cascade reaction was proposed by Du and team on the basis of a dual activation model. In the first Michael addition step, the amine unit of the quinine deprotonates the 3-isothiocyanato oxindole, and it is stabilized by forming two hydrogen bonds with the catalyst. The thiazolidinone is simultaneously activated by hydrogen bonding with the protonated amine. The thiazolidinone is then attacked by the deprotonated 3-isothiocyanato oxindole from the *Re*-face, which then completes the Michael addition-cyclization sequence to furnish the final product.

Squaramides have also been exploited in the development of catalytic systems capable of stimulating Friedel-Crafts initiated cascade reactions. In 2017, Zhao, Hu, and co-workers investigated organocatalyzed cascade reactions, and in this case, they employed an asymmetric Friedel-Crafts alkylation-lactonization sequence to afford α-aryl-β-trifluoromethyl dihydrocoumarin derivatives.[66] Naphthols and 3-trifluoroethylidene oxindoles were reported to undergo the squaramide catalyzed Friedel-Crafts initiated reaction, which represented a novel [3 + 3] strategy for the enantioselective synthesis of dihydrocoumarins bearing a CF_3 moiety at the β position (Scheme 20). A catalyst screen identified squaramide **55** as the catalyst of choice, and enantioselectivity improved slightly upon addition of 4 Å molecular sieves. An exploration of the substrate scope of the methodology determined that a variety of 3-trifluoroethylidene oxindoles and naphthols, including both 1- and 2-naphthols (at 0°C and −30°C, respectively), could be tolerated with high yields

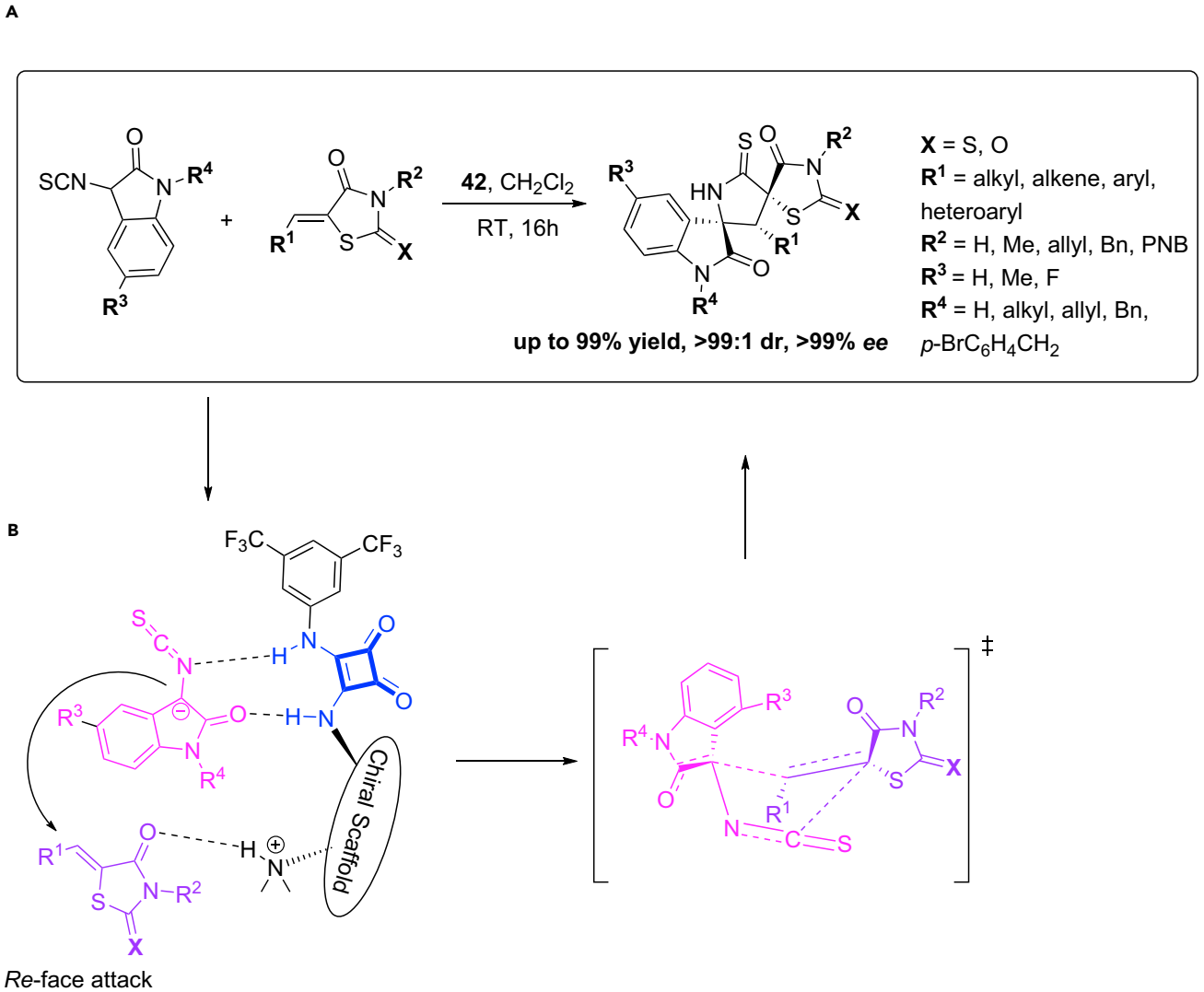

Scheme 19. Michael-Reaction-Initiated Squaramide Catalyzed Cascade for the Construction of Oxindolepyrrolidone-Thiazolidinone Bispirocyclic Heterocycles

(A) General reaction scheme for the Michael-initiated cascade.

(B) Proposed mechanism and transition states for the transformation.

(up to 99%) and high enantio- and diastereoselectivities (up to 98% ee and >20:1 d.r.). The lactonization step was suggested to proceed by nucleophilic attack of the naphthol hydroxyl group at the amide motif of the oxindoles, and this protocol represents a new strategy for the formation of dihydrocoumarins by intramolecular amide C–N bond cleavage and a concurrent esterification process. The absolute configurations of the newly formed chiral centers for one of the products were assigned as αR and βS according to the X-ray crystallographic analysis. Finally, to demonstrate the utility of this asymmetric Friedel-Crafts alkylation-lactonization protocol, the reaction was scaled up to 3 mmol, and the product was obtained with a comparably high yield and stereoselectivity. The products were also shown to be versatile intermediates that could be readily converted into indole derivatives.

Later in 2017, Enders and co-workers reported another Friedel-Crafts initiated cascade, this time an unprecedented domino aza-Friedel-Crafts N,O-acetalization

A

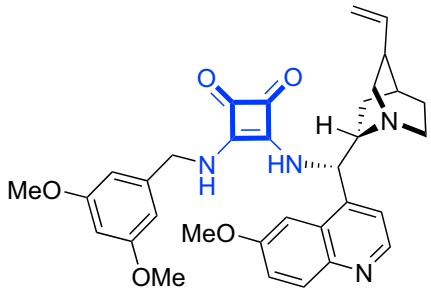

55

B

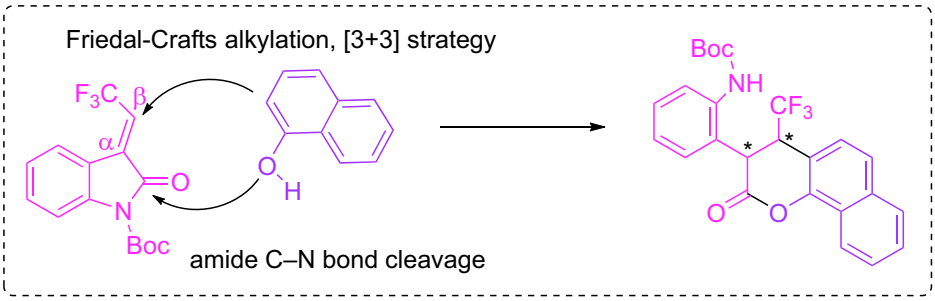

C

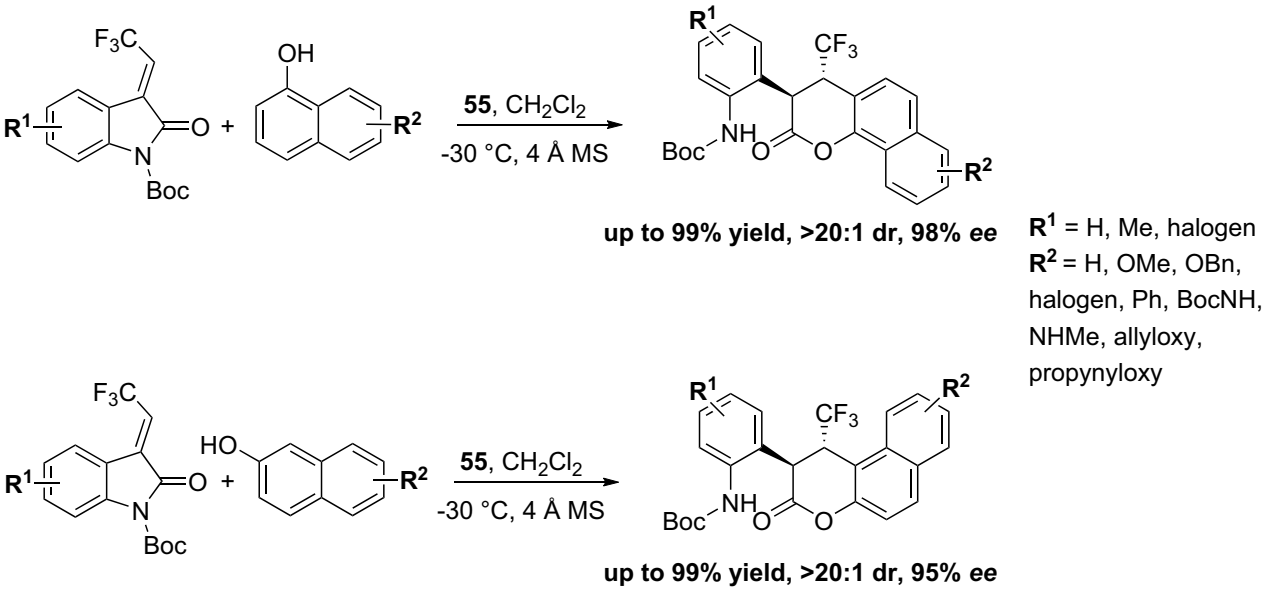

Scheme 20. Asymmetric Friedel-Crafts Alkylation-Lactonization Sequence for the Generation of α-Aryl-β-trifluoromethyl Dihydrocoumarins

(A) The chemical structure of catalyst **55**.

(B) The [3 + 3] strategy for the Friedel-Crafts alkylation and lactonization.

(C) General reaction scheme for the asymmetric Friedel-Crafts alkylation-lactonization cascade.

of N-Boc ketimines with 2-naphthols (Scheme 21).[67] The N-Boc ketimines were derived from pyrazolin-5-ones and upon reaction with a 2-naphthol, in the presence of a bifuncational squaramide catalyst, furnished furanonaphthopyrazolidinone

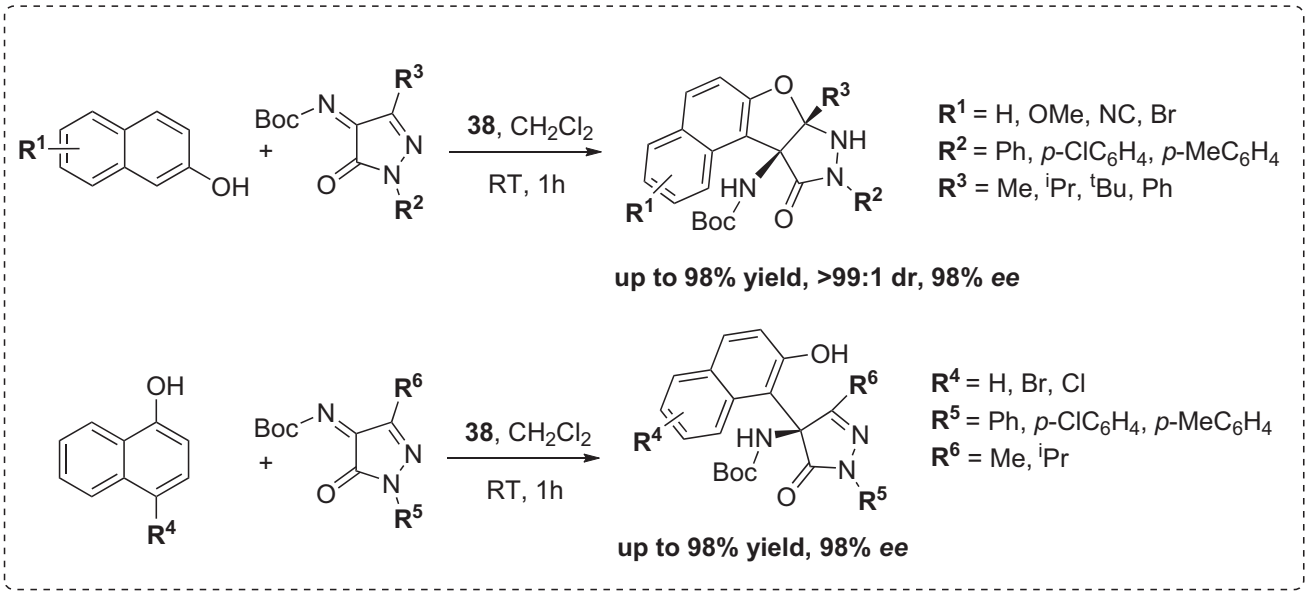

Scheme 21. General Reaction Scheme for the Asymmetric Friedel-Crafts-Initiated Cascade

derivatives bearing two vicinal tetra-substituted stereogenic centers. A screen of reaction conditions revealed squaramide **38** as the catalyst of choice; a loading of only 0.5 mol % was required, and performance was optimal with $CHCl_3$ as the solvent (reaction time of only 10 min with 5 mol % catalyst). Because of the higher toxicity of $CHCl_3$, CH_2Cl_2 was chosen for further studies (reaction time of 25 min with 5 mol % catalyst). A substrate scope study showed that a variety of N-Boc ketimines and 2-naphthols could be successfully employed in the aza-Friedel-Crafts N,O-acetalization with high yields (95%–98%) and stereoselectivity (>99:1 d.r. and 97%–98% ee). However, a different reactivity was observed in the case of 1-naphthols and other electron-rich phenols. For these examples, the acetalization step did not occur, and instead, the aza-Friedel-Crafts adducts were isolated in 70%–98% yield and 47%–98% ee. It was proposed that a possible explanation for this diverse reactivity is that the different rotation barriers around the C–C bond after the aza-Friedel-Crafts reaction of the 2-naphthol and the 1-naphthol might be responsible. The absolute configuration of a product furanonaphthopyrazolidinone was determined as (*S*,*S*) by X-ray crystallographic analysis. The synthetic efficiency of the methodology was demonstrated via a scale-up reaction that prepared gram amounts of product in high yield and stereoselectivity.

Cascade reactions that begin with a squaramide-catalyzed Mannich reaction have also been reported. An example of this is the asymmetric domino reaction of 4-bromo-3-oxobutanoates with isatin-derived ketimines as reported by Wu, Sha, and co-workers in 2014.[68] The work described the enantioselective construction of 3-amino-2-oxindoles, with a quaternary stereocenter, via a Mannich-cyclization cascade (Scheme 22). A catalyst screen was conducted, and although the highest enantioselectivity was achieved with the bifunctional squaramide catalysts **56**, in the presence of 1 equiv of $NaHCO_3$, the yields of the reactions were somewhat unsatisfactory. It was suggested that the low yields might have resulted from the low conversion rate of the substrates and/or the initial Mannich adduct. The use of Na_2CO_3 as a base additive (0.5 equiv) resulted in a significant increase in yield with catalyst **56**. The catalyst loading of **56** could be reduced to 5 mol %, and under these conditions, the desired product was formed in an 82% yield and 97% ee.

A

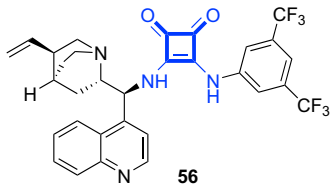

B

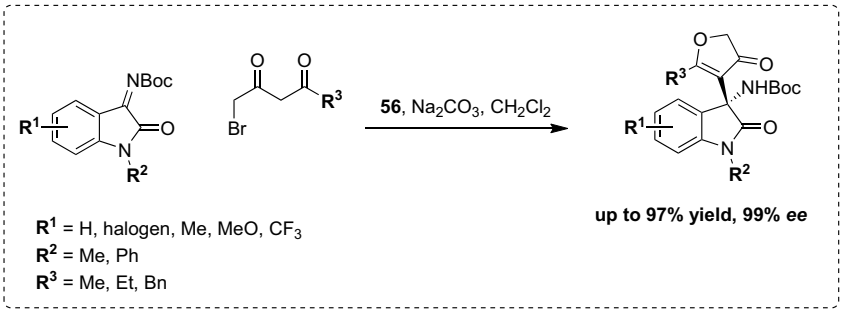

Scheme 22. Enantioselective Construction of 3-Amino-2-oxindoles via a Mannich-Cyclization Cascade

(A) Chemical structure of catalyst **56**.

(B) General reaction scheme for the asymmetric Mannich-initiated cascade.

Interestingly, using Et_3N as a base did promote the domino reaction and gave the product in a 98% yield but with very low enantioselectivity, which was probably due to a background reaction. A solvent screen resulted in the selection of CH_2Cl_2 as the preferred solvent. The subsequent substrate-scope study demonstrated that a variety of 4-bromoacetoacetates and isatin-derived ketimines could furnish the expected products, with 1 equiv of Na_2CO_3 and only 1 mol % of the squaramide catalyst, in high yields (90%–97%) and high enantioselectivities (92%–99% ee). The absolute configuration of one of the products was determined to be *R* by X-ray analysis.

Squaramide-catalyzed aldol reactions have been utilized as the first step in cascade sequences. In 2016, Han and Chang described one such transformation involving the highly enantioselective organocatalytic vinylogous aldol-cyclization cascade reaction of 3-alkylidene oxindoles to isatins.[69] Here, an unexpected intramolecular lactonization that followed the initial aldol reaction and led to cleavage of the oxindole ring and generation of enantioenriched spirooxindole dihydropyranones was reported (Scheme 23). The squaramide catalyst **38** was found, once more, to give the best combination of yield and enantioselectivity when CH_2Cl_2 was used as the solvent and the reaction was performed at RT. Exploration of the substrate scope revealed that a broad range of enantioenriched spirooxindole dihydropyranones could be synthesized in good to high yields and high enantioselectivities (up to 99% yield and 99% ee). The authors were pleased to find that the unprotected isatin also took part in the cascade reaction and furnished the product in a 90% yield and 95% ee. The unprotected oxindole, in contrast, delivered no desired product. However, the N-benzyl-protected oxindole provided the vinylogous aldol product. Here, it was suggested that these results might show that occurrence of the intramolecular lactonization was due to an increase in reactivity of the oxindole ring by replacing the Boc protecting group on the nitrogen atom with a benzyl group. An interesting observation was that only a single spirooxindole was obtained, in high yield and enantioselectivity, regardless of whether the (*E*) or (*Z*) oxindole starting material

A

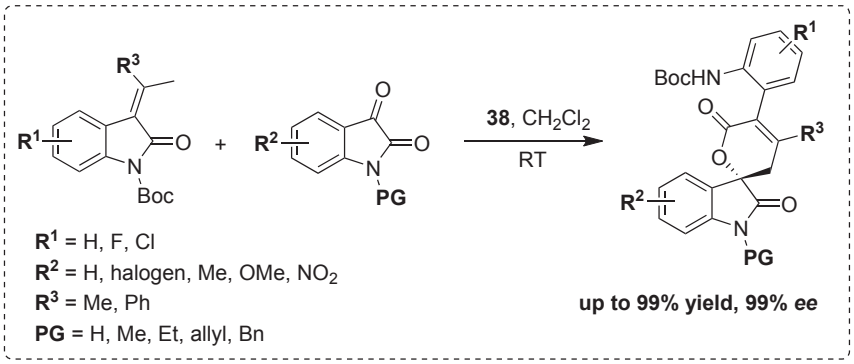

B

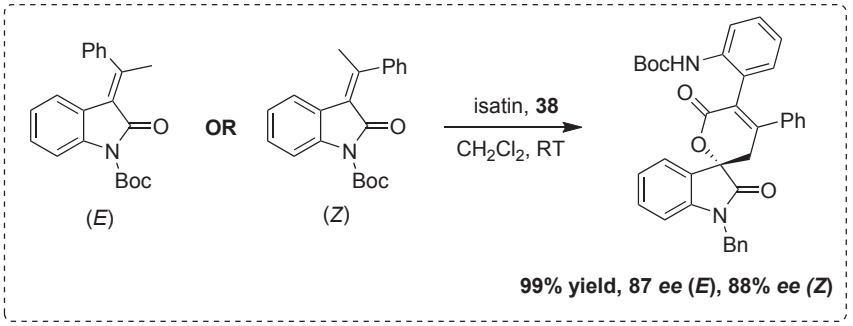

C

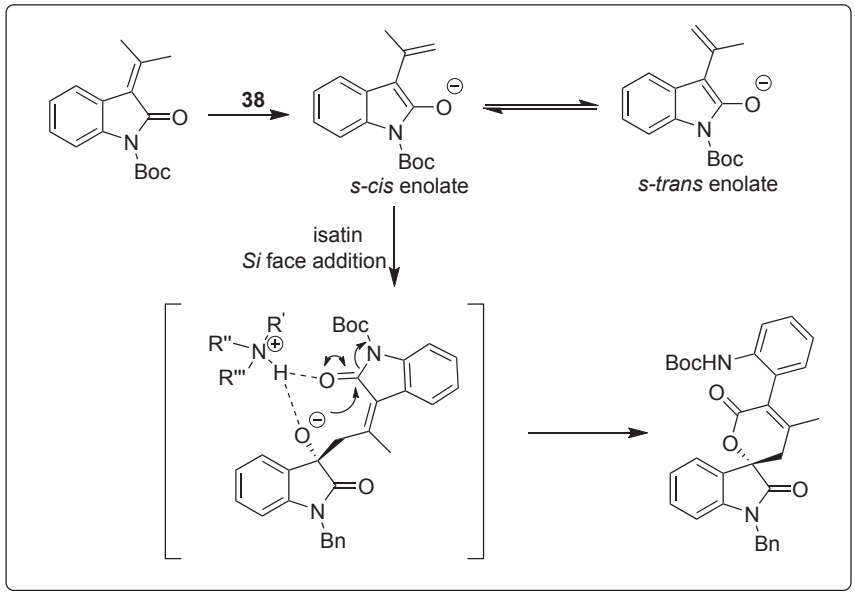

Scheme 23. Enantioselective Organocatalytic Vinylogous Aldol-Cyclization Cascade Reaction of 3-Alkylidene Oxindoles to Isatins

(A) General reaction scheme for the asymmetric aldol cyclization cascade.

(B) Effect of oxindole olefin geometry on reaction outcome.

(C) Proposed mechanism and transition state for the transformation.

was used. The absolute configuration of the products was assigned on the basis of the X-ray crystallographic analysis, and a possible mechanism was proposed. Here, the authors suggested that the oxindole was deprotonated by the catalyst and generated s-*cis* enolate. This enolate then added through the *Si* face to the isatin to give an alkoxide intermediate, which formed the final product upon protonation. It was noted that another possible direct hetero-Diels-Alder reaction pathway cannot be ruled out and that the model of dual activation of both the nucleophile and the electrophile by means of the bifunctional squaramide catalyst was also a possibility.

Squaramide-based molecules have become a leading and powerful family of organocatalysts in a very short time. A large number of publications have shown squaramides to be effective catalysts for the promotion of stereoselective carbon-carbon and carbon-heteroatom bond formations, as well as various domino and cascade sequences involving multiple reactive components.[40,60,61] There is significant potential for squaramides to be used in catalyzing the asymmetric synthesis of additional valuable enantioenriched natural products, drug molecules, and other biologically active compounds. Further expansion of the utility of squaramides as catalysts in important asymmetric transformations can be expected into the future. Such expansion will continue to take advantage of the ability of squaramides to interact and bind to substrates, a characteristic that is also heavily exploited in their use as an anion recognition motif.

SQUARAMIDES AS ANION RECOGNITION MOTIFS

The field of anion recognition has developed dramatically in recent years, and a large body of research has now been reported in the areas of anion receptors,[70] anion sensors,[71,72] and, more recently, anion transporters.[73] A number of binding motifs dedicated to hydrogen bonding have been exploited for anion recognition (including but not limited to imidazoles, pyrroles, calixarenes, amides, ureas, thioureas, amidothioureas, and thiosemicarbazides); thus, it was inevitable that the squaramide, with its many favorable characteristics, would also be explored as an anion recognition motif. Below, we will highlight some of the more recent advances in the field where the use of squaramides has evolved from anion receptors to sensors and most recently as highly effective anion transporters.

The early pioneering work of Costa and co-workers on squaramide-facilitated anion recognition[74,75] was later followed by a report by Fabbrizzi and co-workers, who undertook a direct comparison between the anion-recognition ability of urea-containing **57** and squaramide-containing **58**, which possessed identical aromatic substituents (Figure 22).[76] Using a combination of NMR spectroscopy, UV-visible (UV-vis) analysis, X-ray crystal structure analysis, and theoretical calculations, the authors were able to show that both **57** and **58** were able to form 1:1 receptor/anion complexes with Cl^- via hydrogen-bonding interactions, but the squaramide derivative **58** exhibited a higher binding affinity than urea derivative **57** when measured by spectrophotometric titration ($\log K = 4.55$ for **57** versus $\log K = 6.05$ for **58** when measured in MeCN at 25°C). Indeed, a subsequent study from the same groups also saw superior binding from another squaramide derivative **60** than from urea **59** and sulfonamide-based receptor **61**.[77] The results of spectrophotometric titrations, isothermal calorimetry (ITC), and ^{1}H NMR spectroscopic titrations in acetonitrile again suggested that the squaramide was capable of forming stable 1:1 receptor-anion complexes with Cl^- and with other oxoanions, such as AcO^- and $H_2PO_4^-$.

More recently, a small family of *N*-*tert*-butyl sulfinyl squaramide receptors, **62**–**64**, was synthesized by Li et al. (Figure 23).[78] Using ^{1}H NMR titration studies to establish

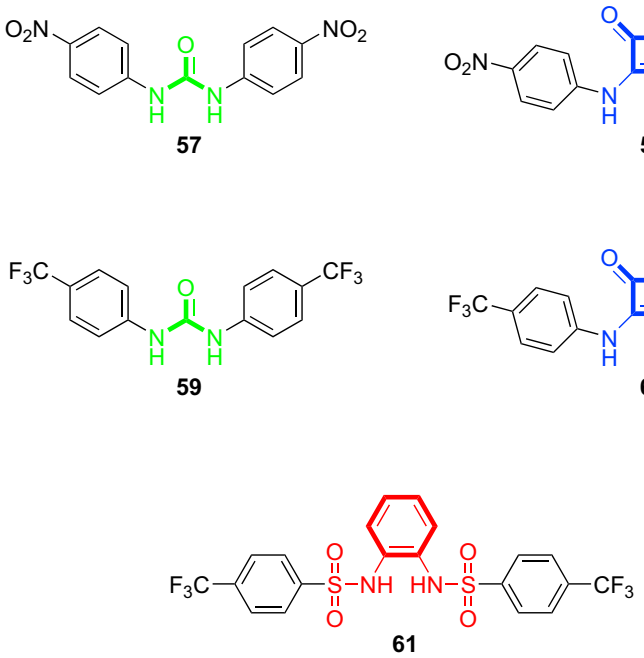

Figure 22. Chemical Structures of 57–61

binding constants of the receptors for a range of anions, the authors found that the receptors had the highest affinity for Cl^- in all cases and that their binding constants in DMSO-d_6 with 0.5% water were similar to those of squaramide analogs containing

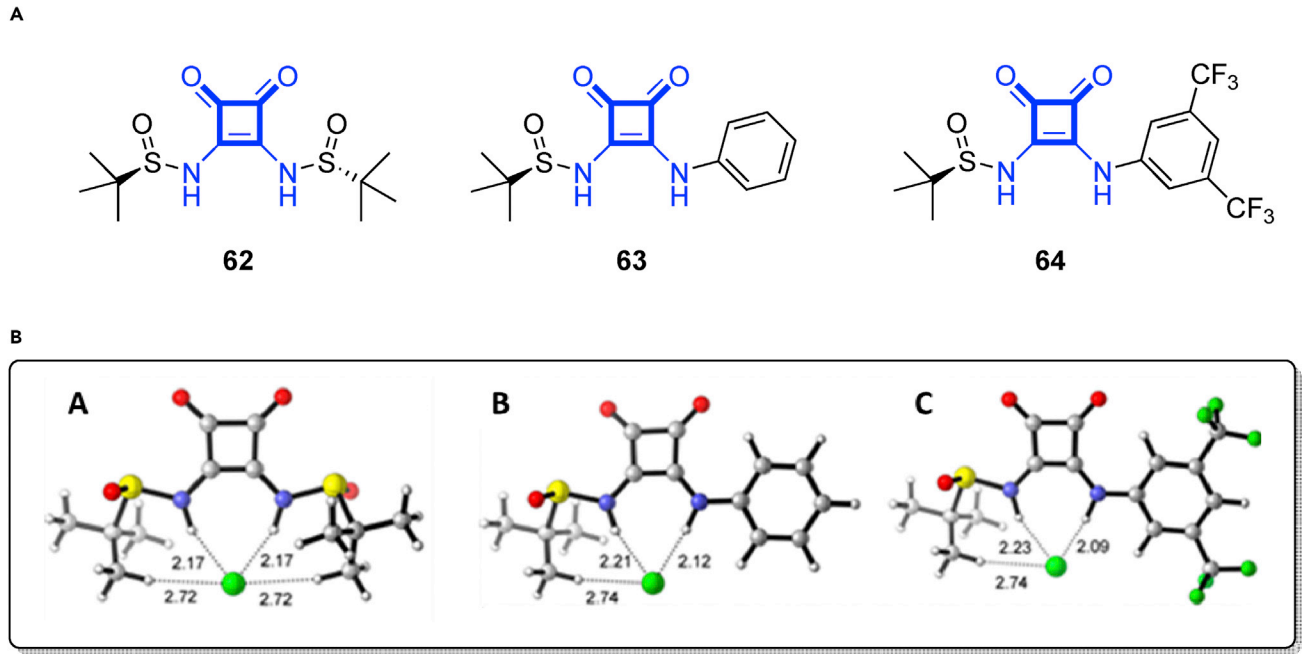

Figure 23. *N-tert*-Butyl Sulfinyl Squaramide Anion Receptors

(A) Chemical structures of **62**–**64**.

(B) DFT optimized geometries for the complexes formed between the Cl^- anion and (A) **62**, (B) **63**, and (C) **64** show the contribution from C–H···Cl^- interactions.

Reproduced with permission from Li et al.[72] Copyright 2017 American Chemical Society.

two aromatic substituents (e.g., K_a = 820 ± 67 M^{-1} in the case of compound **64**). DFT calculations and single-crystal analysis established that there were weak *tert*-butyl C–H···anion interactions in binding to Cl^-, further increasing the binding affinity (Figure 23). These results suggest that not only the acidity of the squaramide NH protons but also the overall structure of the receptor can have a major influence on the binding of squaramides to anionic species.

Indeed, Elmes et al. have synthesized larger constructs by using a solid-phase synthetic strategy to form a small family of amino-acid- and dipeptide-based anion receptors, **65–70**, which incorporated either thiourea or squaramide moieties (Figure 24A).[79] It was demonstrated that these anion receptors, particularly those containing squaramides, displayed a significantly higher affinity for SO_4^{2-} over various other anions (AcO^-, BzO^-, $H_2PO_4^-$, and Cl^-) such that ^1H NMR titrations exhibited large modulations in chemical shift upon titration with SO_4^{2-} (Figure 24B). The stereochemistry of the amino acid backbone showed little influence on the binding affinity of the receptors toward their target anions. However, the presence of the backbone amide NH protons was shown to be particularly important to the receptor-anion interaction given that dipeptide receptors **67–70** displayed significantly higher binding affinities for SO_4^{2-} than their single-amino-acid analogs **65** and **66**.

A subsequent study by Elmes and Jolliffe synthesized L-lysine-based squaramide anion receptors **71–78** by using both solid- and solution-phase methods (Figure 25).[80] Their anion-binding ability was evaluated by ^1H NMR spectroscopic titrations, and all of the receptors demonstrated the ability to bind to anions in aqueous DMSO solution, and selectivity was again observed for SO_4^{2-} over other anions, such as Cl^-, AcO^-, and BzO^-. Additionally, the authors demonstrated that the lipophilicity of the receptors could be fine-tuned by functionalization at the C and N termini without interfering with anion-binding capabilities.

A more recent report by Tzioumis et al. details the synthesis of another small library of peptide-based anion receptors, **79–84**, in order to further examine the effect structure has on SO_4^{2-} recognition (Figure 26).[81] The authors probed the importance of various design features, including shortening the side chain length, increasing the length and flexibility of receptor backbone, increasing the acidity of the squaramide NH protons, and introducing a water-solubilizing group to the N terminus of the peptide scaffold. In all cases, the receptors displayed a strong selectivity for SO_4^{2-}, as seen in earlier reports. Surprisingly, the addition of the hydrophilic TriTEG group did not markedly increase solubility of the receptors in aqueous solution, so the effect of higher concentrations of water on SO_4^{2-} binding in DMSO-d_6 could not be evaluated.

A recent report from the same research group produced a family of macrocyclic squaramides, **21** (vide supra) and **85–89**, containing either two or three squaramide units (Figure 27).[32] ^1H NMR titration studies confirmed that the macrocyclic squaramide (MSQ) receptors **21**, **85**, **88**, and **89** also displayed very high selectivity for SO_4^{2-} in aqueous DMSO-d_6 solution. Upon complexation to SO_4^{2-}, the ^1H NMR spectrum of **21** showed large modulations in chemical shift, and interestingly, the signal for the methylene protons was seen to split into two distinct signals. The authors suggested that the free macrocycle was capable of adopting several conformations in solution at RT but upon SO_4^{2-} complexation became fixed in a single conformation. Indeed, X-ray crystal-structure analysis revealed that in the presence of SO_4^{2-}, the conformation adopted by **21** was markedly different from the chair-like conformation found for the free macrocycle. Instead, **21** was shown to form a 1:1 (receptor/anion) complex with SO_4^{2-} whereby the receptor adopted a bowl-like conformation reminiscent of a calixarene in the

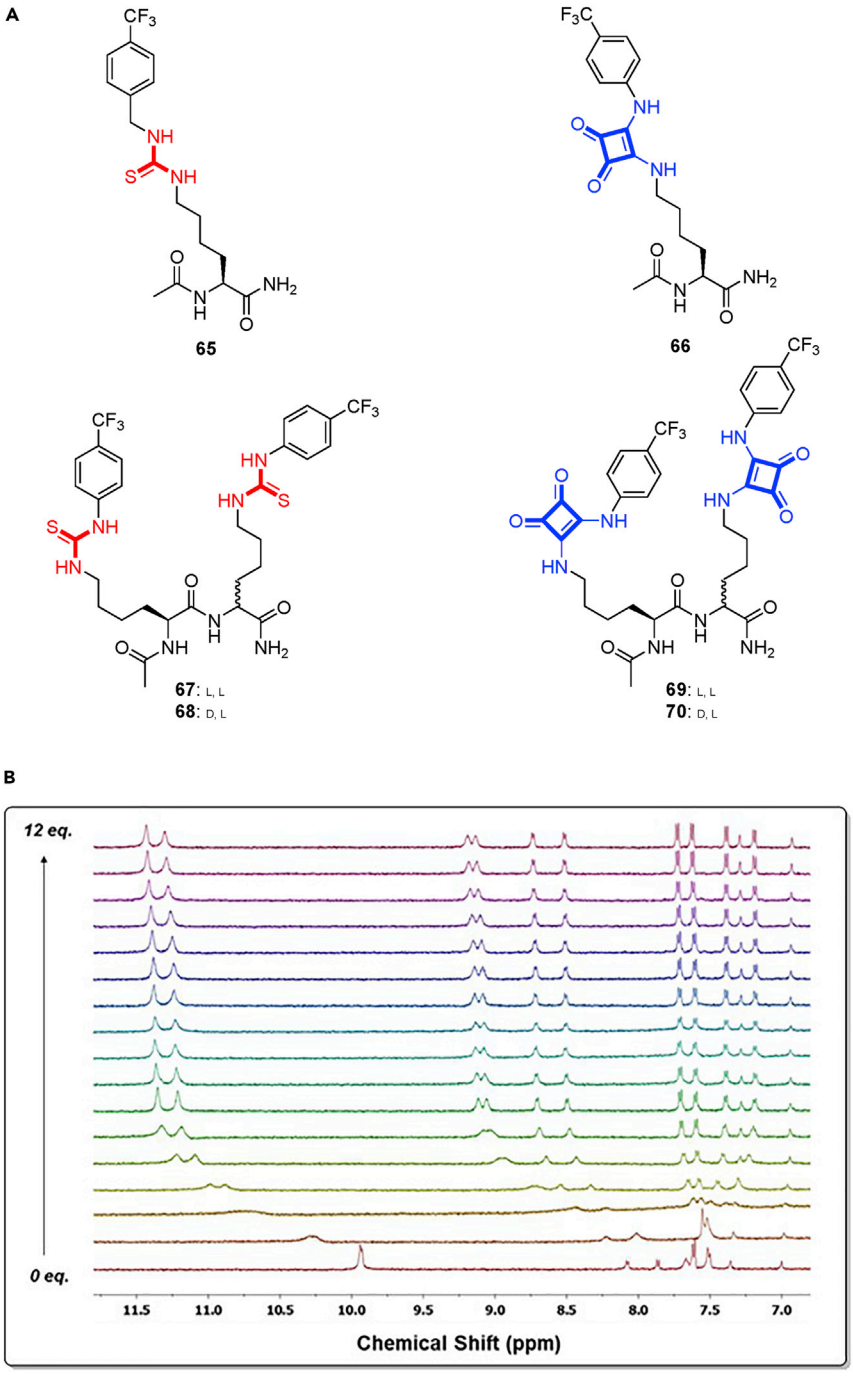

Figure 24. Peptide-Squaramide Anion Receptors

(A) Chemical structures of **65**–**70**.

(B) Stack plot of ^{1}H NMR spectra of **69** upon addition of $(TBA)_2SO_4$ (0–12 equiv) in 20% H_2O in DMSO-d_6 at 25° C shows large modulations in chemical shift.

Reproduced with permission from Elmes et al.[79] Copyright 2014 Wiley-VCH Verlag GmbH & Co. KGaA.

cone conformation (Figure 28). Furthermore, the larger MSQs containing three squaramide units (**85** and **89**) were found to better match the size and shape of the SO_4^{2-} ion than their smaller counterparts (**21** and **88**) and provided high affinity and selectivity for

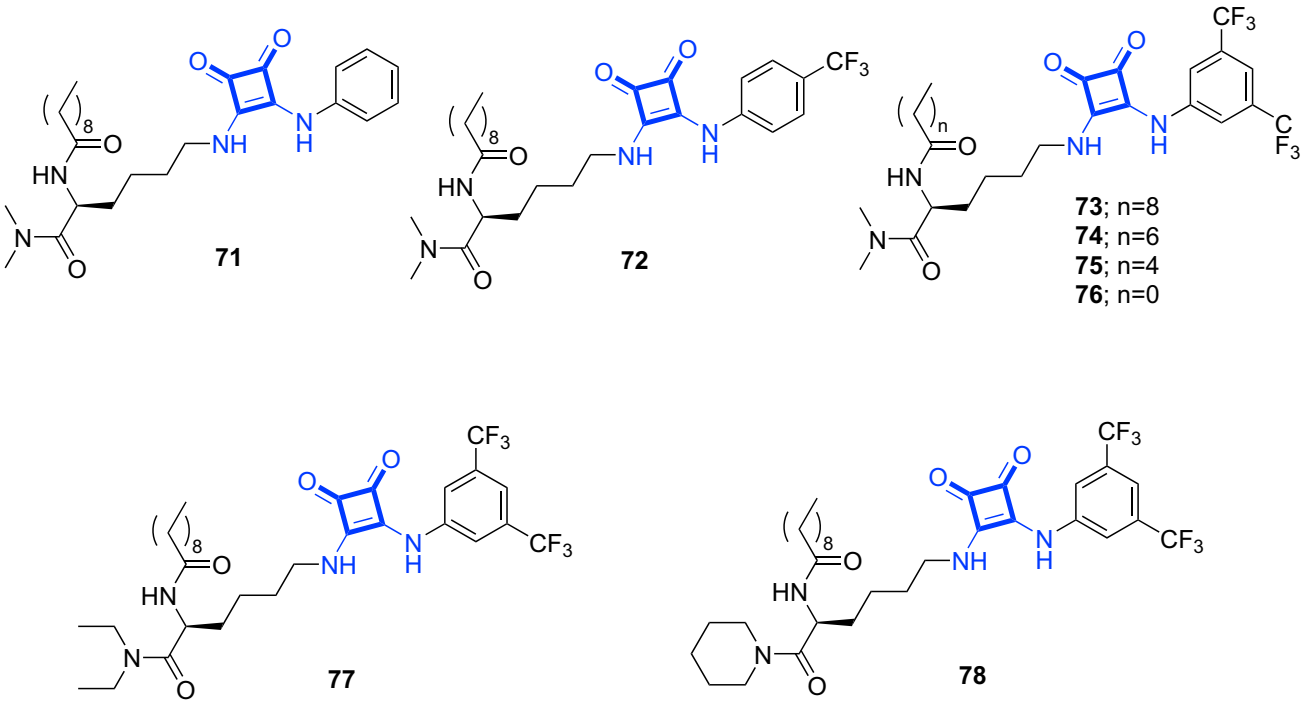

Figure 25. Chemical Structures of 71–78

SO_4^{2-} even in mixtures of anions mimicking the composition of either nuclear waste or blood plasma.

Calix[4]arene-based anion receptors incorporating the squaramide moiety **90–92** have been reported by Wang and co-workers (Figure 29).[82] The anion-binding capability of each receptor was examined via UV-vis spectroscopy and ^{1}H NMR analysis, which showed that the receptors could selectively recognize F^-, AcO^-, and $H_2PO_4^-$ over other anions. **90** was shown to bind to anions via hydrogen-bond interactions,

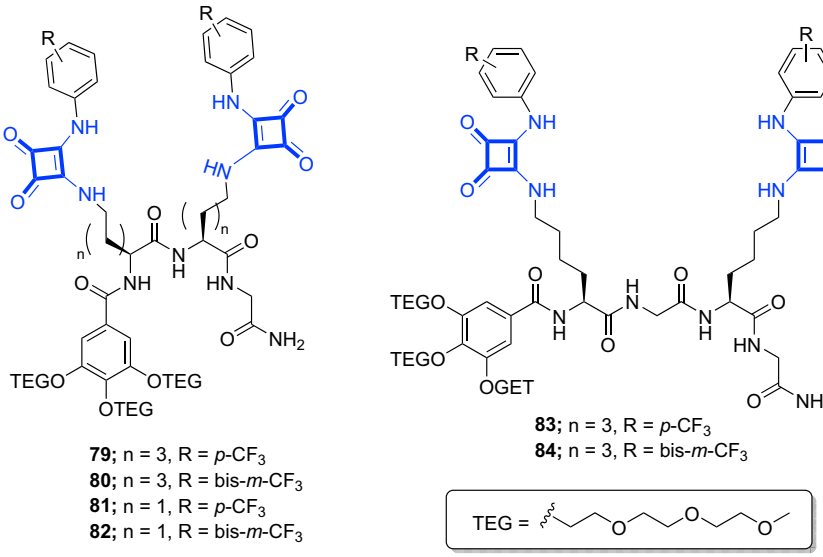

Figure 26. Chemical Structures of 79–84

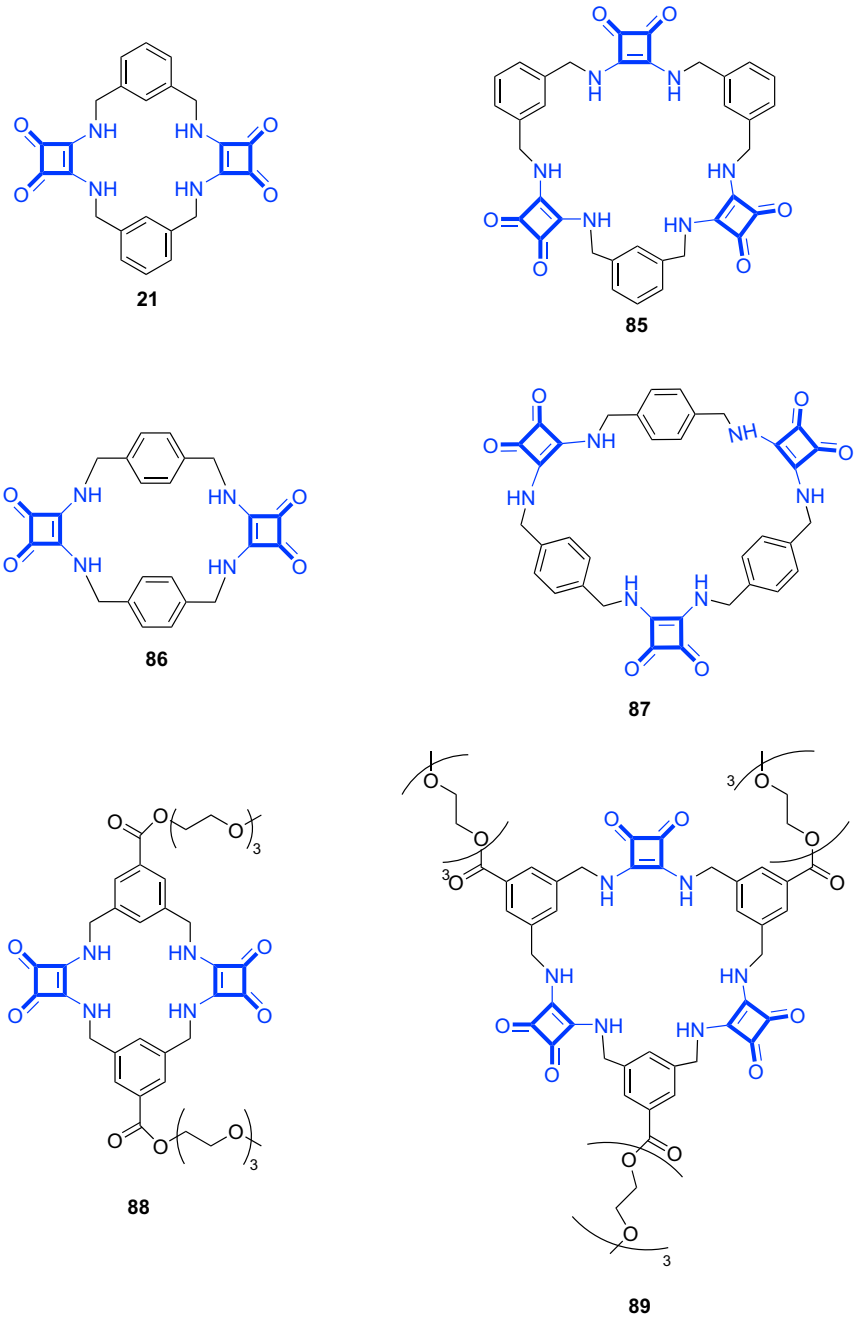

Figure 27. Chemical Structures of 21 and 85–89

resulting in downfield shifts of the NH protons in the ^{1}H NMR spectra, concomitant with bathochromic shifts in the UV-vis spectra. Meanwhile, **91** and **92** both displayed an acid-base interaction between the receptor and anion, resulting in a naked-eye color change. This was purported to be due to the increased acidity of the squaramide NH protons of **91** and **92** as a result of the electron-withdrawing nitro groups. A subsequent study by the same research group reported the synthesis of two mono-squaramide-functionalised pillar[5]arenes, **93** and **94** (Figure 29).[83] Using ^{1}H NMR titrations, Job's plot analysis , ESI-MS, and 2D NMR techniques, the authors showed that **93** forms a 1:1 stoichiometric complex with both *n*-hexylphosphonic

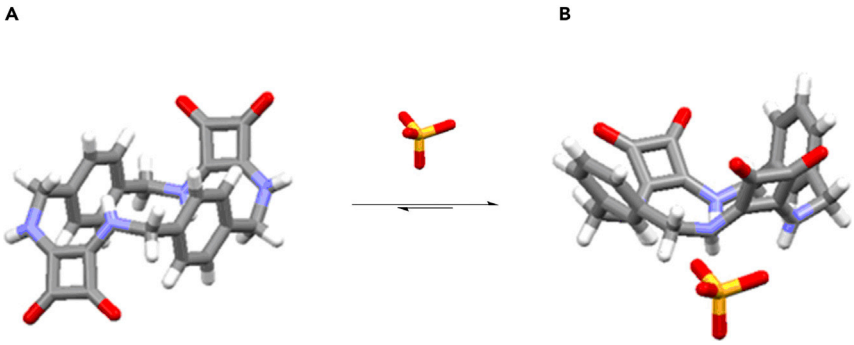

Figure 28. Sulfate Recognition Using Macrocyclic Squaramides
Single-crystal XRD structures of (A) **21** and (B) the complex formed between **21** and SO_4^{2-} clearly show the interaction between SO_4^{2-} and the squaramide NH protons inside the macrocyclic cavity.

acid (HPA) and *n*-heptanoic acid (HA) with high affinity (log *K* = 3.83 and 1.98, respectively). As expected, **94**, with a strongly electron-withdrawing CF_3 group, showed a similar ability to recognize HPA and HA but with slightly higher affinity (log *K* = 5.74 and 2.06, respectively).

Squaramides have also been incorporated into polymeric materials. Manesiotis et al. synthesized a series of polymerizable squaramides, **95–100**, and compared their anion-binding ability to urea analog **101** by using UV-vis spectroscopy (Figure 30).[84] As seen previously, the squaramides with the most electron-withdrawing groups attached to the aromatic substituents exhibited the highest association constant values for anions tested (Table 1). The more acidic NH protons of **98** and **100** underwent a color change due to deprotonation in the presence of excess fluoride, as seen with the

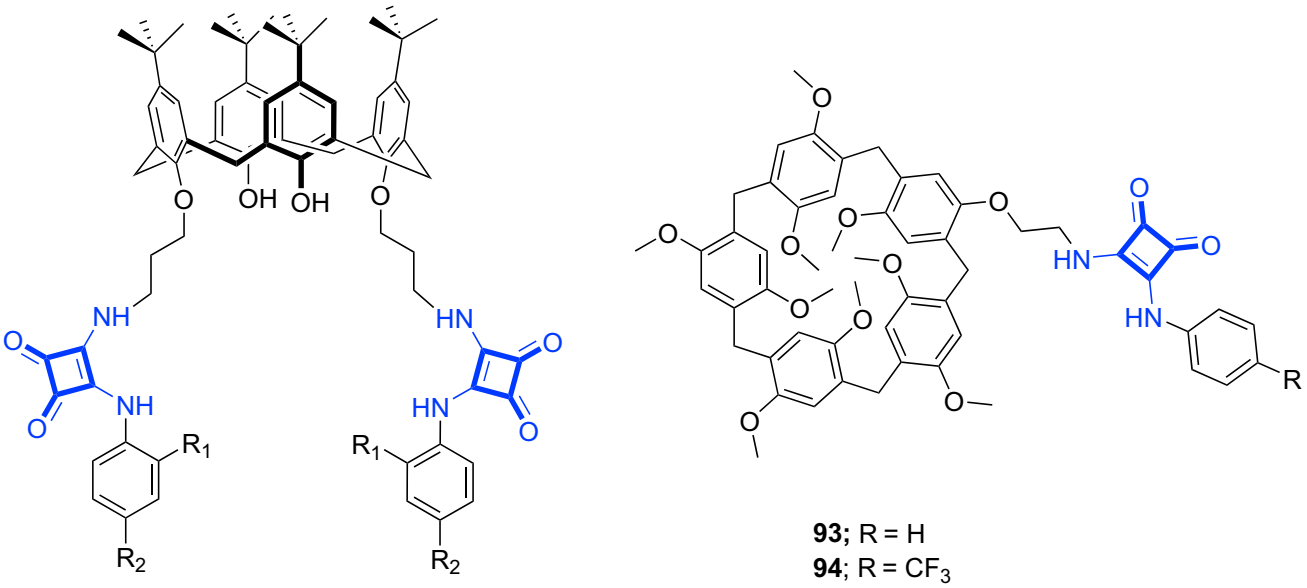

90; R_1 = H; R_2 = H
91; R_1 = H; R_2 = NO_2
92; R_1 = NO_2; R_2 =H

93; R = H
94; R = CF_3

Figure 29. Chemical Structures of 90–94

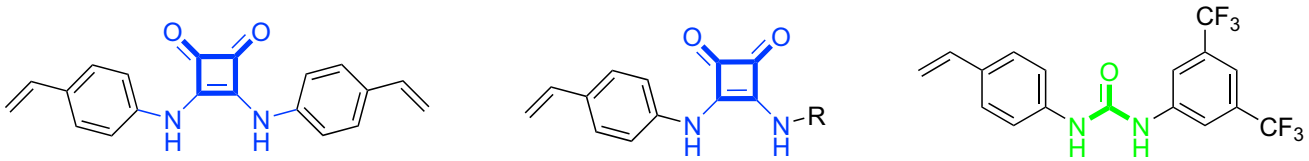

95

96; R = Phenyl
97; R = 3-nitrophenyl
98; R = 3,5-bis(trifluoromethyl)phenyl
99; R = benzyl
100; R = 3,5-bis(trifluoromethyl)benzyl

101

Figure 30. Chemical Structures of 95–101

appearance of an absorbance band at 470 nm, which indicated a charge transfer between two species. Molecularly imprinted polymers (MIPs) were also prepared from squaramide **95**, and its binding performance to a model anion, tetrabutylammonium benzoate (TBAOBz), was compared with that of a polymer prepared with urea monomer **101**. **MIP95** exhibited both the highest affinity and capacity toward its template, higher than that of **MIP101**, the urea-based polymer, as measured by UV-absorption-based rebinding experiments. These results confirmed that the squaramide MIP retained a stronger affinity for anionic species than the equivalent ureas after polymerization. Moreover, a MIP prepared with **98** and TBAF as the template resulted in polymer particles capable of rapid and reversible association of TBAF in acetonitrile, as evidenced by intense color changes clearly visible to the naked eye.

Another interesting example is the switchable rotaxane organocatalyst **102**, synthesized by Beswick et al. (Figure 31).[85] **102** contains two catalytic sites, one of which is blocked by a macrocycle under a given set of conditions. The positioning of the macrocycle is switched via acid-base mediation whereby under acidic conditions, the crown ether portion of the macrocycle interacts with the protonated secondary amine, inhibiting catalytic activity at this site while exposing the squaramide catalytic site. Conversely, under neutral or basic conditions, the macrocycle preferentially binds to the squaramide moiety, inhibiting its ability to hydrogen bond and thus deactivating the catalytic activity at this site. This exposes the secondary amine and permits it to promote iminium catalysis. The rotaxane was found to successfully catalyze Michael additions and demonstrated a high level of selectivity in both modes.

It is of note that the vast majority of squaramide-based compounds reported in the area of ion recognition deal specifically with anion recognition. Given the ability of

Table 1. Association Constants (K_a, L mol^{-1}) between 95 and 101 and Tetrabutylammonium Salts of Common Anions as Determined by UV Titration Experiments in DMSO

Receptor	$C_6H_5COO^-$	$H_2PO_4^-$	F^-	I^-
95	1.0×10^5	3.6×10^5	6.7×10^5	$<10^3$
96	5.1×10^4	6.5×10^4	4.1×10^5	$<10^3$
97	7.8×10^5	4.0×10^5	$>10^6$[a]	9.8×10^4
98	9.1×10^5	5.1×10^5	$>10^6$[a]	3.8×10^5
99	3.0×10^3	1.3×10^4	6.4×10^4	$<10^3$
100	1.2×10^4	2.1×10^4	1.5×10^5	$<10^3$
101	5.1×10^5	8.2×10^4	6.3×10^5	7.1×10^3

[a]Deprotonation occurred upon addition of excess TBAF.

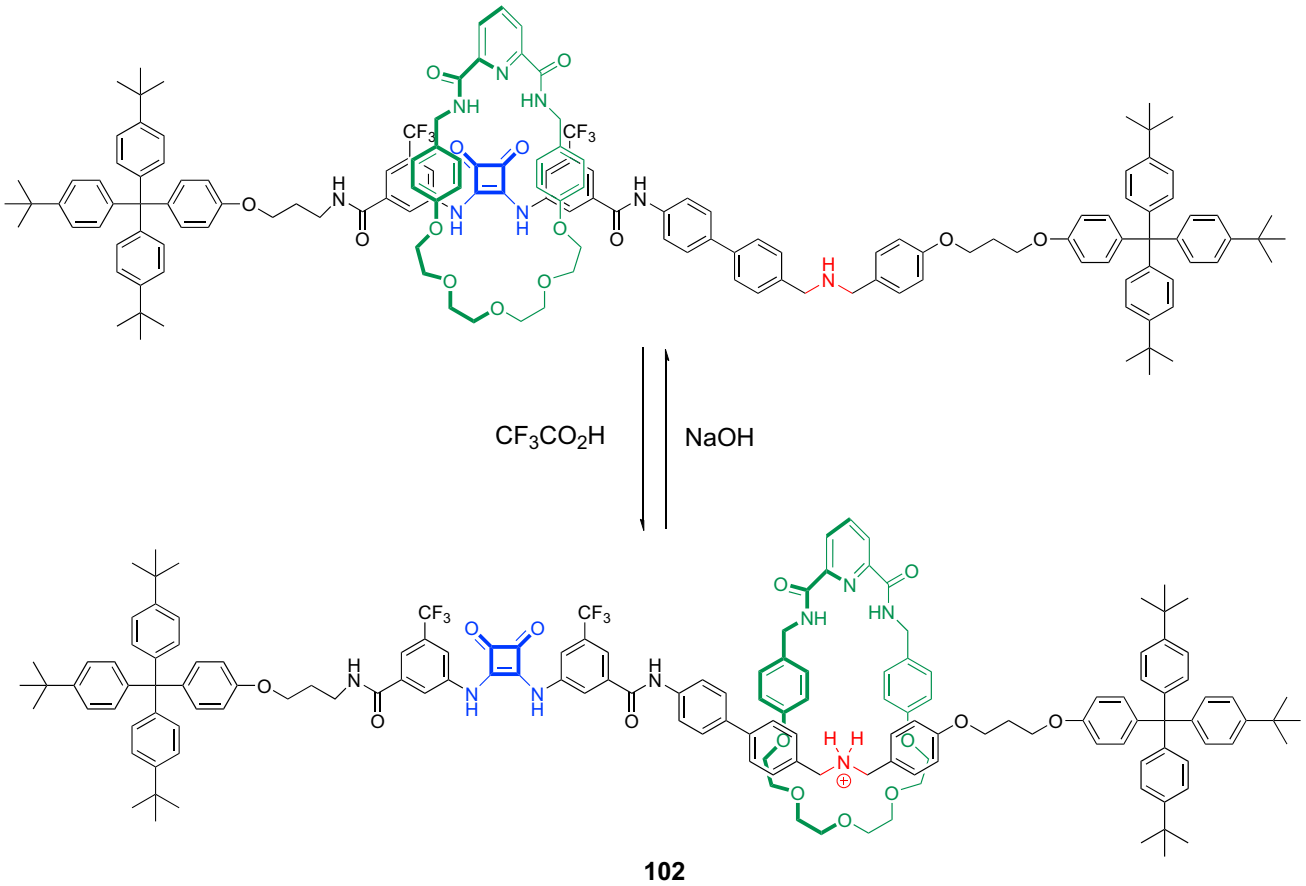

102

Figure 31. Chemical Structure of 102 Showing the Shuttling of a Macrocycle as a Function of Acid-Base Equilibrium

squaramides to act as both a hydrogen-bond acceptor and a hydrogen-bond donor, it is surprising that the squaramide moiety has not been exploited to the same degree as a cation recognition motif by taking advantage of the two squaramide carbonyl functionalities. Some early examples of cation recognition include two pioneering papers by Ballester, Costa, and co-workers, who outline the use of squaramide-based tripodal receptors for the recognition of tetraalkylammonium compounds such as choline, acetylcholine, and related ammonium salts.[86,87] These examples of cation recognition and fluorescent sensing of membrane phospholipids were rare until more recent reports of the use of squaramides for the construction of ion-pair zwitterion receptors.

Costa and co-workers reported a self-complementary amidosquarate-squaramide host for miltefosine **103** (Figure 32).[88] The authors exploited the charged amidosquarate unit as the binding site for the cationic quaternary amine of miltefosine and a neutral squaramide unit, located at a precise distance away to act as a binding site for the anionic phosphate. The combination of two different squaramide units effectively enhanced the affinity and selectivity for miltefosine by using a structurally simple receptor. In another study, Costa and co-workers reported the synthesis of Janus-like tripodal squaramide-based ditopic receptors such as **104** and **105** for ion-pair recognition (Figure 32).[89] ^{1}H NMR spectroscopy and UV dilution experiments revealed that compound **105** could form dimeric assemblies in organic solution. Further microscopic analysis showed that aggregation of **105** resulted in the

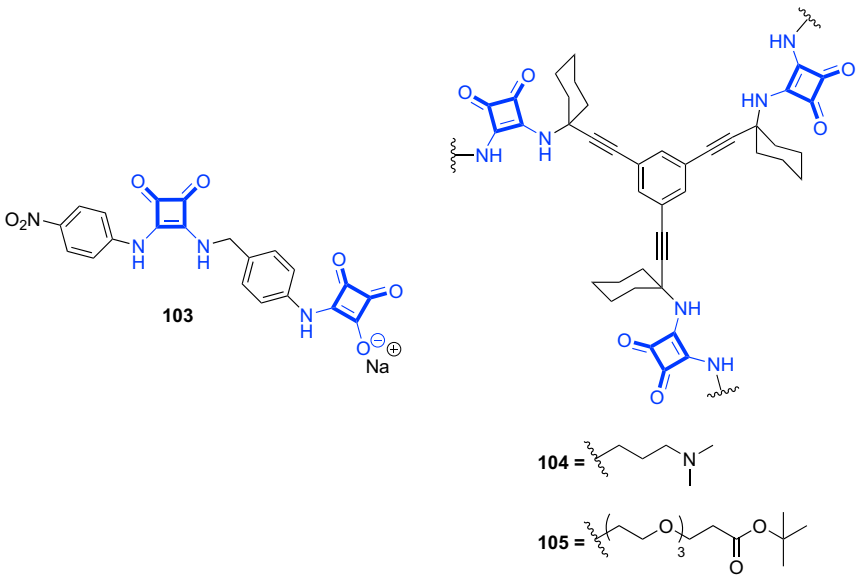

Figure 32. Chemical Structures of 103–105

formation of a network of bundled fibers and a macroscopic gel-like morphology in $CDCl_3$. Studies with tetraalkylammonium tricarboxylate and iodide salts showed that **105** exhibited two different and mutually exclusive binding modes whereby reorganization of the squaramide groups could be effected depending on the nature of the ion pair introduced. Indeed, the authors suggest that such conformational transitions driven by ion-pair recognition could have application in controlling more elaborate movements within molecular devices.

The group of Piatek and co-workers has also reported ion-pair receptors, **106** and **107**, which incorporate two anion-binding functionalities and a sodium-selective *N*-acyl aza-18-crown-6 domain (Figure 33).[90] Through single-crystal XRD analysis, it was found that a methyl group effectively aligns the binding domains in one direction, thus optimizing the binding of the ion pair. Their study showed that binding at one domain increases the binding affinity at the other binding site, demonstrating a cooperative binding effect. For example, upon the binding of chloride to **106**, the strength of sodium complexation increased by up to 23 times. Squaramide-based receptor **107** was shown to bind at a similar strength but at a lower cooperativity with log K_a = 6.52 M^{-1}. However, receptor **107** was found to bind to sodium cations more than twice as strongly than receptor **106**. This is believed to be due to a complimentary interaction of the squaramide carbonyl groups with the crown ether where cation complexation of the squaramide provides a more favorable interaction than the urea carbonyls.

A related study from Zdanowski et al. investigated the use of **108** as an ion-pair receptor capable of facilitating the extraction of chloride from an aqueous to an organic environment (Figure 34).[91] The study found that the presence of two anion-binding sites was optimal for the formation of anion-receptor complexes where **108** was found to bind both NaCl and TBACl with association constants (K_a) in the region of 10^6 M when measured in MeCN via UV spectroscopy. Given the strong affinity of **108** toward Cl^- anions, a series of salt extraction and transport studies were performed to assess its ability to transport salts from an aqueous phase into an organic phase. Toluidine blue with a Cl^- counteranion was used to monitor the transfer of the salt, and **108** was shown to effectively transfer Cl^- salts from the

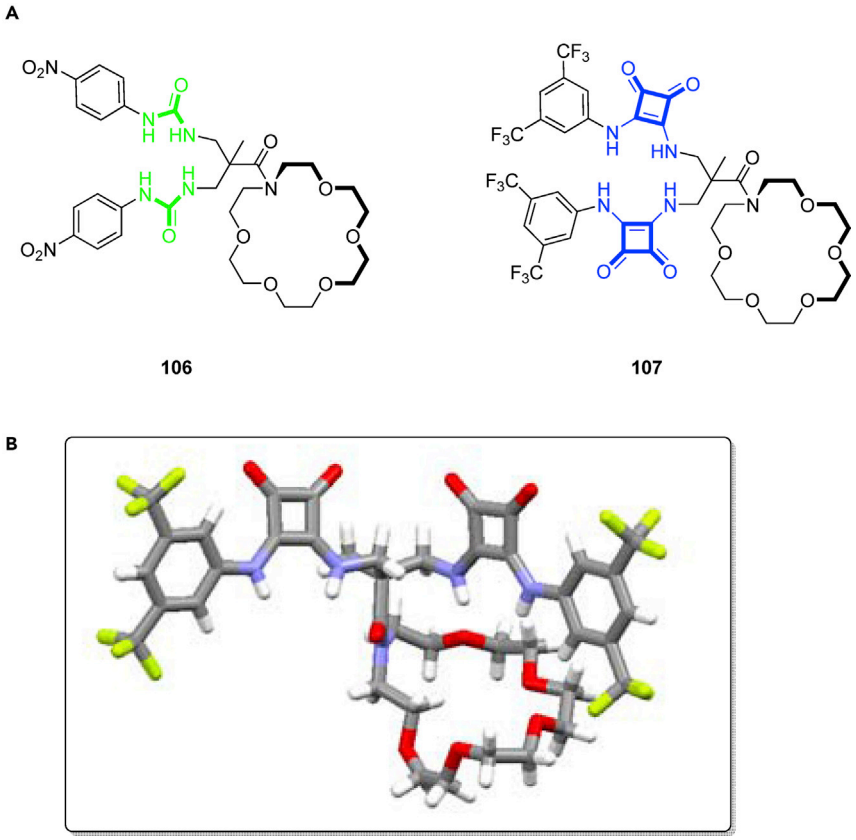

Figure 33. Squaramide-Based Ion-Pair Receptors

(A) Chemical structures of **106** and **107**.

(B) X-ray crystal structure of **107** shows the alignment of both squaramide binding domains in a single direction.

aqueous to the organic phase (Figure 34). The transport of Cl^- was facilitated by soft counter cations such as TBA^+; however, the transport study failed when a salt consisting of two hard ions was used.

Most recently, the Romański group has reported ion-pair receptors **109** and **110**, which also consist of a crown ether cation-binding site coupled to either a squaramide or a urea anion-binding domain (Figure 35).[92] Spectrophotometric and spectroscopic studies revealed that salt binding occurred in both acetonitrile and acetonitrile-water mixtures, where a host of anions (nitrate, nitrite, bromide, and chloride) were found to associate with receptor **109** and **110** more strongly in the presence of sodium cations than in the presence of tetrabutylammonium cations. Single-crystal XRD analysis was also used to demonstrate the ability of **109** to form complexes with sodium chloride, even in the presence of water. Moreover, in contrast to the urea-based compound **110**, compound **109** was shown to be able to extract sodium chloride from the aqueous to the organic phase by ^1H NMR, mass spectrometry, and atomic absorption spectroscopy analysis.

While squaramide-based anion receptors have received significant research attention in recent years, in parallel, squaramide-based sensors that are capable of reporting colorimetrically or fluorometrically on the binding event have also been explored. Initially taking advantage of dye-displacement-based sensors, such as

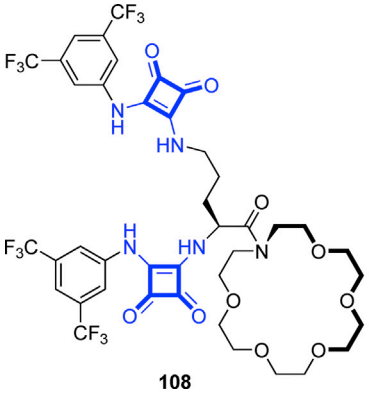

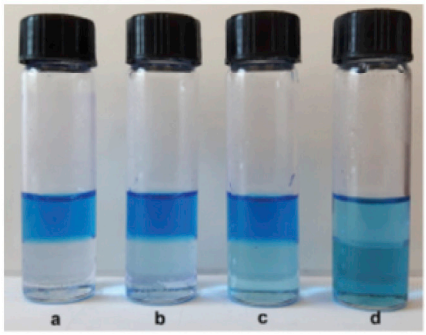

Figure 34. Chloride Extraction with Squaramides

Chemical structure of **108** and extraction of aqueous solution of toluidine blue (top layers) with (A) 20% n-butanol in chloroform, (B) 1 equiv of receptor **108** in the organic phase, (C) 10 equiv of receptor **108** in the organic phase, and (D) 100 equiv of receptor **108** in the organic phase (bottom layers). Adapted from Zdanowski et al.[91] with permission from the Royal Society of Chemistry.

those developed by Costa,[74,93,94] in more recent years, a number of other approaches have been explored.

Elmes et al. synthesized a family of squaramide-based colorimetric and luminescent anion sensors, **111–114**, by covalently appending an anthracene moiety to the squaramide scaffold (Figure 36).[95] The sensors exhibited little interaction with non-basic anions, such as Br^-, I^- and NO_3^-; however, upon addition of Cl^- to **111** and **112**, their absorption spectra underwent hyperchromic shifts at 393 nm, with a hypochromic shift at 355 nm, resulting in a naked-eye color change from colorless to yellow. The addition of chloride to the nitro-substituted derivative **113** resulted in similar hyperchromic and hypochromic shifts but also underwent a hypsochromic shift of approximately 5–10 nm, resulting in a stark color change from orange to deep red, which was clearly visible to the naked eye (Figure 36). Moreover, the fluorescence properties of these receptors were also found to be significantly modulated upon interaction with Cl^-, whereby fluorescence excimer emission centered at 530 nm was significantly "switched off" by 66% for **111** in the presence of Cl^- ions. The authors suggested that the observed spectroscopic changes were related to the acidity of the squaramide that can be effectively tuned by various aryl substituents, thus giving the ability to selectively recognize anions via deprotonation of the squaramide NH proton.

Marchetti et al. found similar behavior with a small family of squaramidoquinoxaline chemosensors, **115–117** (Figure 37).[96] Compound **116** displayed a sensitivity for F^- over other halides and exhibited a stark color change from purple to green in organic solvent. This was attributed to the enhanced acidity of the NH protons due to the presence of the electron withdrawing nitro substituent. Moreover, computational analysis predicted that the observed color change would arise from a reduced

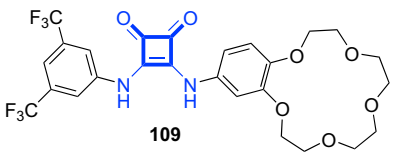

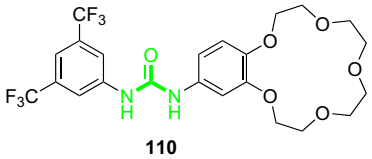

Figure 35. Chemical Structures of 109 and 110

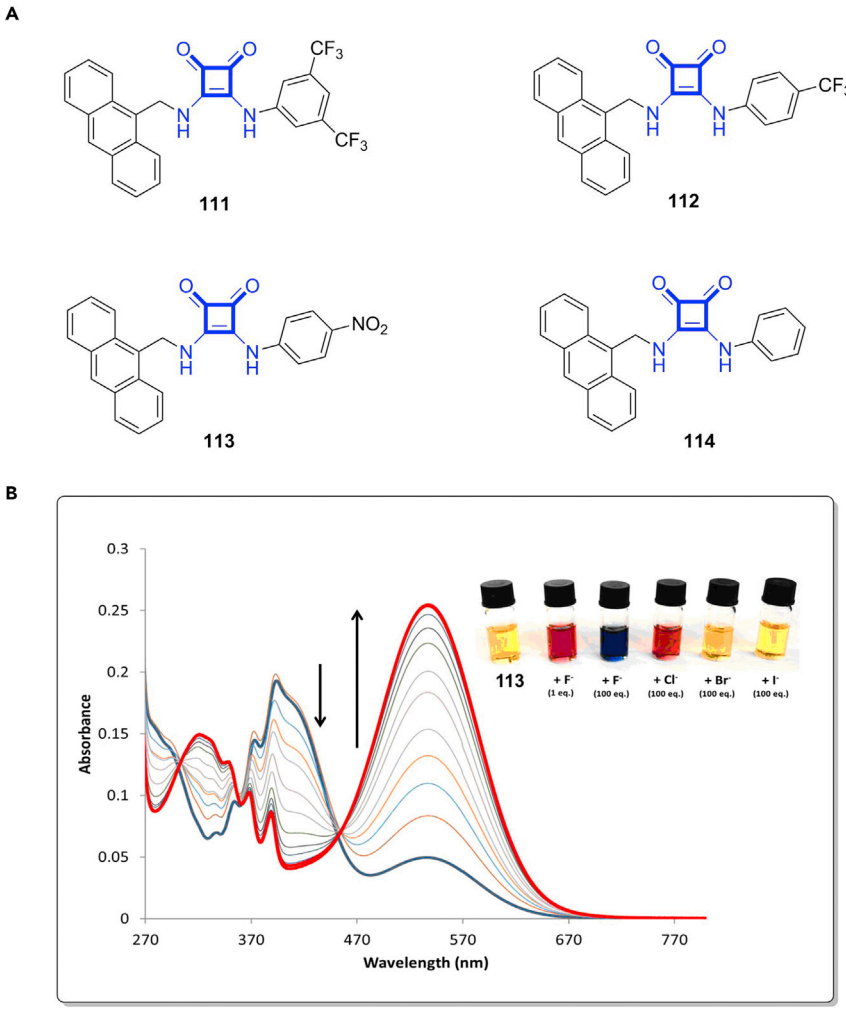

Figure 36. Squaramide-Based Colorimetric and Luminescent Anion Sensors

(A) Chemical structures of **111**–**114**.

(B) Changes observed in the absorption spectrum of **113** upon addition of TBACl in DMSO. Inset: the corresponding changes seen by the naked eye with various halide anions.

Adapted with permission from Elmes et al.[95] Copyright 2013 American Chemical Society.

HOMO-LUMO gap in the intramolecular charge-transfer process between the squaramide ring system and the nitro group upon deprotonation of one of the NHs. The authors were able to demonstrate the utility of **116** as a F^- chemosensor by using a paper-based colorimetic assay where the sensor was easily able to detect F^- by the naked eye but did not display any sensitivity for other halide anions in either organic or aqueous solution.

Muthyala and co-workers reported an alternative strategy for fluorescent Cl^- detection based on suppression of an excited-state intramolecular proton transfer (ESIPT).[97] Squaramides **118** and **119** (Figure 38) had been reported previously[98] and showed a fluorescence "turn on" response in the presence of Cl^- in acetonitrile solution as a result of a conformational change brought about by the binding event. A later article explored the origin of the Cl^--induced emission enhancement in these ortho-substituted squaramides, where it was suggested by computational analysis that two degenerate excited states exist because of two charge-transfer pathways.[99]

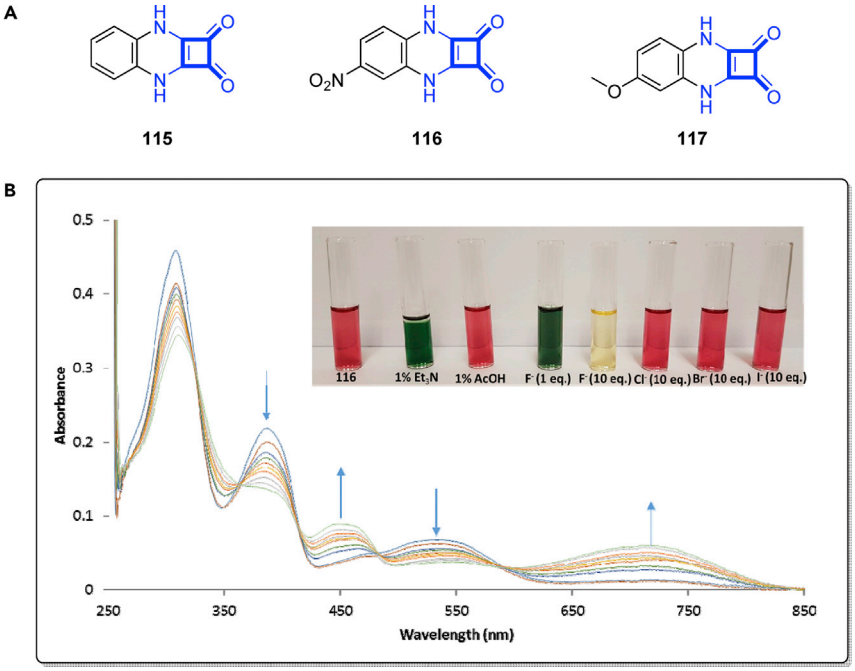

Figure 37. Squaramidoquinoxaline Colourimetric Anion Sensors

(A) Chemical structures of **115**–**117**.

(B) Changes observed in the absorption spectrum of **116** upon addition of TBAF in 0.5% H_2O in DMSO solution. Inset: colorimetric changes observed for **116** under acidic conditions, under basic conditions, and in the presence of various halides in DMSO at 25°C.

In the unbound state, competition between the two pathways decreases the fluorescence intensity of the receptor. However, upon Cl^- recognition, a suppression of the charge transfer into the cyclobutenedione ring occurs, thereby enhancing the observed emission intensity from the anthranilate portion of the molecule.

An article by Rostami et al. reported the design and synthesis of two squaramide-based polymers, **120** and **121**, and an investigation of their spectroscopic response to various anions.[100] The authors were able to demonstrate that polysquaramide **120** exhibits a selective "turn-on" fluorescence response to dihydrogenphosphate ($H_2PO_4^-$) ions in aqueous *N*-methylpyrrolidinone (NMP) (10% H_2O) (Figure 39). **120** was synthesized by condensation of a 9,9-dioctylfluorene-2,7-diamine derivative with diethyl squarate, and it was suggested that upon addition of $H_2PO_4^-$ to compound **120**, the ions engage in hydrogen bonding with multiple squaramide groups along the polymer. Non-polymeric control receptor **122** showed a minimal spectroscopic response to $H_2PO_4^-$; thus, it was proposed that the cooperative aggregation of the organic polymer in response to the anion exploited the repeating

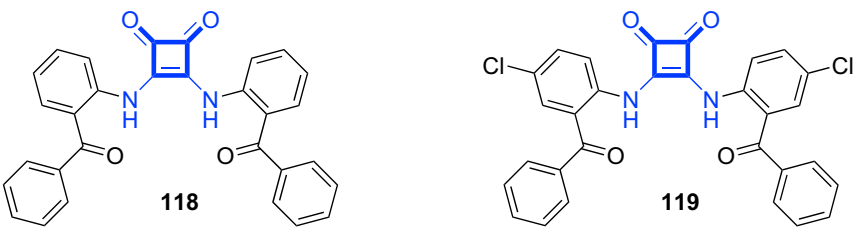

Figure 38. Chemical Structures of 118 and 119

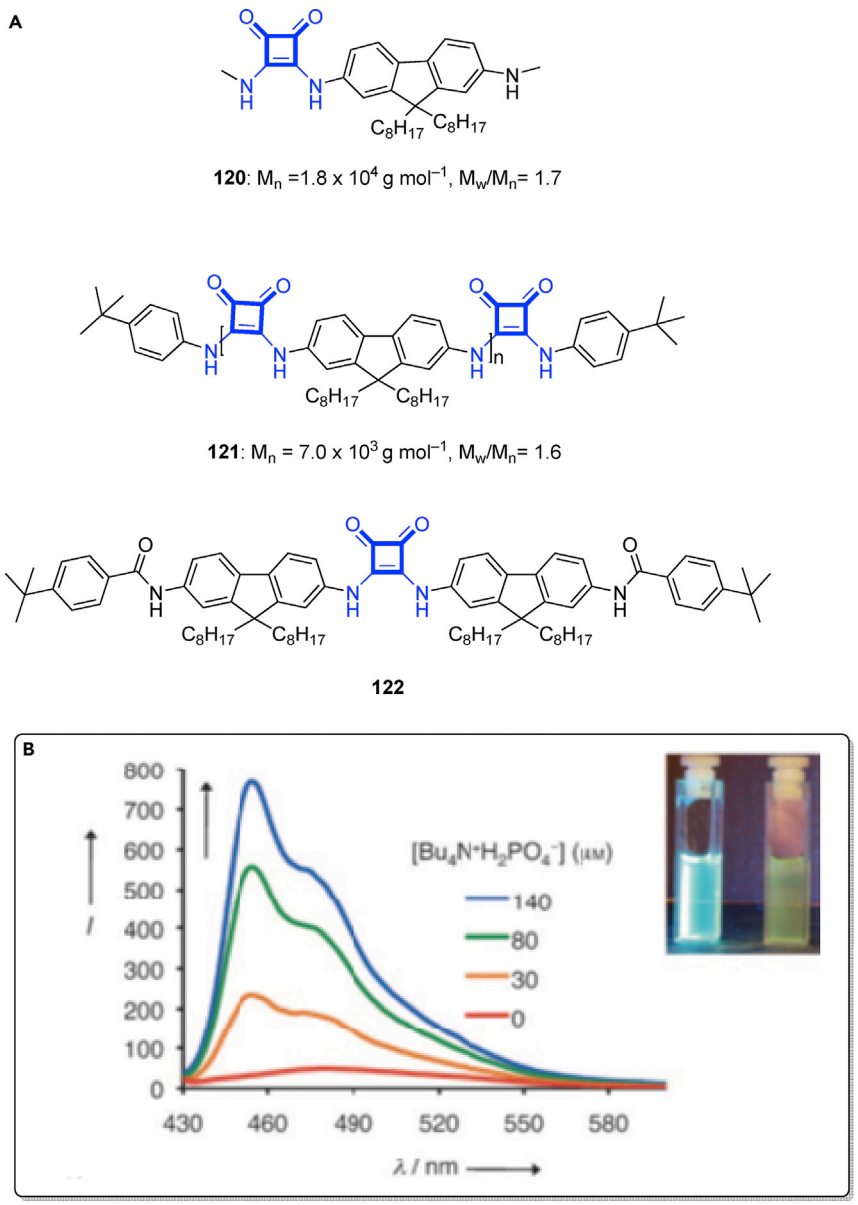

Figure 39. Fluorescent Squaramide-Based Polymers

(A) Chemical structures of poly(squaramide) compounds **120** and **121** and non-polymeric control receptor **122**.

(B) Fluorescence response of polymer 120 to increasing concentrations of $Bu_4N^+H_2PO_4^-$ in 10% water in NMP (λ_{ex} = 415 nm).

Reproduced with permission from Rostami et al.[100] Copyright 2011 Wiley-VCH Verlag GmbH & Co. KGaA.

hydrogen-bond donor groups and resulted in large enhancements in anion affinity and selectivity compared with those of the non-polymeric reference.

Delgado-Pinar et al. created a simple indicator displacement assay system of boehmite (γ-AlO(OH)) or silica-coated boehmite based on a squaramide scaffold with a quaternized amine group, **123** (Figure 40).[101] UV-vis spectrometry showed that these nanoparticles could selectively bind to SO_4^{2-} over $H_2PO_4^-$ and halide anions in pure water. The signaling in this system arises from the displacement of

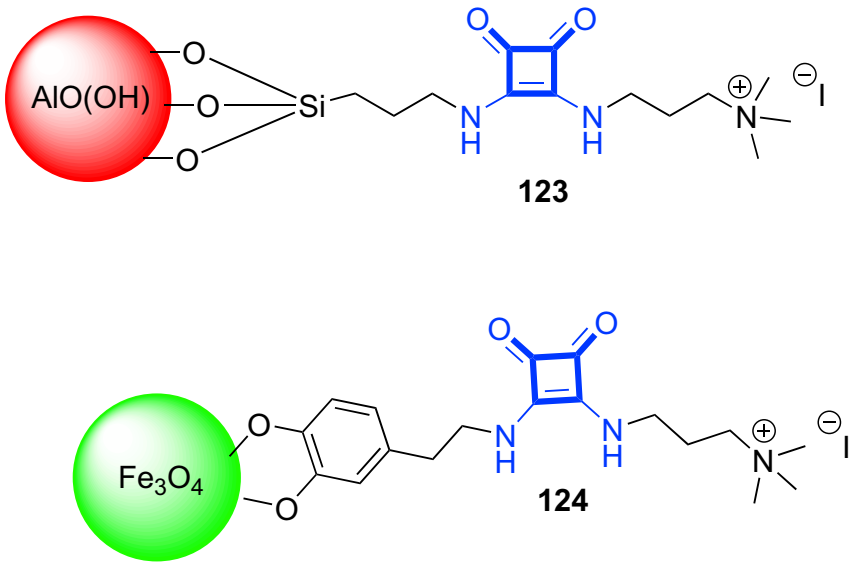

Figure 40. Schematic Representations of the Nanoparticle Appended Squaramides 123 and 124

Bromocresol Green when an anion binds to the receptor, resulting in a color change from blue to yellow.

López et al. followed a similar approach with iron nanoparticles functionalized with compound **124** (Figure 40), which could efficiently detect the presence of mono- and dicarboxylates in aqueous solution.[102] On their surface, these nanoparticles contained a high density of **124** capable of complexing the fluorescent dye fluorescein. Once complexed to the surface of the nanoparticles, fluorescein's fluorescence was quenched and subsequently restored upon release of the fluorescein when the carboxylate anion bound to the receptor. The nanoparticles were easily removed from solution magnetically and could detect mono- and dicarboxylates at mM levels in water.

As outlined above, a number of approaches have been reported for the use of squaramides for anion recognition and sensing, but more recently, one of the emerging applications of squaramides has been toward anion transport through lipid membranes. The development of synthetic anion transporters has been driven by the potential application of anion receptors in the treatment of various diseases caused by dysregulated anion transport or as a means of perturbing anion homestasis in cells.[73] Busschaert et al. were the first to evaluate squaramides as potential anion transporters by synthesizing a family of analogous squaramide-, thiourea-, and urea-based anion transporters, **125–133** (Figure 41), to establish and compare the anion-transport ability of squaramides against ureas and thioureas.[103] Using POPC liposomes, the authors found that these compounds acted as extremely efficient transporters promoting both nitrate-chloride exchange and bicarbonate-chloride exchange in an antiport process. The squaramides, in particular **131**, displayed considerably lower EC_{50} values than their urea and thiourea analogs, establishing them as superior anion transporters with potential biological applications (vide infra).

Analogous systems **134–136** (Figure 41) were reported by Busschaert and Elmes et al., who found that these thiosquaramide-based anion transporters exhibit pH-switchable anion-transport behavior.[104] Anion-binding studies showed that thiosquaramide **134** had a greater binding affinity for Cl^- than the oxosquaramide

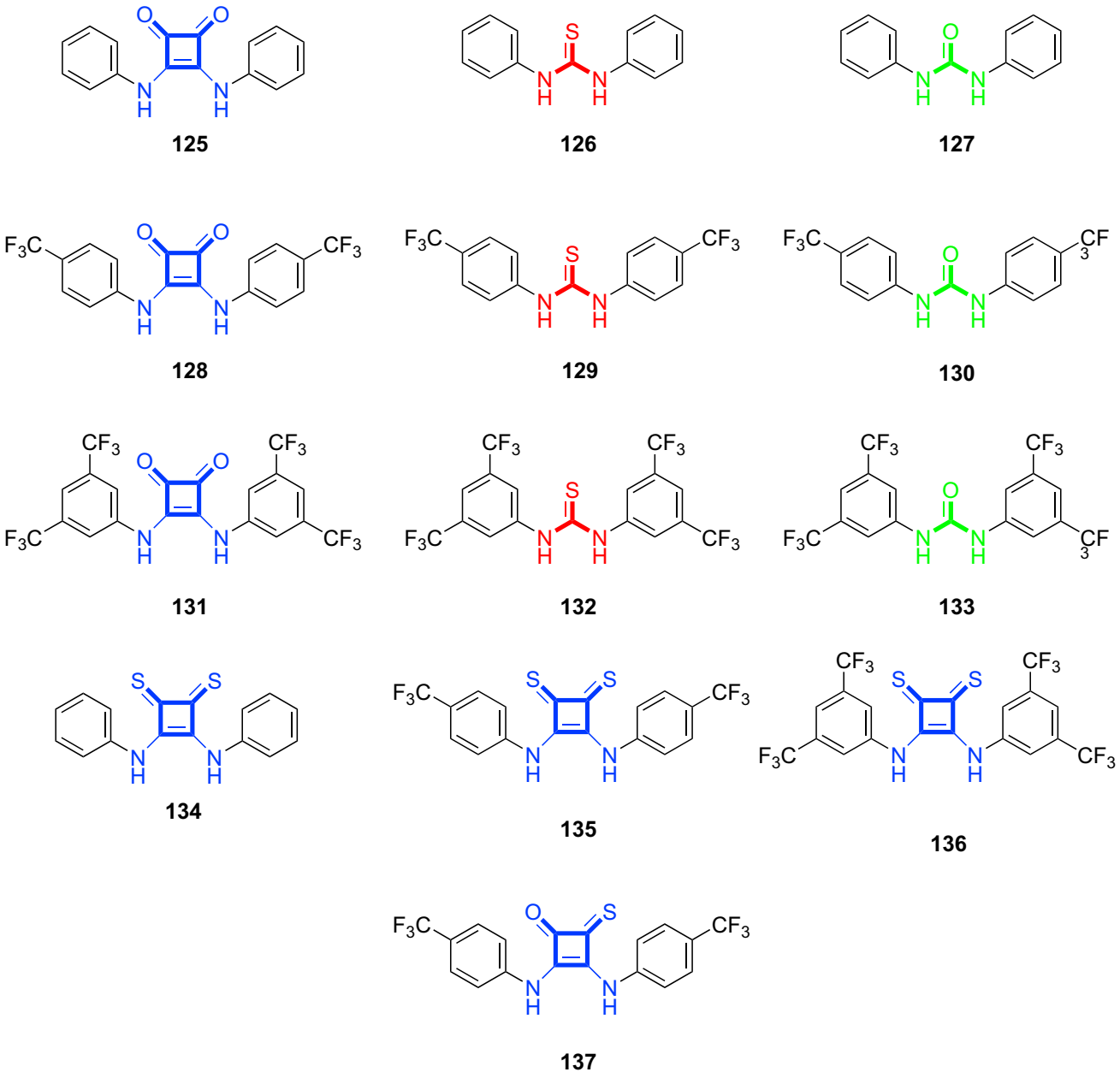

Figure 41. Chemical Structures of 125–137

analog **125**; however, the CF_3-substituted thiosquaramides **135** and **136** had significantly lower anion-binding affinity. Computational and experimental data established that the thiosquaramide NHs display lower pK_a values in aqueous solution than their oxosquaramide analogs and predominately exist in their deprotonated form at neutral pH, thus leading to extremely weak anion binding due to electrostatic repulsion. Indeed, using POPC liposomes loaded with NaCl solution, buffered at pH 7.2, the authors were able to determine that the anion transport ability of **134**–**136** was limited at this pH. However, when the anion-transport studies were repeated at pH 4.0, a significant increase in the transport abilities of **134** and **135** was observed, demonstrating the ability to switch anion transport "on" or "off" depending on the pH of the environment (Figure 42). A subsequent report from Elmes,

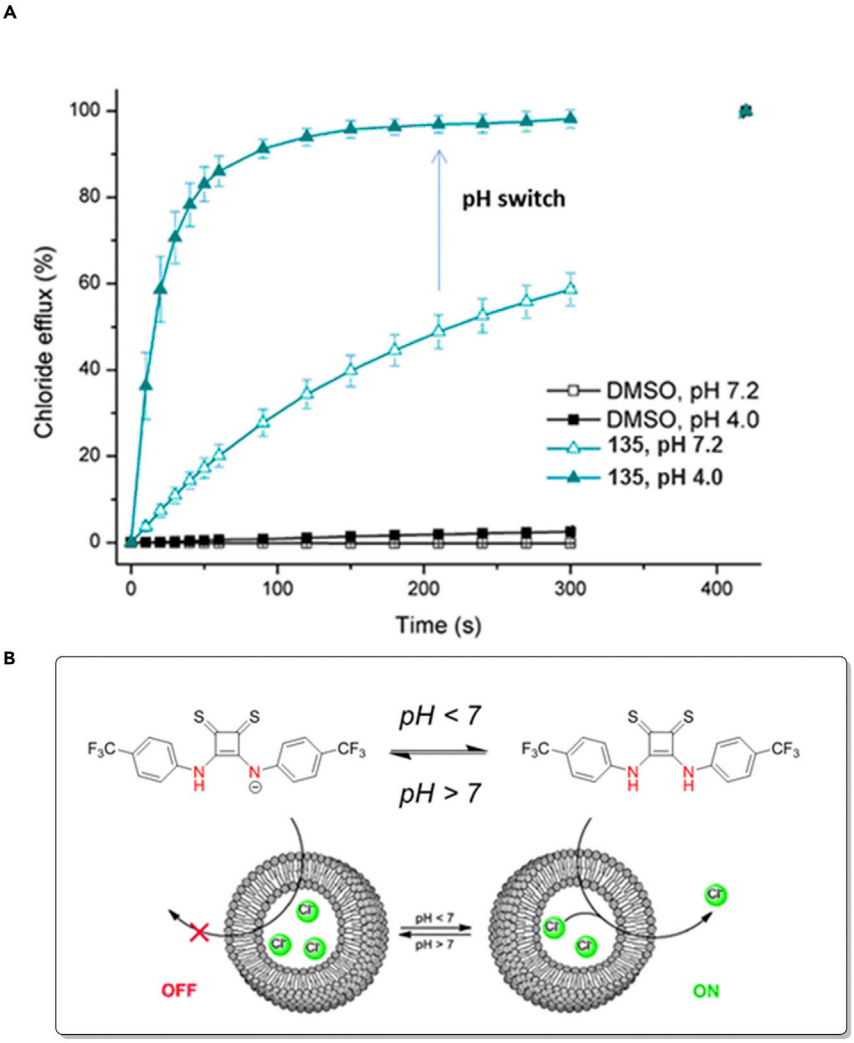

Figure 42. Thiosquaramide-Based pH-Switchable Anion Transporters

(A) Chloride efflux from POPC vesicles at pH 7.2 (empty symbols) and pH 4.0 (filled symbols) mediated by thiosquaramide **135** (1 mol % with respect to lipid) as measured by an ion-selective electrode (ISE). DMSO was used as a control.

(B) Schematic representation of the pH-switchable anion transport exhibited by compound **135**. Adapted from Busschaert et al.[104] with permission from the Royal Society of Chemistry.

Busschaert, et al. also demonstrated the pH-switchable nature of the oxothiosquaramide derivative **137**.[105]

Gale and co-workers have also exploited the squaramide motif to create a three-component assembly that can facilitate the transmembrane transport of amino acids.[106] Taking advantage of a combination of squaramide **131** (Figure 42) and 3,5-bistrifluoromethylbenzaldehyde (BTFMB), the authors proposed that the amino portion of glycine can form a hemiaminal or imine with the lipophilic aldehyde before **131** subsequently forms non-covalent hydrogen bonds to the glycine carboxylate group, thus facilitating reversible binding and releasing of the amino acid. This dynamic covalent approach increases the lipophillicity of the hydrophilic glycine, thus allowing facile transmembrane transport. Influx of glycine was measured by a novel fluorescence assay involving a Cu^{2+}-calcein complex whereby sequestration of the

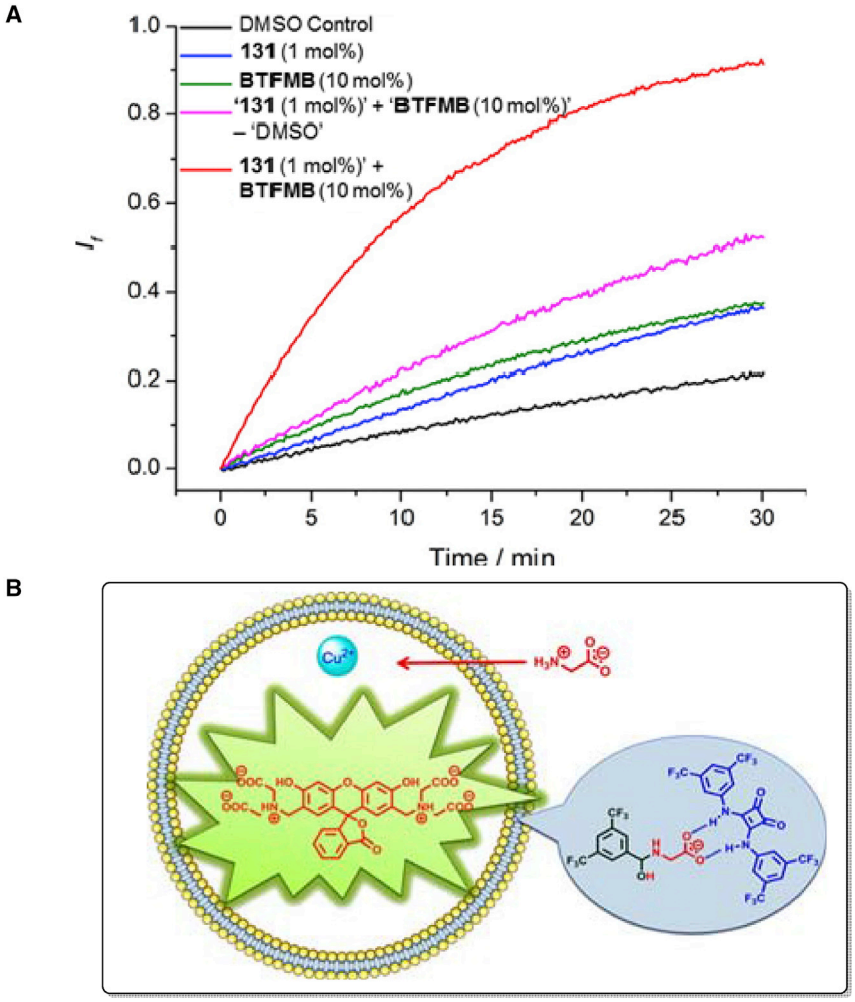

Figure 43. Squaramide-Facilitated Transmembrane Transport of Amino Acids

(A) Glycine transport kinetics mediated by squaramide **131** and **BTFMB** as measured by the Cu^{2+}-calcein assay. DMSO was used as a control.

(B) Schematic representation of the dynamic covalent chemistry approach to amino acid transport mediated by compound **131** and **BTFMB**.

Adapted with permission from Wu et al.[106] Copyright 2015 American Chemical Society.

copper from the calcein by the amino acid resulted in a restoration of calcein fluorescence, which was quenched by Cu^{2+} (Figure 43).

Gale, Davis, and co-workers have recently developed a family of steroid-based anion receptors with squaramides appended at the axial position, **138**–**143** (Figure 44).[107] The squaramide NH protons were shown to co-operatively bind to target anions, and the steroid ensured solubility in nonpolar media and efficient transmembrane transport ability. The acidic NH protons of the squaramide were shown to increase the binding affinity to a greater extent than those of urea and thiourea analogs synthesized previously.[108] Receptor **143** demonstrated the highest binding affinity to Cl^-, which can be attributed to the presence of the electron-withdrawing bis-3,5-trifluoroaniline moiety attached to the squaramide. Interestingly, the transmembrane transport abilities did not correlate with the anion affinities, which would suggest an upper limit to the binding strength of this class of anion receptors in the context of transmembrane anion transport.

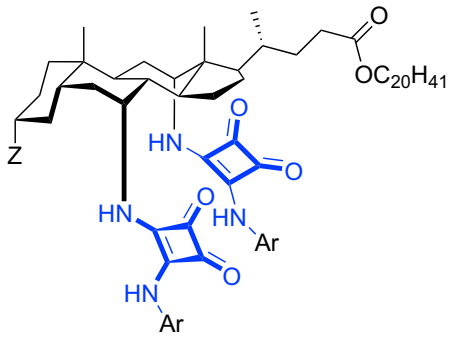

138; Z = OAc, Ar = 4-$MeOC_6H_4$
139; Z = OAc, Ar = Ph
140; Z = OAc, Ar = 4-$CF_3C_6H_4$
141; Z = OAc, Ar = 3,5-$(CF_3)_2C_6H_3$
142; Z = $NHCOCF_3$, Ar = 4-$CF_3C_6H_4$
143; Z = $NHCOCF_3$, Ar = 3,5-$(CF_3)_2C_6H_3$

Figure 44. Chemical Structures of Steroid-Based Anion Receptors 138–143

Jin et al. developed tripodal squaramide-based anion receptors **144–146** (Figure 45) and assessed their anion-binding abilities via ^{1}H NMR titration studies in DMSO-d_6.[109] The receptors displayed a higher affinity for SO_4^{2-} than for $H_2PO_4^-$, HSO_4^-, AcO^-, and Cl^- (Table 2). Receptors **145** and **146** with electron-withdrawing moieties displayed acid-base interactions with the more basic AcO^- and $H_2PO_4^-$ anions because of the increased acidity of the squaramide NH protons. X-ray crystal-structure analysis showed that receptor **144** bound to SO_4^{2-} via encapsulation and hydrogen bonding, where a dimeric complex was observed, whereas in organic solution, a 1:1 complex was observed through ^{1}H NMR analysis.

Liu et al. subsequently used **144–146** to produce a SO_4^{2-} ion-selective electrode.[110] The ionophore was added into a solution of THF, PVC, and a plasticizer, which was then drop cast onto gold electrodes, effectively embedding the ionophore in a polymeric membrane on the electrode. The tripodal squaramides mimicked the sulfate-binding protein by providing a cavity in which the SO_4^{2-} anion can participate in hydrogen bonding, in this case to the squaramide NH protons. The electrode containing ionophore **145** demonstrated the ability to determine the SO_4^{2-} concentration in drinking water from as low as 1 μM to 100 mM. The electrodes were also able to detect the presence of sulfate in cell lysate from 10 μM to 100 mM.

Cai et al. explored the transmembrane anion-transport ability of tripodal squaramide conjugates **146** and **147** (Figure 45) by measuring Cl^- efflux across egg yolk phosphatidylcholine (EYPC)-based liposomal membranes, monitored by a chloride-ion-selective electrode.[111] A pyranine assay was also used to characterize the efficiency of the Cl^-

Table 2. Binding Constants of Receptors 144–146 with Various Anions Determined by ^{1}H NMR

Anion[a]	Receptor 144	Receptor 145	Receptor 146
SO_4^{2-}	4.75 ± 0.11	4.95 ± 0.12	4.87 ± 0.07
$H_2PO_4^-$	4.15 ± 0.14	NA[b]	NA[b]
HSO_4^-	3.65 ± 0.12	3.78 ± 0.05	3.65 ± 0.14
AcO^-	2.82 ± 0.07	NA[b]	NA[b]
Cl^-	2.58 ± 0.08	2.61 ± 0.11	2.65 ± 0.09

NA, not applicable.
[a]Anions were used as tetrabutylammonium salts.
[b]Deprotonation was observed.

A

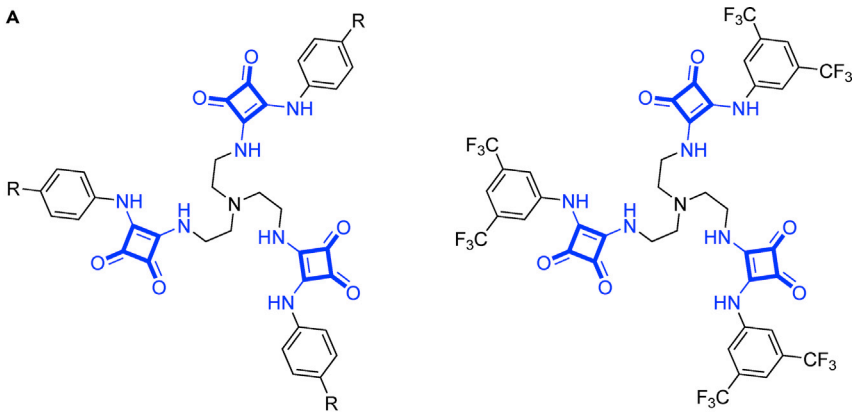

144; R = H, **145**; R = NO_2, **146**; R = CF_3 **147**

B

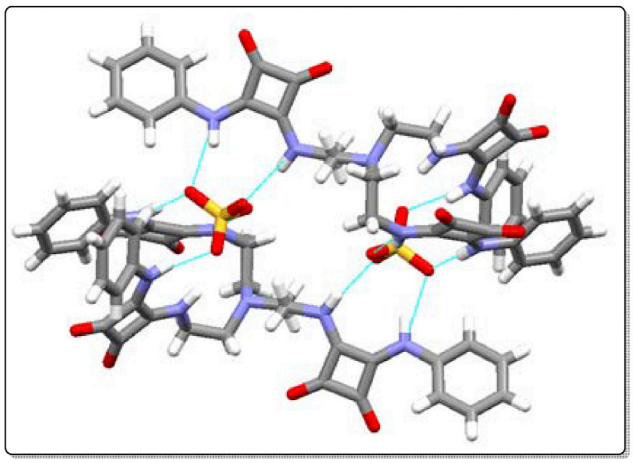

Figure 45. Tripodal Squaramide-Based Sulfate Receptors

(A) Chemical structures of tripodal receptors **144**–**147**.

(B) X-ray crystal structure of the dimeric complex formed between **144** and SO_4^{2-} in the solid state.

transport, where EC_{50} values of 0.14 and 0.75 mol % were determined for **146** and **147**, respectively, indicating that both receptors represent an effective class of anion transporters. Although compound **146** demonstrated a high binding affinity for SO_4^{2-} anion, as seen previously, it displayed minimal transport of SO_4^{2-} across liposomal membranes. In addition, the presence of SO_4^{2-} inside the liposomes inhibited Cl^- efflux, possibly as a result of the receptors' greater affinity for SO_4^{2-} anions than for Cl^- anions.

A squaramide-linked bis(choloyl) conjugate, **148**, was also successfully synthesized by members of the same research group: Deng et al. reported an evaluation of its anionophoric activity (Figure 46).[112] Using techniques similar to those previously described (pyranine assay and chloride-ion-selective electrode measurements), the authors observed potent ionophoric activity across EYPC-based liposomal membranes. The authors found that the rate of Cl^- release was independent of external cations and highly hydrophilic sulfate but was affected by external monoanions, suggesting that **148** functions via an anion-cation co-transport or symport process and highlighting the fact that the squaramide portion alone does not determine anionophoric ability and that the linker plays a crucial role in the process.

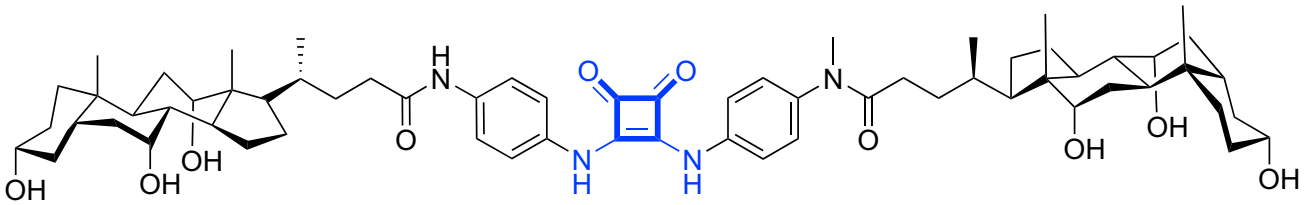

148

Figure 46. Chemical Structure of Squaramide-Linked Bis(choloyl) Conjugate 148

Gale and co-workers have recently reported a small series of fluorescent squaramide-based anion transporters, **149–152**, containing the 1,8-naphthalimide moiety (Figure 47).[113] These transporters displayed a strong binding affinity toward Cl^- and facilitated chloride transport via Cl^-/NO_3^- anti-port and Cl^-/H^+ symport mechanisms. Compound **149** was found to be the most active transporter in the series, correlating

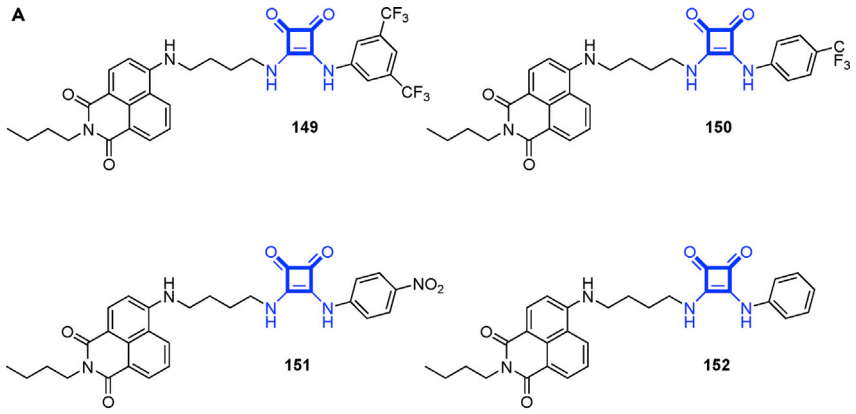

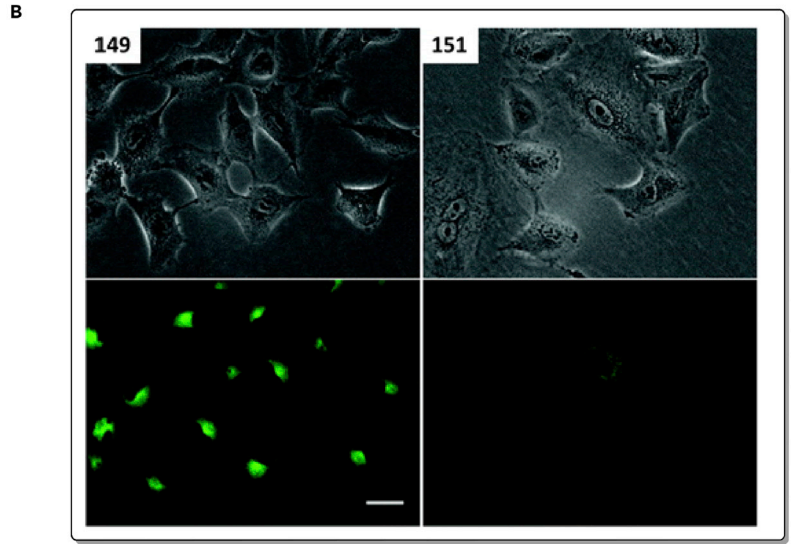

Figure 47. Fluorescent Squaramide-Based Anion Transporters

(A) Chemical structures of 1,8-naphthalimide-conjugated squaramides **149–152**.

(B) Fluorescent micrographs of A549 cells after incubation with compounds **149** (1.0 μM, left) and **151** (1.0 μM, right) for 24 h. The bright-field and fluorescent images are displayed in the upper and lower rows, respectively. Scale bar: 25 μm.

Reproduced from Bao et al.[113] with permission from the Royal Society of Chemistry.

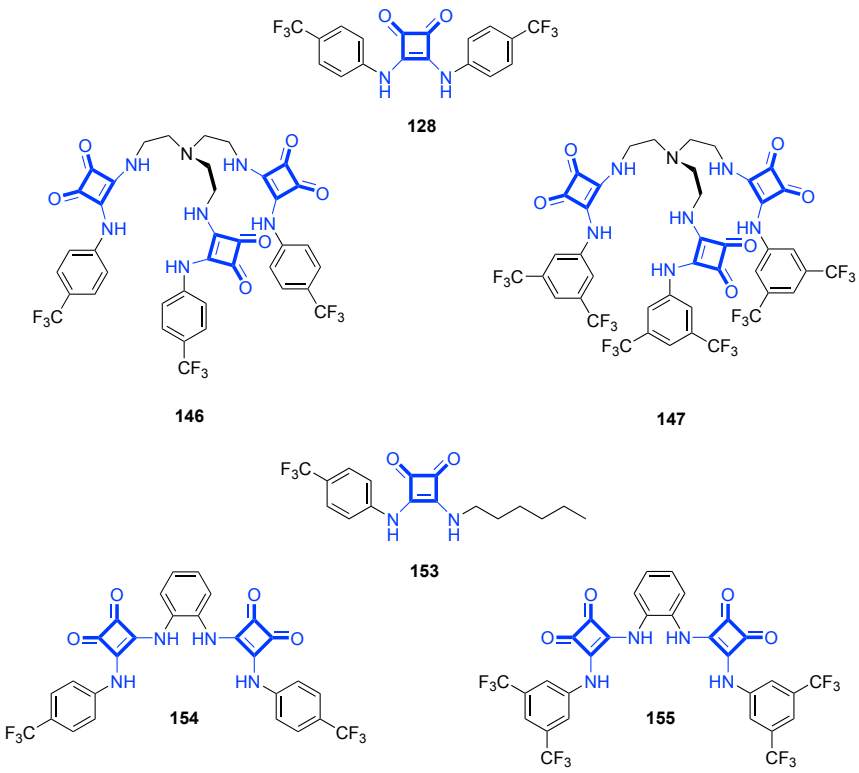

Figure 48. Chemical Structures of Squaramides 128, 146, 147, and 153–155

with its superior chloride affinity, and importantly, it was found to exhibit homogenous bright-green fluorescence within the cytoplasm of A549 cells (Figure 47). In addition, a CCK-8 toxicity assay showed that **149** had no toxicity in A549 cells. Such fluorescent transmembrane anion transporters will be useful for studying the sub-cellular localization and pharmacokinetics of anion transporters, where their development as potentially new drug candidates is another burgeoning area.

Indeed, Busschaert, Park, et al. recently examined the biological effect of squaramide-based anion transporters **128**, **146**, **147**, and **153–155** on a range of mammalian cell types (Figure 48).[114] The transport ability of the anionophores was first examined in POPC vesicles, where the efflux of Cl^- was monitored via a chloride-ion-selective electrode. Receptor **128** proved to be the most efficient anionophore across the POPC vesicles, followed by **154** and **155**. The tripodal receptors **146** and **147** were found to be inactive transporters, most likely because their binding affinity for Cl^- is too high, thereby inhibiting the release of the anion even after it crosses the membrane. Transporters **128**, **154**, and **155** were found to function as Cl^- transporters in combination with channel-mediated sodium co-transport in Fischer rat thyroid epithelial (FRT) cells. The effects of the anion transporters in HeLa and A549 cells were also investigated and shown to have the ability to induce caspase-dependent apoptosis by disrupting the intracellular chloride concentrations. **128** alone exhibited the ability to transport chloride anions out of lysosomes, decreasing the lysosomal chloride concentrations while increasing the pH, thereby reducing the activity of lysosomal enzymes, disrupting autophagy, and inducing apoptosis. This discovery is a major step toward elucidating the effects of transmembrane transporters in cells and could pave the way toward their use as a new class of anti-cancer agents. Indeed, a more recent report by Gale, Felix, and co-workers further investigated the transmembrane

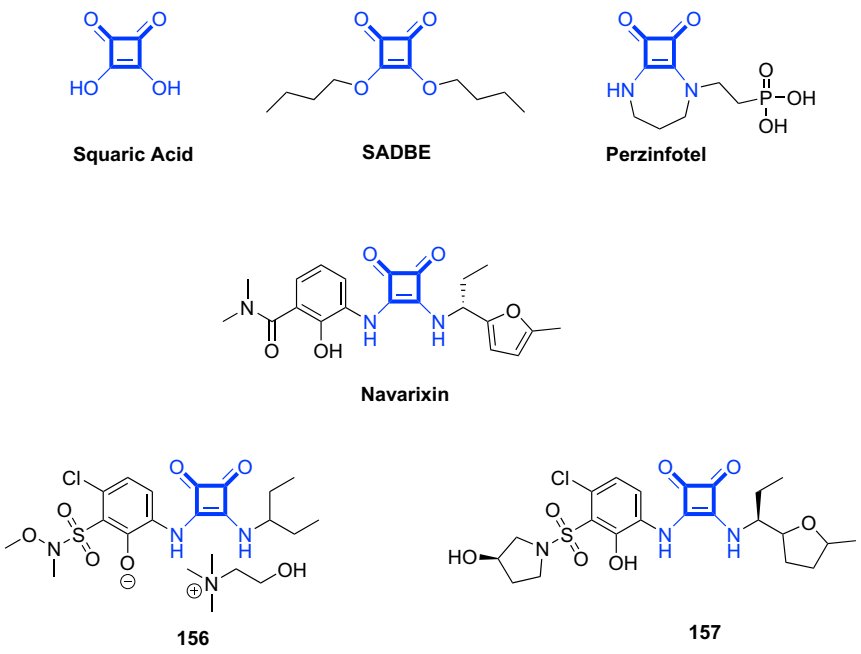

Figure 49. Chemical Structures of Some Squaramide-Based Drug Candidates under Investigation

anion-transport mechanism of squaramides by using *in silico* investigations; it found that compounds such as **128** showed assisted chloride translocation across phospholipid bilayers, which is thermodynamically favored.[115]

Although utilizing squaramides as anion transporters and exploiting their ability to disrupt normal cell function is a novel approach in medicinal chemistry, squaramides have also been reported in more traditional medicinal chemistry drug candidates and show potential across a broad range of illnesses.

SQUARAMIDES IN MEDICINAL CHEMISTRY

Squaric acid itself is known for the treatment of warts, and squaric acid dibutylester (SADBE) is also marketed as a treatment for alopecia. However, in more recent times, a number of squaramide-containing small-molecule drugs have entered clinical trials (Figure 49). Perzinfotel (EAA-090), a drug developed by Wyeth (now a wholly owned subsidiary of Pfizer), acts as a potent NMDA antagonist and was brought to phase 2 clinical trials for the treatment of neuropathic pain associated with diabetic neuropathy.[116,117] Navarixin (MK-7123) is an antagonist of the cysteine-X-cysteine chemokine receptor 2 (CXCR2) and is under development by Merck. This compound was brought to phase 2 clinical trials for chronic obstructive pulmonary disease (COPD) and is currently being investigated in phase 2 clinical trials as a combination therapy against a range of metastatic solid tumors.[118,119] Both Novartis and Boehringer Ingleheim have also reported squaramide-based drug candidates (**156** and **157**, respectively) for COPD treatment and even an early process-development study; however, despite multiple patent filings relating to CXCR2 antagonists, neither company appears to have progressed a candidate into development.[120,121] Nevertheless, with such fervent squaramide-based research activity within industry, it is clear that the potential of squaramides is now being realized, and early-stage development of small-molecule drugs containing the squaramide motif has continued apace. Below, we review some of the more recent advances showing the versatility and potential of squaramide-based therapeutics across a broad range

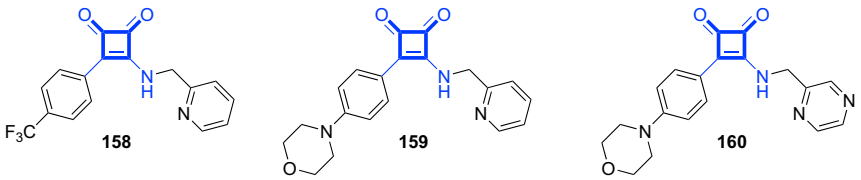

Figure 50. Chemical Structures of Squaramide-Based Drug Candidates 158–160, under Investigation

of disease states from anti-malarials to anti-cancer agents and treatments for more neglected diseases, such as Chagas disease.

A team of scientists led by Ravishankar and Hameed at AstraZeneca recently reported the synthesis of potent squaramide-based inhibitors of mycobacterial adenosine triphosphate (ATP) synthase as a new approach to fighting tuberculosis infection.[122] A structure-activity relationship (SAR) study for potency and selectivity identified a series of squaramide-based inhibitors, such as **158–160** (Figure 50), which were then evaluated in an ATP synthesis inhibition assay, where potencies in the nanomolar range were reported. Moreover, the lead compound, **160**, was found to be extremely specific as an inhibitor of ATP synthase without any observed cytotoxicity and retained activity against a panel of drug-sensitive and single-drug-resistant strains of *Mycobacterium tuberculosis*.

The Santos group has used the squaramide moiety in the search for a novel class of anti-malarial drugs that provide anti-parasitic activity against drug-resistant strains

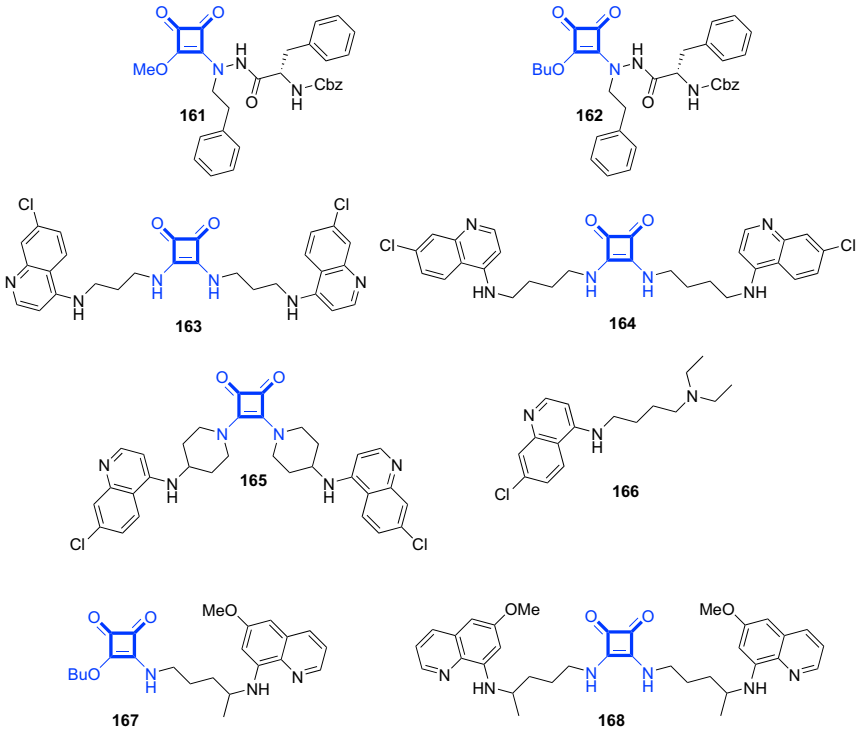

Figure 51. Chemical Structures of Squaramide-Based Anti-malarial Drugs 161–168, Reported by Santos and Co-workers

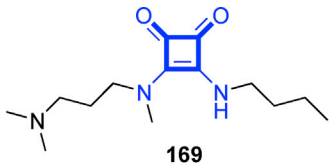

169

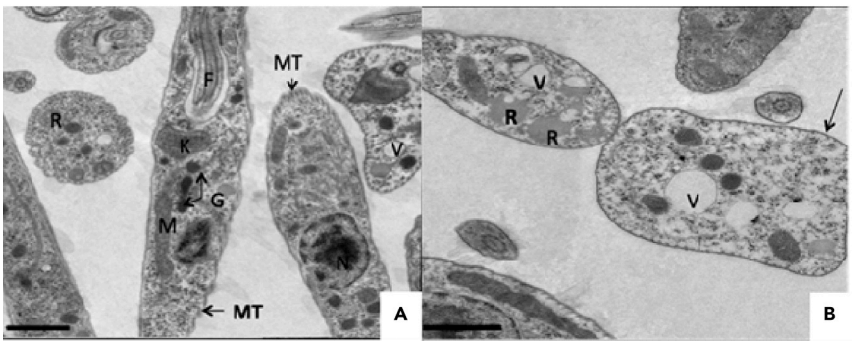

Figure 52. *N,N'*-Squaramides for Treating Chagas Disease

Chemical structure of squaramide **169** and TEM images of (A) a *Trypanosoma cruzi* control parasite showing typical organelles, such as mitochondria (M), glycosomes (G), microtubules (MT), vacuoles (V), reservosomes (R), kinetoplast (K), and flagellum (F) and (B) treatment with squaramide **169** showing ultrastructural alterations. Scale bar: 1 μm. Reproduced with permission from Olmo et al.[126] Copyright 2014 American Chemical Society.

of *Plasmodium falciparum*. The synthesis of a library of 38 squaric derivatives was reported, whereby each candidate was evaluated against several drug-resistant strains of *P.falciparum*.[123] Aza-dipeptidyl squaric acid derivatives displayed good anti-plasmodial activity, and the most active compounds, such as **161** and **162**, contained an "azahomoPhe" moiety and displayed IC_{50} values in the μM range (Figure 51). No cysteine protease inhibition was observed for these compounds, thus leading the authors to speculate that the anti-plasmodial activities of **161** and **162** might stem from inhibition of other proteases involved in the parasite life cycle—a key point of difference to many known anti-malarial drugs.

A subsequent report detailed the synthesis and a SAR analysis of a series of hybrid compounds containing a squaramide moiety conjugated to the heteroaromatic core of 4-amino-7-chloroquinoline (Figure 51).[124] Three of the reported structures, **163**, **164**, and **165** (IC_{50} values = 99, 95, and 105 nM, respectively), had greater *in vitro* potency than the known anti-malarial chloroquine **166** (IC_{50} = 140 nM) against a chloroquine resistant strain of *P. falciparum*. Moreover, these compounds were found to be non-cytotoxic against NIH-3T3 and Hek 293T cells, thus representing a promising new class of anti-plasmodial agents.

Most recently, a report from the same group detailed a SAR study generating ten 8-aminoquinoline-squaramide conjugates that are active against liver stage malaria parasites.[125] In human hepatoma cells (Huh7) infected by *Plasmodium berghei* parasites, conjugates **167** and **168** showed 7.3-fold more potency against the liver stage of *P. berghei* infection than the known anti-malarials primaquine and bulaquine, again highlighting the importance of the squaramide moiety for anti-plasmodial activity in this class of compounds.

In a related therapeutic area, Costa and co-workers synthesized a series of *N,N'*-squaramides with high *in vivo* efficacy and low toxicity for treating Chagas disease,

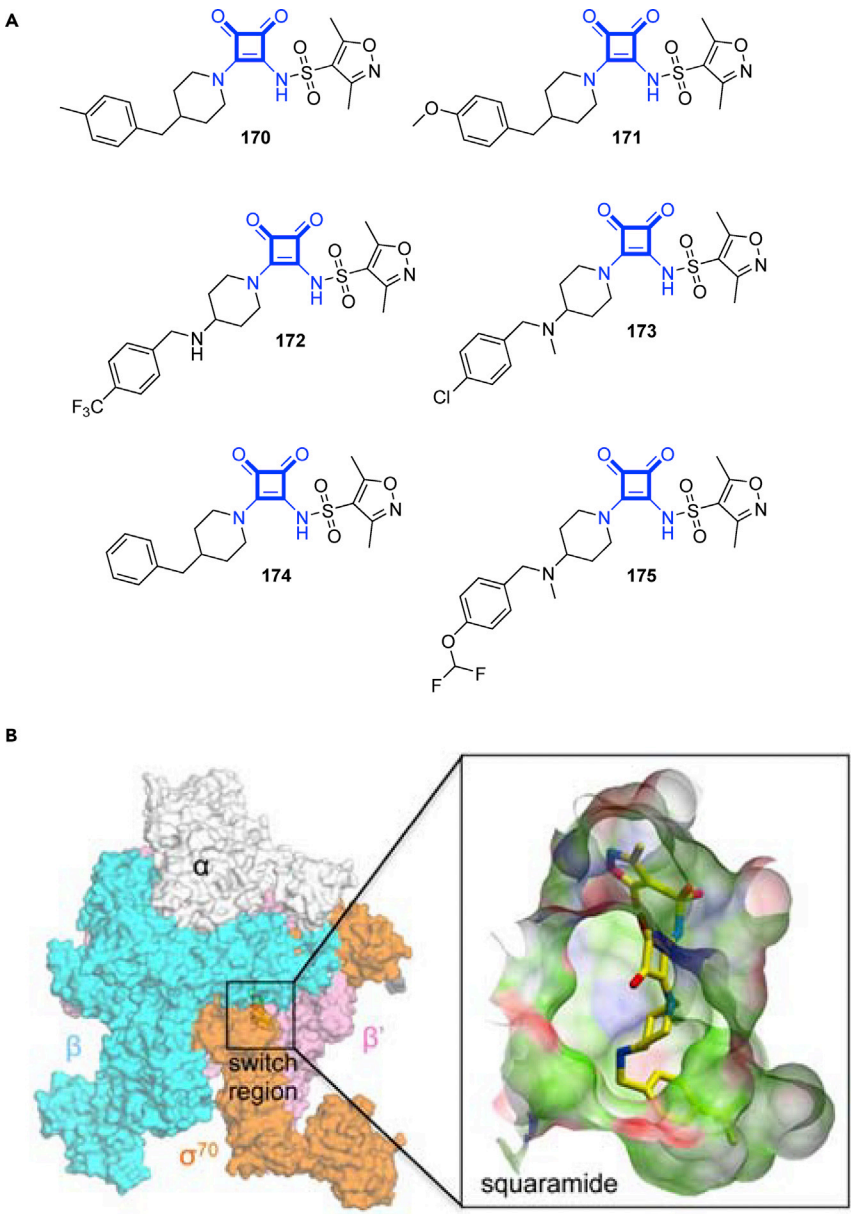

Figure 53. Squaramides as Antimicrobials

(A) Chemical structures of some squaramide-based anti-bacterial drugs under study at Astra Zeneca.

(B) Schematic representation of the RNA polymerase-squaramide complex structure showing the overall structure of the *E. coli* RNAP in complex with compound **172** and a representation of the squaramide-binding pocket.

Reproduced with permission from Molodtsov et al.[128] Copyright 2015 American Chemical Society.

a *Trypanosoma cruzi* infection that is considered one of the world's neglected tropical diseases with the highest death rates.[126] Compound **169** was found to be the most effective and gave rise to a 67% decrease in the infection rate of Vero cells, making it much more effective than other clinically available drugs, such as benznidazole. Moreover, *in vivo* studies revealed that compound **169** was an effective treatment in both the acute and chronic phases of Chagas disease in that minimal toxicity was observed. From transmission electron microscopy (TEM) analysis 169

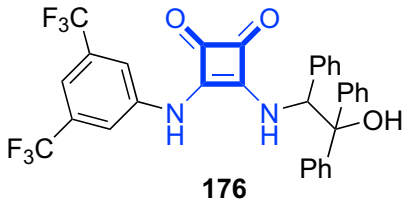

176

Figure 54. Chemical Structure of Potent Cytotoxic Squaramide 176

was shown to induce a complete breakdown of the parasites cellular structure characterized by significant modifications to many cytoplasmic organelles (Figure 52). This promising *in vivo* activity together with its minimalist molecular structure and simple synthesis prompted the authors to patent the drug in advance of preclinical development.

Squaramides have also been exploited as a novel class of antimicrobials. Fleming and co-workers at AstraZeneca originally reported the synthesis of a series of squaramide-based anti-bacterials, **170–173** (Figure 53).[127] Although the series of compounds displayed weak to moderate antimicrobial activity against a range of bacteria, their mode of action was found to be through inhibition of RNA and protein synthesis, specifically via inhibition of the switch region of RNA polymerase—a known target of naturally occurring antimicrobials, such as myxopyronin, corallopyronin, and ripostatin. Importantly, these squaramides were the first reported non-natural-product-related inhibitors of the switch region of RNA polymerase, and with their ease of synthesis and facile derivatization, a subsequent report led by Murakami and co-workers soon followed.[128] From the starting point of **174**, a SAR study determined that the terminal isoxazole and a benzyl group appended to a squaramide are crucial for biochemical potency and bind into distinct relatively narrow, hydrophobic pockets in the enzyme. Moreover, **172**, **173**, and **175** were found to display 20- to 60-fold higher *in vitro* antimicrobial activity against an efflux-negative strain of *Haemophilus influenzae* than **174**. Through X-ray crystal-structure analysis of *Escherichia coli* RNA polymerase co-crystallized with compound **172** (Figure 53), the authors predicted that drug binding in this region interfered with the conformational change of the clamp domain and/or with binding of template DNA to RNA polymerase, a mechanism similar to that of natural product myxopyronin.

The use of squaramides in the development of novel anti-cancer agents has also gained research attention in recent years. Triola and co-workers synthesized a large series of squaramates and squaramides and conducted an investigation into their cytotoxic activity in different cancer cell lines.[129] Compound **176** (Figure 54) was revealed as the lead compound because it exhibited potent and selective cytotoxicity against the human gastric cancer cell line HGC-27. Cell-cycle distribution analysis and cell-death studies showed that compound **176** induces cell-cycle arrest at the G1 phase and subsquent caspase-dependent apoptosis, leading the authors to pursue squaramide **176** as a novel agent for the treatment of gastric carcinoma.

Very recently, Fournier et al. at Nestlé Skin Health reported a series of squaramide-based hydroxamic acids, **177–180** (Figure 55), that were found to act as histone deacetylase (HDAC) inhibitors. Such HDAC inhibitors, which can disrupt chromatin folding, have been exploited in recent years for the oral treatment of cutaneous T cell lymphoma (CTCL), culminating in the FDA approval of vorinostat and romidepsin. Squaramides **177** and **178** were found to exhibit subnanomolar binding values to HDAC1 and nanomolar EC_{50} values against the HuT78 cell line (cutaneous T

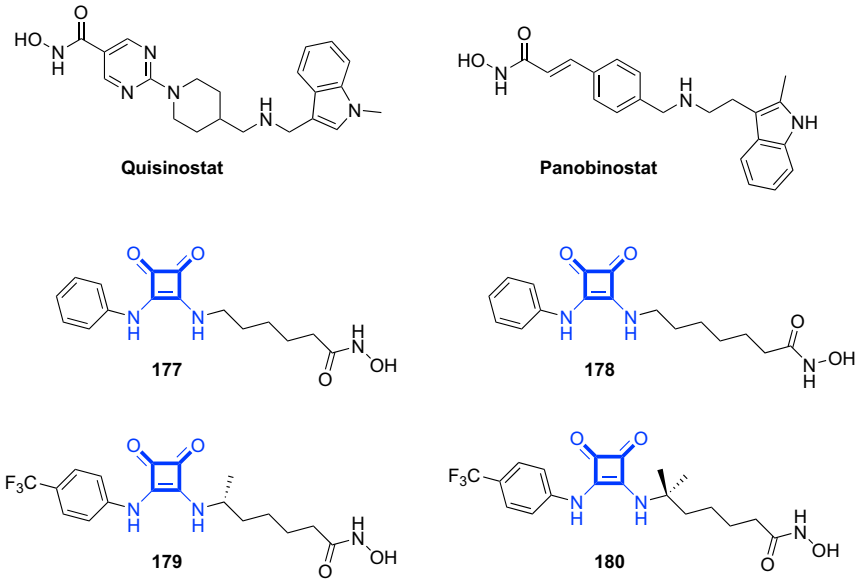

Figure 55. Chemical Structures of Clinically Approved HDAC Inhibitors Quisinostat and Panobinostat and Squaramide-Based HDAC Inhibitors 177–180

lymphocyte). Several series of compounds were explored, and it was found that many candidates suffered from problems of solubility but showed high potency, whereas those with improved solubility suffered from a reduction in potency. Overall, compound **180** displayed the most promising activity with cellular potency comparable to those of investigated or approved drugs, such as quisinostat and panobinostat, but with a profile better suited for topical treatment of CTCL.

In a further example of squaramide-based anti-cancer agents, Zhou and co-workers have reported several novel estrogen-derived metal complexes, in which the squaramide moiety was used as a metal chelator.[130] Ligand **181** was prepared by a four-step synthetic strategy before reaction with three transition metals (Pd, Ni, and Zn) yielded metal complexes **182a–182c** (Figure 56). Estrogen receptor (ER)-binding affinities of complexes **182a–182c** were measured by a competitive fluorescence polarization binding assay using both purified human subtypes (ERα and ER_β) and compared with estradiol. The authors demonstrated that all complexes retained binding affinity for both subtypes (except **182c**, which was selective for ER_α); **182b** showed the highest affinity for ER_α (2.3% ± 0.5%), and **182a** showed the highest affinity for ER_β (0.85% ± 0.05%). Furthermore, transcriptional activity tests using Luciferase reporter gene assays in human embryonic kidney (HEK-293T) cells showed that all of the complexes were agonists of ER_α, and **182a** and **182c** showed greater agonist activity than the neutral free ligand **181**. Several ER agonists are clinically approved for the treatment of breast cancer; thus, the results of this study could yield a new approach for novel squaramide-based breast cancer therapeutics.

Wan et al. have also reported squaramide-based metal complexes for medicinal application; for example, bisperoxovanadium(pyridine-2-squaramide) **183** has been shown to exert a neuroprotective effect in cerebral ischaemia-reperfusion (Figure 57).[131]

The study demonstrated that **183** inhibited the activity of phosphatase and tensin homolog deleted on chromosome 10 protein (PTEN) (a phosphatase that dephosphorylates proteins and lipids; IC_{50} = 39.44 ± 5.92 nM) and increased Akt activity

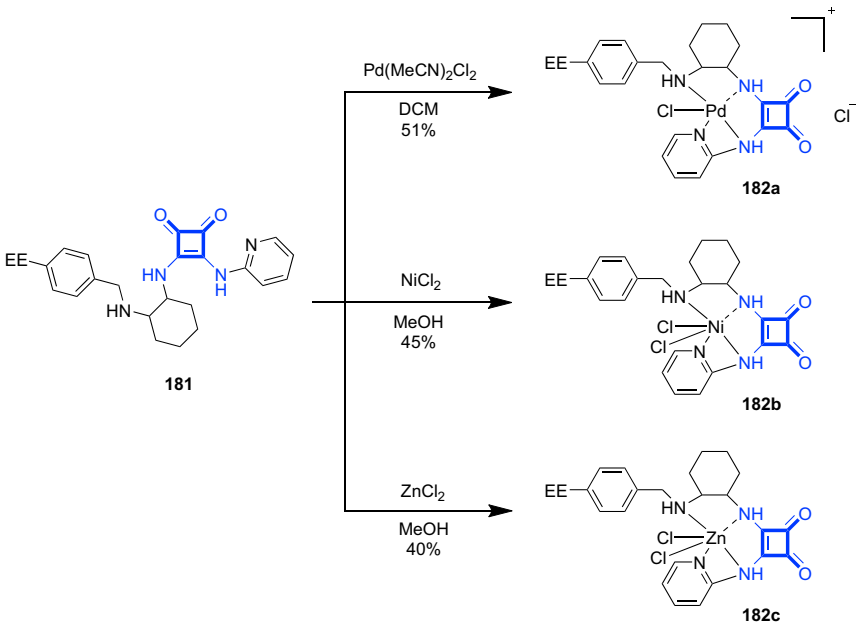

Figure 56. Synthesis of Estrogen-Derived Squaramide Metal Complex Inhibitors 182a–182c from Ligand 181

(Akt is a multi-isoform serine/threonine kinase implicated in cell survival and growth). Moreover, **183** was also shown to elevate ERK1/2 (believed to mediate cell survival, neuronal plasticity, and migration) albeit via an independent pathway, thus preventing neuronal death *in vitro* and promoting functional recovery in stroke animals. The authors concluded that **183** confers its neuroprotective action by suppressing PTEN and activating ERK1/2 and thus yields a bi-target neuroprotectant that could be developed as a future treatment for stroke.

Although this has been a non-exhaustive list, we have used the above examples to highlight recent progress in the use of squaramides in both academic and industrial research programs for new drug candidates. The breadth of disease states under investigation in addition to the diverse structures involved shows the vast scope and potential of squaramides for use in medicinal chemistry. The recent increased interest in drug-based squaramides serves to further highlight the future potential of this class of compounds, where the surface has barely been scratched. The final area that we focus on in this review is the utility of squaramides in bioconjugation

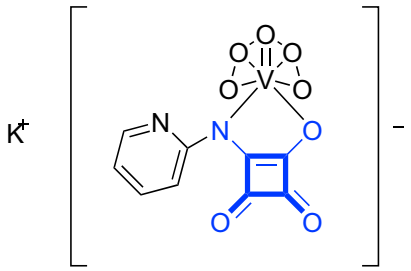

183

Figure 57. Chemical Structure of Bisperoxovanadium(pyridine-2-squaramide) 183

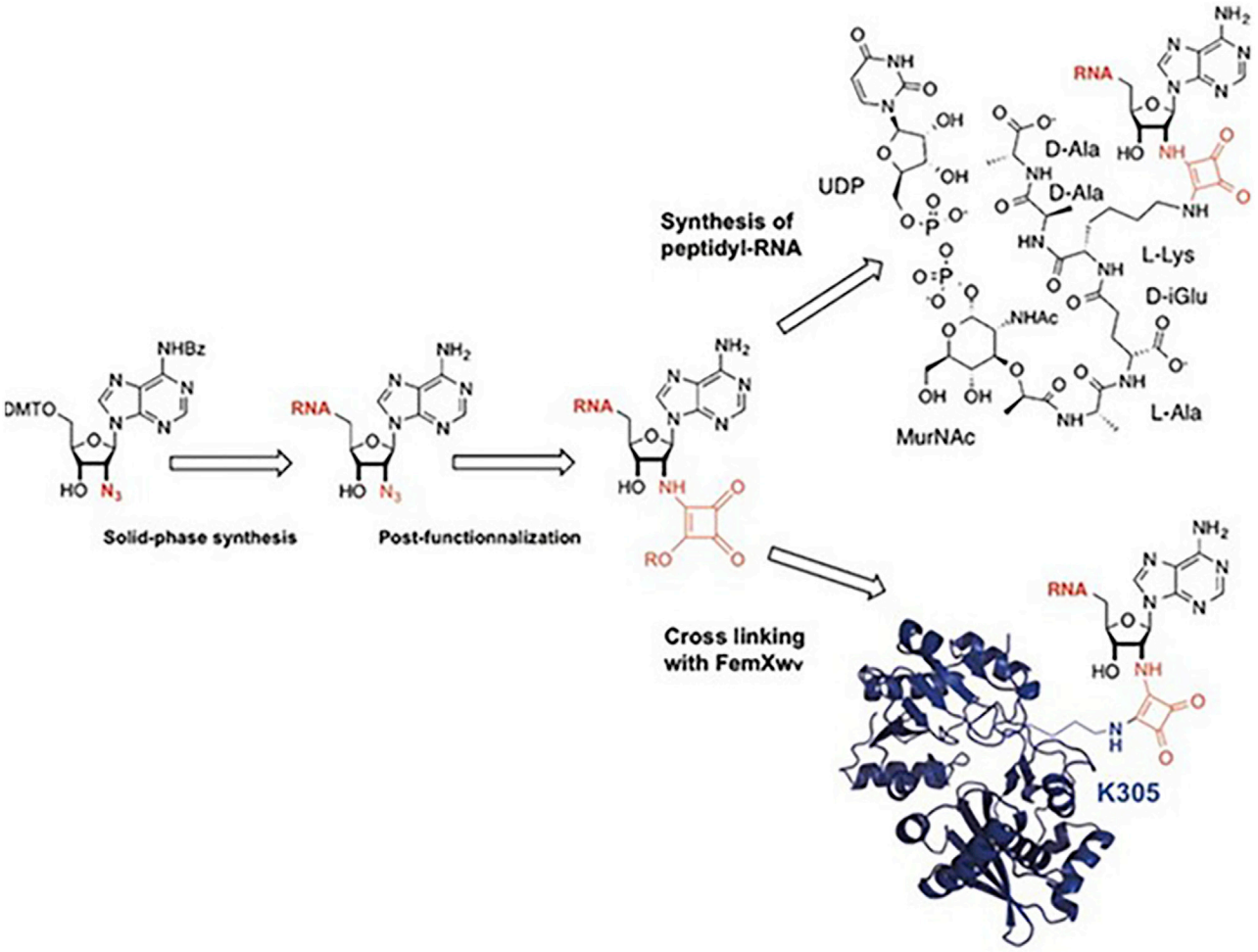

Figure 58. Synthesis of Squaramate-RNA for Peptidyl-RNA Synthesis and Cross-Linking with Active Site K^{305} of the Aminoacyl-Transferase $FemX_{Wv}$
Reproduced with permission from Fonvielle et al.[133] Copyright 2016 Wiley-VCH Verlag GmbH & Co. KGaA.

reactions, where again, the versatility and simplicity of the squaramide moiety serve many advantages for the chemistry and biology communities.

SQUARAMIDES AS A TOOLS FOR BIOCONJUGATION

Coupling reactions with squaric acid derivatives, such as diethyl-, dimethyl, ditertbutyl, and dichloro squarate, have found increased utility as a useful method of bioconjugation because of facile reaction protocols, high reaction yields and high functional-group tolerance, and usually very high conversions. Glüsenkamp et al. were some of the first authors to recognize the potential of squaric acid derivatives as useful bioconjugation scaffolds; they synthesized a range of squaric acid amides containing lysine, biotin, bovine serum albumin, and adenine.[132] Since then, many examples of squarate-mediated bioconjugations covering a diverse range of biomolecules have been reported. Below, we review some recent examples.

Etheve-Quelquejeu, Arthur, and co-workers utilized a squarate conjugation strategy toward facile RNA functionalization whereby the introduction of a squaramide monoester provides an electrophilic site at the 3′ end of RNA (Figure 58).[133] The authors showed that they could synthesize peptide-RNA conjugates in a facile manner

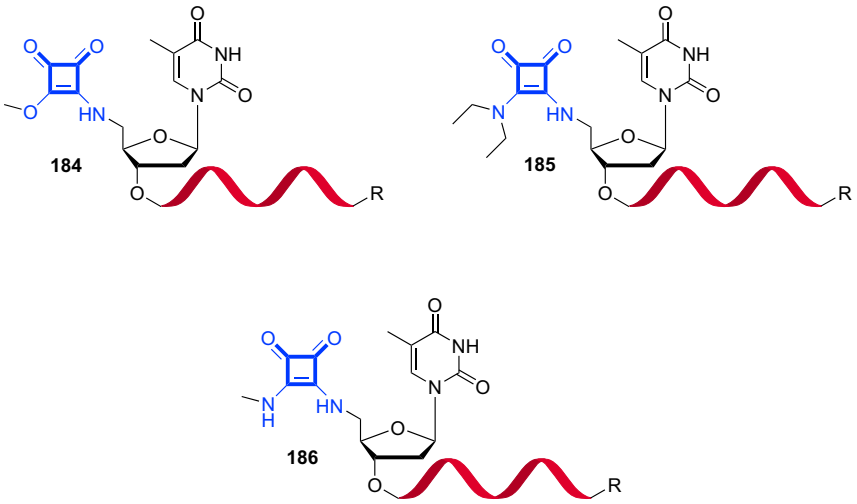

Figure 59. Chemical Structures of Modified Oligonucleotides 184–186, Containing Squaramides as Phosphate Replacements at the 5′ End

R = either OH or the cyanine-based Cy3 fluorophore.

by taking advantage of the reduced reactivity of the monosquaramide resulting from the first amidation step. This feature enabled sequential amidation reactions leading to asymmetric squaramide containing peptidyl-RNA conjugates with high selectivity and in high yields. The strategy proved particularly attractive because the electrophilic squaramate-RNAs had the ability to specifically react with the primary amines of the targeted unprotected peptides in spite of the presence of phosphate, hydroxyl, and carboxylic acid functional groups. The authors used the protocol to synthesize an RNA-UDP-MurNAc-pentapeptide in 23% yield in aqueous buffer (500 mM borate at pH = 9.2) and also showed that increasing the size of the RNA moiety did not reduce the efficiency of the coupling reactions. Indeed, a newly synthesized RNA-UDP-MurNAc-pentapeptide conjugate was further biologically evaluated where it was shown to successfully inhibit the aminoacyltransferase FemXWv from *Weissella viridescens*, an aminoacyl-transferase involved in bacterial cell wall synthesis, with an IC_{50} value of 123 $\pm$ 6 nm. A squaramate-RNA was also found to specifically react with FemXWv enzyme at the catalytic Lys 305 residue despite the presence of several other lysines. This result further highlights the useful properties of the squarate moiety and its ability to act as a versatile tool for the synthesis of both peptidyl- and protein-RNA conjugates.

McGouran and co-workers recently reported the first example of a squaramide modification at the 5′-terminal position of oligonucleotides. The authors reported the synthesis of oligonucleotides **184–186** (Figure 59), where the 5′-phosphate was replaced by different squaramides introduced chemoselectively after solid-phase synthesis.[134] The resulting oligonucleotides were evaluated for their ability to perform as phosphate isosteres by using the Zn^{2+}-dependent exonuclease SNM1A. This enzyme has 5′-to-3′ activity and requires a terminal 5′-phosphate for substrate recognition and catalysis. This model system revealed that introduction of the squaramide modification yielded minimal recognition as a 5′ phosphate mimic; however, inhibition of SNM1A was observed and thought to occur through Zn^{2+} coordination at the enzyme active site.

Donnelly, Hicks, and co-workers reported the synthesis of a squarate derivative of desferrioxamine B, a hexadentate bacterial iron siderophore that can act as a ligand

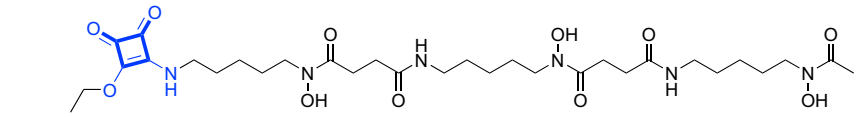

187

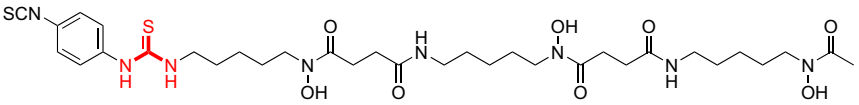

188

Figure 60. Chemical Structures of 187 and 188

for $^{89}Zr^{IV}$ radiopharmaceuticals.[135] The study reported a simple squaramate derivative of desferrioxamine B, **187** (Figure 60), which was found to be an excellent ligand with potential to label antibodies, proteins, and peptides with $^{89}Zr^{IV}$ while having the desired shelf stability and the ability to react rapidly with amino groups in proteins and peptides under mild conditions (labeling was complete in $\leq$30 min, ca. 100% labeling was measured by iTLC, and the ligand was found to be stable for $\geq$5 months when stored at 20°C). Moreover, the use of the squaramide linker provided the possibility that the dione backbone of the squaramide might coordinate to Zr^{IV} to give putative 8-coordinate complexes. The versatility of **187** to partake in antibody conjugations was demonstrated in separate conjugation reactions with the anti-CD20 antibody, rituximab, the metalloprotein transferrin, and trastuzumab, an antibody that binds to the extracellular domain of human epidermal growth factor receptor 2 (HER2) and is used as a therapy for treatment of HER2-positive breast cancer. Imaging studies with human ovarian high-copy HER2 cell line SKOV3 xenograft models demonstrated enhanced imaging capability of the ^{89}Zr-**187**-trastuzumab conjugates compared with the thiourea derivative **188**, for which reduced liver and bone uptake and increased tumor and spleen uptake were measured.

Ito and co-workers reported a similar approach for the conjugation of the BODIPY-modified $Man_9GlcNAc_2$derivative **189**, equipped with a reactive squarate (Figure 61).[136] Probe **189** was evaluated for its ability to label UDP-glucose:glycoprotein glucosyltransferase (UGGT), an enzyme with the ability to transfer a glucose residue to N-glycan moieties of incompletely folded glycoproteins. As in the previous examples, the authors exploited the electrophilic nature of the squarate moiety to promote bioconjugation with nucleophilic amino acid residues in the aglycon-recognition site of human UGGT, resulting in squaramide formation. Indeed, the authors were able to successfully label the UGGT active site by reaction at a unique lysine residue (K1424), thus gaining valuable insight in to the folding sensing mechanism of human UGGT1 (HUGT1).

After the original work of Glüsenkamp et al.[132] nucleotide conjugation was further explored by Sekine and co-workers, who designed novel analogs of 2′-deoxynucleotides and ribonucleotides that incorporated the squaramide moiety.[137] By replacing the phosphoric acid residues of natural nucleotides with squaric acid the authors suggested that such molecules might act as electronic isosters of 5′-nucleotides. Because of their strong acidity (pK_a= 2.3), the nucleotide analogs were thought to exist in the mono-anionic form; thus, under physiological conditions, they would display unique structural, electronic, and conformational properties that would mimic those of the natural nucleotides and could give rise to potential biologically

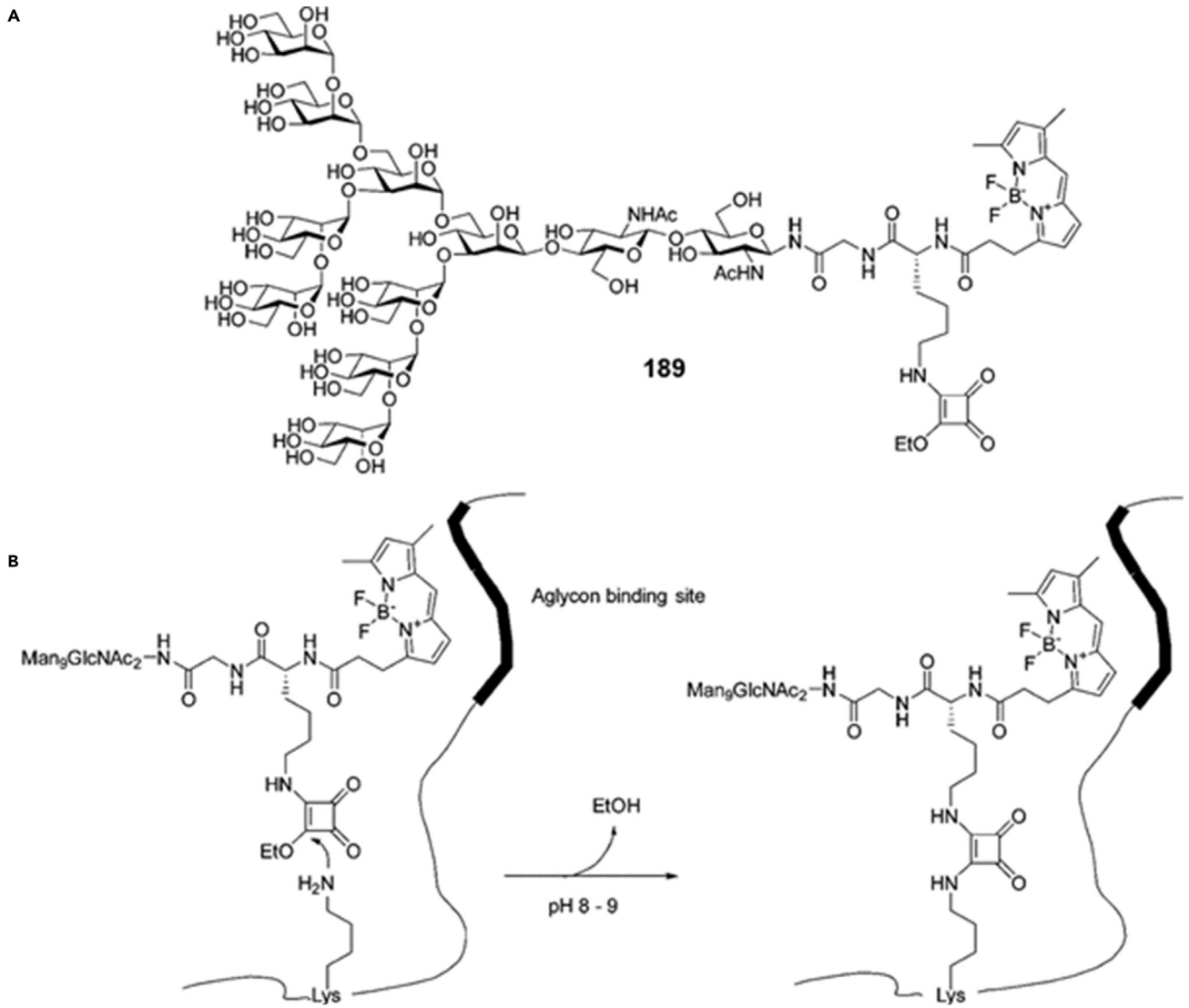

Figure 61. Squaramide-Based Protein Labeling

(A) Chemical structure of probe **189**.

(B) Labeling of UGGT with probe **189**.

Reproduced with permission from Ohara et al.[136] Copyright 2015 American Chemical Society.

active compounds, such as anti-viral or anti-cancer agents. Indeed, Honek and co-workers subsequently investigated some novel squarate-based carbocyclic nucleosides for their anti-viral and anti-cancer properties (Figure 62).[138] Although compounds **190–192** displayed some modest anti-cancer activity against a range of cancer cell lines (including non-small cell lung cancer [NCI-H522], ovarian cancer [OVCAR-8]), leukemia [CCRF-CEM], renal cancer [UO-31], colon cancer [KM12], melanoma [UACC], and CNS cancer [SF-295]), no anti-viral properties were reported.

Another interesting example of squaramide conjugation to nucleotides was recently reported by Kieltyka and co-workers, who investigated the use of bis-squaramide **24** as a supramolecular polymer (vide supra).[4] They subsequently synthesized squaramide bola-amphiphile DNA oligonucleotide conjugates **193** (DNA sequence = 5-hexynyl/TTAACCCACGCCGAAT) and **194** (5-hexynyl/TATACGTGCATACGAT)

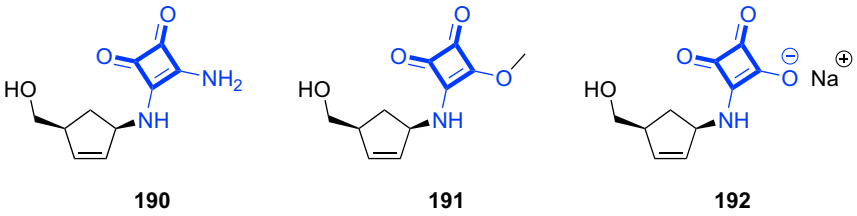

Figure 62. Chemical Structures of Squarate-Based Carbocyclic Nucleosides 190–192

and demonstrated their capacity to act as effective multi-component supramolecular polymers capable of recognizing DNA-labeled gold nanoparticles (Figure 63).[139] Through TEM analysis, gel electrophoresis, fluorescence quenching, and thermal denaturation experiments, they observed reversible loading and exchange of AuNPs by orthogonal self-assembly. Moreover, the recognition event could be addressed in a programmable and reversible fashion through the orthogonal self-assembly of varying DNA strands. Taking advantage of azide-alkyne coupling chemistry, the authors could tether nanoparticles of different sizes to the same DNA-conjugated squaramide polymer. They highlighted the potential of this strategy for the reversible labeling of DNA-grafted squaramides with various complex biological molecules (e.g., peptides or proteins), which could enable selective presentation of biochemical signals on the surface of such squaramide-based supramolecular polymers.

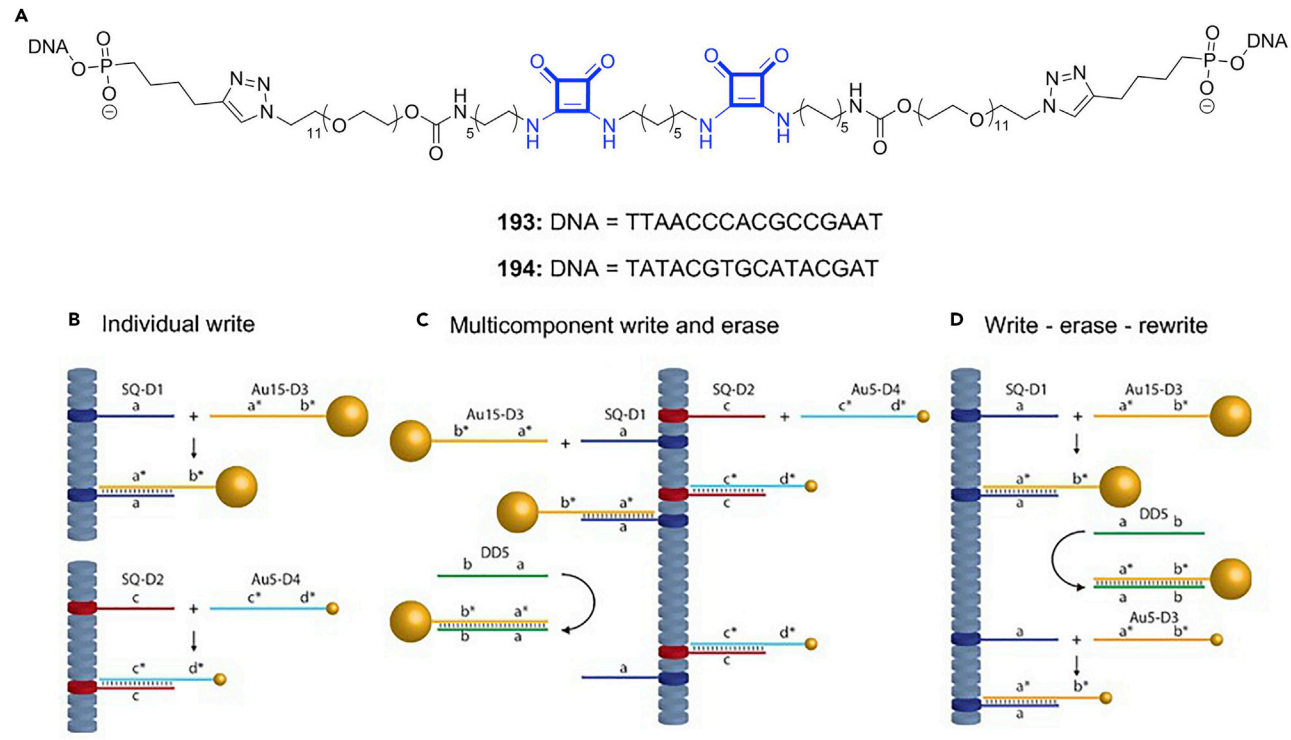

Figure 63. Squaramide Conjugation to Nucleotides for Reversible Labeling of DNA

(A) Chemical structures of bis-squaramide bola-amphiphiles **193** and **194**.

(B–D) Schematic illustration of the reversible loading of squaramide-based supramolecular polymers with AuNPs by orthogonal self-assembly. Adapted with permission from Noteborn et al.[139] under CC BY-NC 4.0.

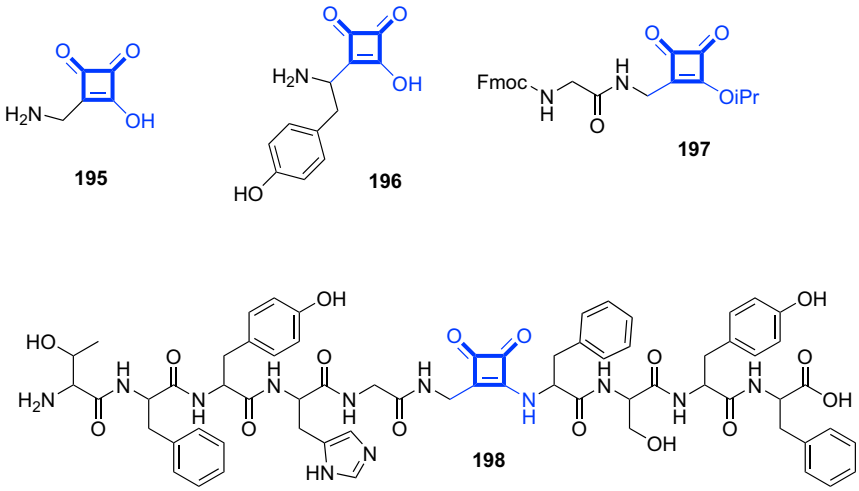

Figure 64. Chemical Structures of α-Amino Squaric Acids 195–197 and Squaramide-Containing Peptide 198

Shinada and co-workers have reported a number of examples of α-amino acid analogs in which the carboxylic acid group of an α-amino acid is replaced with a 2,3-dioxocyclobut-1-enyl group to form so-called α-amino squaric acids (α-Asq), such as **195** and **196** (Figure 64).[140,141] Recently, they further developed their methodology to allow the synthesis of α-Asq-containing peptides by using a solid-phase peptide synthesis approach. FmocHN-Gly[α-Asq]-Oi-Pr **197** was successfully exploited as a bioconjugation moiety, allowing the construction of a selection of squaramide containing hexapeptides, including Sq-peptide **198**. **198**, containing the squaramide moiety, was subjected to enzymatic hydrolysis with carboxypeptidaseY, and MALDI-TOF MS analysis indicated that the α-Asq moiety was stable to cleavage under these conditions. Such results suggest that the inclusion of α-Asqs could be an effective strategy for increasing the metabolic stability of peptides—a significant limitation to the development of peptide-based drugs.[142]

Rotger and co-workers have exploited the squaramide motif as a method of inducing folds and turns in peptides and peptidomimetics and as a preorganization strategy for the macrocyclization of oligosquaramides.[143–145] One of their more recent examples reported a N-methylated squaramide, **199**, that was capable of inducing folding in short peptidomimetic structures (Figure 65).[146] Using Fmoc strategy solid-phase peptide synthesis, **199** was incorporated into α-peptide sequence **200**, where it was shown by various NMR experiments (TOCSY, NOESY, and ROESY), X-ray crystallography, and circular dichroism (CD) that the inclusion of **199** in the sequence induces the formation of hairpin structures in water through the formation of both α- and β-turns (Figure 65).

The squarate ester bioconjugation strategy has been exploited by Luk and co-workers, who reported the synthesis of a new class of squaramides, **201–205**, that mimic the natural tripeptide ligand Arg-Gly-Asp (RGD), a well-known integrin ligand that mediates mammalian cell adhesion (Figure 66).[147] By exploiting diethyl squarate, the authors were able to construct a number of RGD mimics that contained a positive and a negative charge separated by the rigid and hydrophobic cyclobut-3-ene-1,2-dione moiety. Indeed, squaramides **201** and **202** were shown to inhibit cyclic RGD-mediated cell adhesion at concentrations at least 5-fold lower than that of the linear natural peptide GRGDS, whereas **204**, when immobilized on a gold surface, facilitated faster and

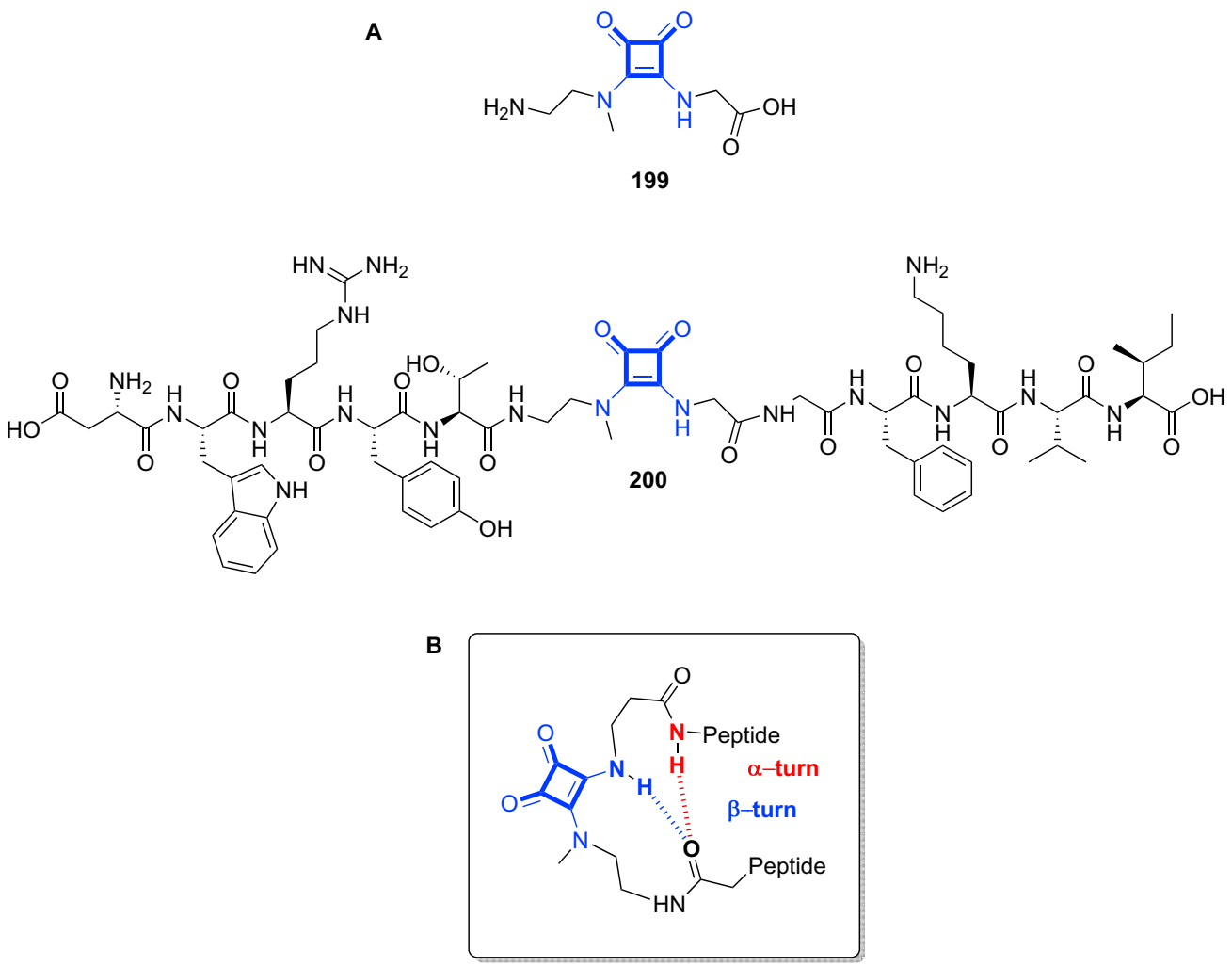

Figure 65. Squaramide for Inducing Folds and Turns in Peptides and Peptidomimetics

(A) Chemical structures of squaramide-based turn inducer **199** and the model peptido-squaramide **200**.

(B) Schematic representation of typical β-turn and α-turn induced by the squaramide **199**.

stronger cell adhesion than that measured for GRGDS. Interestingly, the authors also reported the bioconjugation of cyclic(RGDfK) with an alkanethiol to form self-assembled monolayers of the alkanethiol **205** on a gold surface.

Fluorophore conjugation to squaramides has also become an active area of research. A recent report from Rotger, Costa, and co-workers described the synthesis of two fluorescent cyclosquaramides, **206** and **207**; an analog of the known cyclosquaramide **208** was appended to either a bodipy or a FITC fluorophore via an amino alkyl linker.[31] Photopysical evaluation of **206** and **207** demonstrated emission maxima at 510 and 525 nm, respectively, in aqueous solution, where at physiological pH the emission was largely switched on in both cases. Interestingly, **206** showed a 5-fold increase in emission under acidic conditions (pH < 6) with the emission quantum yield at pH 5.5 = 0.15, slightly higher than that measured at neutral pH. Moreover, flow cytometry and confocal fluorescence microscopy analysis revealed that both **206** and **207** were rapidly uptaken by human glioblastoma cells (U87MG) and nontransformed mouse fibroblast cells (NIH-3T3); both

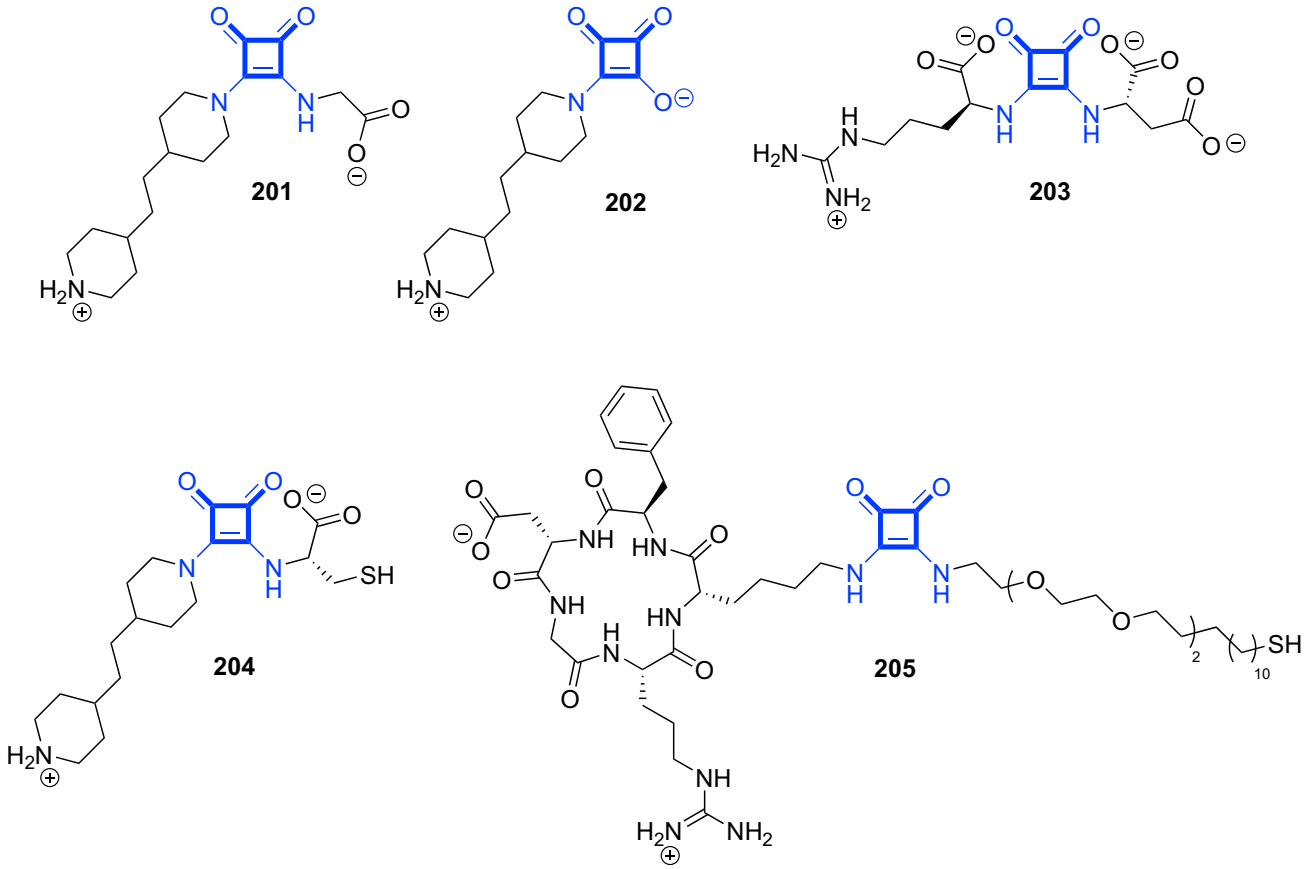

Figure 66. Chemical Structures of Squaramides 201–205

probes were shown to localize largely in vesicle-like structures in the cytosol (Figure 67). Further co-localization experiments with **206** demonstrated that the observed staining pattern in well-defined punctated sub-cellular structures was most likely a result of accumulation within early and late endosomes; the slightly acidic nature of these organelles led to optimal emission characteristics. The process is thought to arise through an endocytotic receptor-mediated mechanism that disturbs late endosome maturation and causes compound **206** to be sequestered in the late endosome for a prolonged period of time and presents an application of **206** as a fluorescent probe for selective imaging of late endosomes in live cells.

Direct conjugation of a fluorophore to the squaramide ring has also been demonstrated recently by Herrera, Concepcion Gimeno, and co-workers, who synthesized a series of luminescent squaramide monoesters, **209–216** (Figure 68).[148] The compounds that exhibited wide-ranging emission maxima from 474 to 616 nm in DMSO solution were, in some cases, also found to be highly cytotoxic to HeLa cells. Conversely, those with modest cytotoxicity (**210**, **212**, and **213**) were found to be readily uptaken by the cells and showed varied cellular distribution such that both lysosomal (**210** and **213**) and nuclear localization (**212**) were observed (Figure 68). The authors highlighted the potential of such monoesters for chiral and non-planar bioprobes given the synthetic versatility of squarate esters.

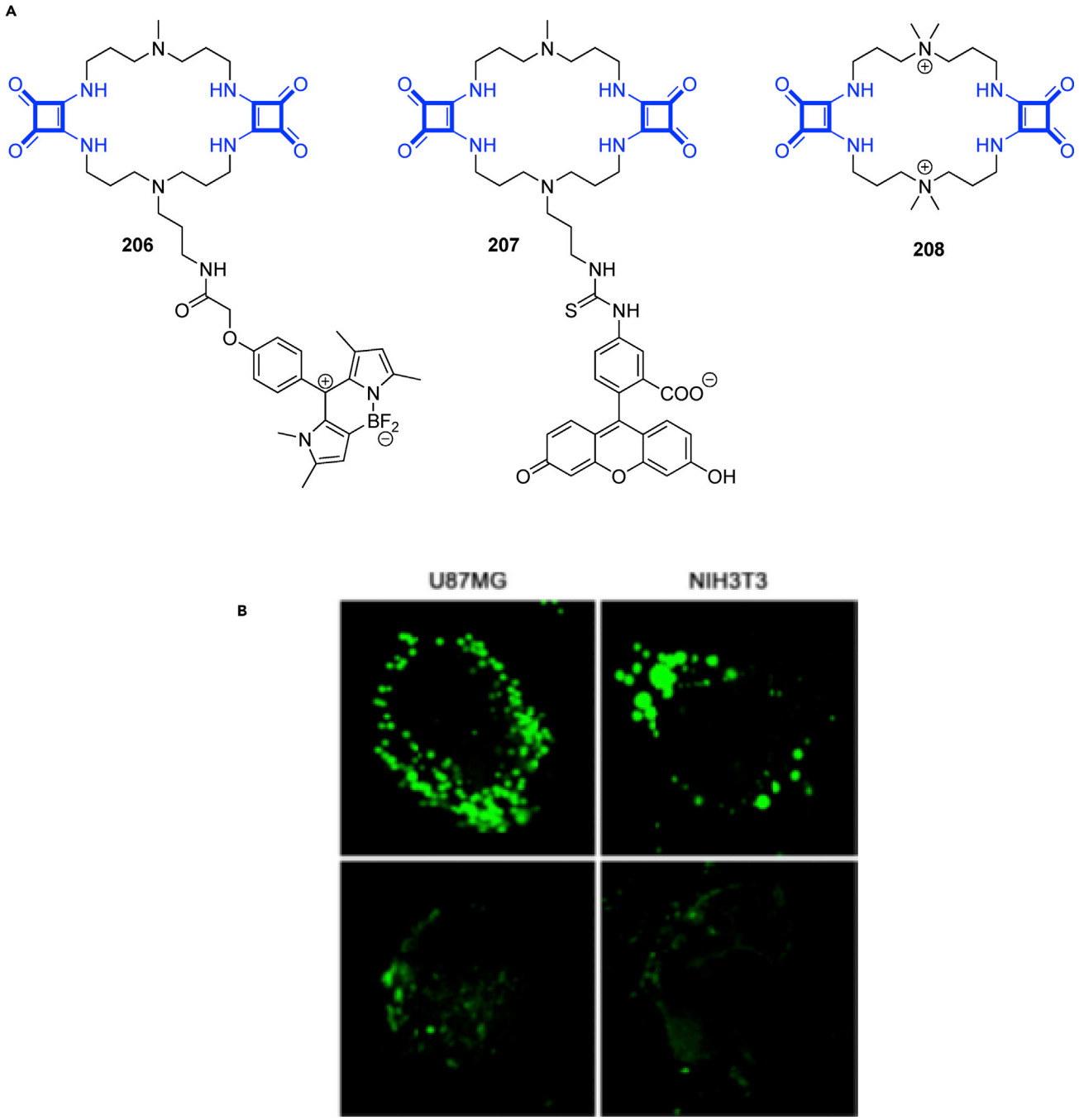

Figure 67. Fluorophore Conjugation with Squaramides

(A) Chemical structures of cyclosquaramides **206**–**208**.

(B) Confocal images of U87MG and NIH-3T3 cells stained with cyclosquaramides **206** (top) and **207** (bottom). Reproduced with permission from Sampedro et al.[31] Copyright 2014 American Chemical Society.

CONCLUSIONS

The use of squaramides has developed rapidly in recent years with the number of research articles reporting that the four-membered ring structure has increased over 5-fold in the past 10 years. Numerous advantageous properties, such as aromaticity, structural rigidity, stability, and facile synthetic approaches, have rendered the

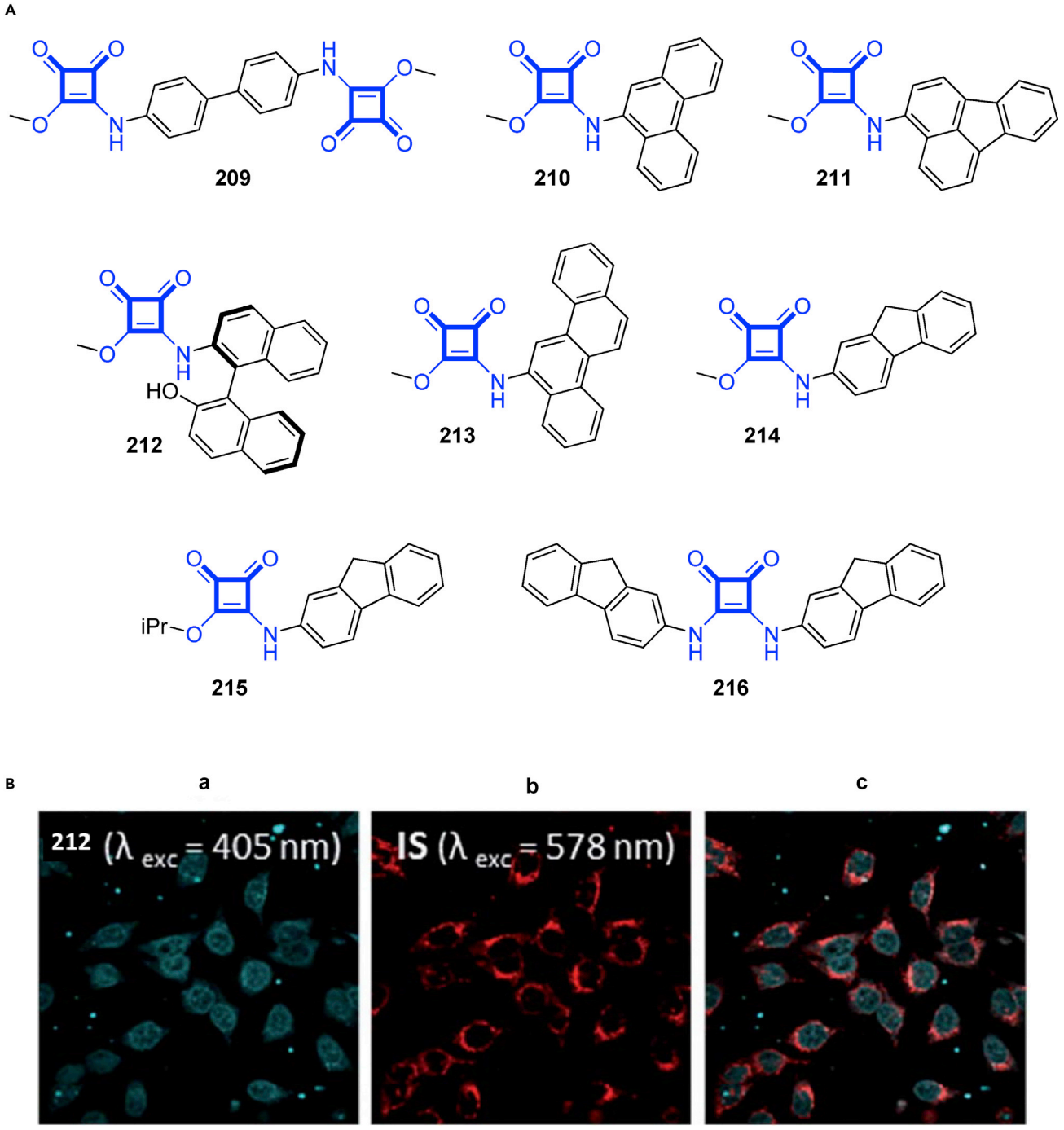

Figure 68. Luminescent Squaramide Monoesters for Cellular Imaging

(A) Chemical structures of luminescent squaramide monoesters **209**–**216**.

(B) Fluorescence microscopy images of HeLa cells incubated with compound **212**. (a) Image upon excitation at 405 nm. (b) Image upon excitation at 578 nm. (c) Superimposed image of (a) and (b). IS, internal standard LysoTracker Red DND-99.

Reproduced from Fernández-Moreira et al.[148] with permission from the Royal Society of Chemistry.

squaramides as an attractive scaffold for use across a diverse set of the chemical sciences. This review has attempted to give an overview of recent developments where major advances have been reported in the use of squaramides to construct large and

complex self-assembly structures and materials, to catalyze a diverse set of synthetic transformations, to bind anionic guests, to sense anionic analytes, and most recently to stimulate transmembrane anion transport. Similarly, medicinal chemists have taken note of the scaffold, thought of as a bioisostere for biologically ubiquitous phosphate, where both academic research programs and pharmaceutical companies are pursuing new drug candidates containing the squaramide scaffold in a diverse range of therapeutic areas. The field of chemical biology is also gaining advantage from this useful class of compounds; for example, the sensitive and selective reaction of squarate esters with amines is being exploited as a mild and robust method for bioconjugation of peptides, proteins, carbohydrates, nucleosides, and fluorescent dyes. It is exciting to see such diverse development of squaramide chemistry, and this points to a natural evolution toward more applied uses of the scaffold. This class of simple organic building blocks has the potential to affect our lives through solving problems faced by the modern world; sensors for environmental pollution, new drug candidates, improved biomolecular assays, and novel functional materials are all possible. The future is bright for squaramides, and new and exciting developments are on the horizon as many more applications emerge and their true potential is fully realized.

ACKNOWLEDGMENTS

Maynooth University is gratefully acknowledged for departmental support and a Hume Scholarship to L.A.M. L.K.K. thanks the Irish Research Council for awarding the Government of Ireland Postdoctoral Fellowship (GOIPD/2017/1091).

REFERENCES AND NOTES

1. Storer, R.I., Aciro, C., and Jones, L.H. (2011). Squaramides: physical properties, synthesis and applications. Chem. Soc. Rev. *40*, 2330–2346.

2. Wurm, F.R., and Klok, H.A. (2013). Be squared: expanding the horizon of squaric acid-mediated conjugations. Chem. Soc. Rev. *42*, 8220–8236.

3. Xiong-Jie, C., Zhi, L., and Wen-Hua, C. (2018). Synthesis, anion recognition and transmembrane anion-transport properties of squaramides and their derivatives. Mini. Rev. Org. Chem. *15*, 148–156.

4. Saez Talens, V.S., Englebienne, P., Trinh, T.T., Noteborn, W.E.M., Voets, I.K., and Kieltyka, R.E. (2015). Aromatic gain in a supramolecular polymer. Angew. Chem. Int. Ed. *54*, 10502–10506.

5. Prohens, R., Portell, A., Font-Bardia, M., Bauzá, A., and Frontera, A. (2014). Experimental and theoretical study of aromaticity effects in the solid state architecture on squaric acid derivatives. Cryst. Growth Des. *14*, 2578–2587.

6. Cohen, S., and Cohen, S.G. (1966). Preparation and reactions of derivatives of squaric acid. Alkoxy-, hydroxy-, and aminocyclobutenediones. J. Am. Chem. Soc. *88*, 1533–1536.

7. Ito, M., and West, R. (1963). New aromatic anions. IV. Vibrational spectra and force constants for $C_4O_4^{-2}$ and $C_5O_5^{-2}$. J. Am. Chem. Soc. *85*, 2580–2584.

8. von Ragué Schleyer, P., Najafian, K., Kiran, B., and Jiao, H.A. (2000). Are oxocarbon dianions aromatic? J. Org. Chem. *65*, 426–431.

9. Quiñonero, D., Frontera, A., Ballester, P., and Deyà, P.M. (2000). A theoretical study of aromaticity in squaramide and oxocarbons. Tetrahedron Lett. *41*, 2001–2005.

10. Liu, H., Tomooka, C.S., and Moore, H.W. (1997). An efficient general synthesis of squarate esters. Synth. Commun. *27*, 2177–2180.

11. Rostami, A., Colin, A., Li, X.Y., Chudzinski, M.G., Lough, A.J., and Taylor, M.S.N. (2010). N,N′-Diarylsquaramides: general, high-yielding synthesis and applications in colorimetric anion sensing. J. Org. Chem. *75*, 3983–3992.

12. Hu, L., Yan, Z., and Xu, H. (2013). Advances in synthesis and application of near-infrared absorbing squaraine dyes. RSC Adv. *3*, 7667–7676.

13. Rombola, M., and Rawal, V.H. (2018). Dicyclopentyl dithiosquarate as an intermediate for the synthesis of thiosquaramides. Org. Lett. *20*, 514–517.

14. Ozin, G.A., Hou, K., Lotsch, B.V., Cademartiri, L., Puzzo, D.P., Scotognella, F., Ghadimi, A., and Thomson, J. (2009). Nanofabrication by self-assembly. Mater. Today *12*, 12–23.

15. Sacanna, S., Pine, D.J., and Yi, G.-R. (2013). Engineering shape: the novel geometries of colloidal self-assembly. Soft Mater. *9*, 8096–8106.

16. Ward, M.D., and Raithby, P.R. (2013). Functional behaviour from controlled self-assembly: challenges and prospects. Chem. Soc. Rev. *42*, 1619–1636.

17. Davis, A.P., Draper, S.M., Dunne, G., and Ashton, P. (1999). The N-carbamoyl squaramide dimer: a compact, strongly associated H-bonding motif. Chem. Commun. 2265–2266.

18. Rotger, M.C., Piña, M.N., Frontera, A., Martorell, G., Ballester, P., Deyà, P.M., and Costa, A. (2004). Conformational preferences and self-template macrocyclization of squaramide-based foldable modules. J. Org. Chem. *69*, 2302–2308.

19. Portell, A., Barbas, R., Braga, D., Polito, M., Puigjaner, C., and Prohens, R. (2009). New polymorphic hydrogen bonding donor–acceptor system with two temperature coincident solid-solid transitions. CrystEngComm *11*, 52–54.

20. Prohens, R., Portell, A., Puigjaner, C., Tomàs, S., Fujii, K., Harris, K.D.M., Alcobé, X., Font-Bardia, M., and Barbas, R. (2011). Cooperativity in solid-state squaramides. Cryst. Growth Des. *11*, 3725–3730.

21. Prohens, R., Portell, A., and Alcobé, X. (2012). Effect of preorganization on the polymorphism and cocrystallization of a squaramide compound. Cryst. Growth Des. *12*, 4548–4553.

22. Portell, A., and Prohens, R. (2014). Single-stranded molecular helical assembly from a self-complementary squaramide compound. Cryst. Growth Des. *14*, 397–400.

23. Portell, A., Font-Bardia, M., and Prohens, R. (2013). Self-assembling of zwitterionic squaramides through electrostatically compressed face-to-face π-stacking: a new supramolecular synthon. Cryst. Growth Des. *13*, 4200–4203.

24. Rotger, C., Soberats, B., Quiñonero, D., Frontera, A., Ballester, P., Benet-Buchholz, J., Deyà, P.M., and Costa, A. (2008). Crystallographic and theoretical evidence of anion–π and hydrogen-bonding interactions in a squaramide–nitrate salt. Eur. J. Org. Chem. *2008*, 1864–1868.

25. Prohens, R., Portell, A., Font-Bardia, M., Bauzá, A., and Frontera, A. (2018). H-Bonded anion–anion complex trapped in a squaramido-based receptor. Chem. Commun. *54*, 1841–1844.

26. Ximenis, M., Pitarch-Jarque, J., Blasco, S., Rotger, C., García-España, E., Costa, A., and Squaramide, W.-S. (2018). Water-soluble squaramide dihydrates: N-methylation modulates the occurrence of one- and two-dimensional water clusters through hydrogen bonding and dipolar interactions. Cryst. Growth Des. *18*, 4420–4427.

27. Furukawa, H., Cordova, K.E., O'Keeffe, M., and Yaghi, O.M. (2013). The chemistry and applications of metal-organic frameworks. Science *341*, 1230444.

28. McGuirk, C.M., Katz, M.J., Stern, C.L., Sarjeant, A.A., Hupp, J.T., Farha, O.K., and Mirkin, C.A. (2015). Turning on catalysis: incorporation of a hydrogen-bond-donating squaramide moiety into a Zr metal–organic framework. J. Am. Chem. Soc. *137*, 919–925.

29. Cohen, S.M., Zhang, Z., and Boissonnault, J.A. (2016). Toward "metalloMOFzymes": metal–organic frameworks with single-site metal catalysts for small-molecule transformations. Inorg. Chem. *55*, 7281–7290.

30. Zhang, X., Zhang, Z., Boissonnault, J., and Cohen, S.M. (2016). Design and synthesis of squaramide-based MOFs as efficient MOF-supported hydrogen-bonding organocatalysts. Chem. Commun. *52*, 8585–8588.

31. Sampedro, A., Villalonga-Planells, R., Vega, M., Ramis, G., Fernández de Mattos, S., Villalonga, P., Costa, A., and Rotger, C. (2014). Cell uptake and localization studies of squaramide based fluorescent probes. Bioconjug. Chem. *25*, 1537–1546.

32. Qin, L., Hartley, A., Turner, P., Elmes, R.B.P., and Jolliffe, K.A. (2016). Macrocyclic squaramides: anion receptors with high sulfate binding affinity and selectivity in aqueous media. Chem. Sci. *7*, 4563–4572.

33. Sindt, A.J., Smith, M.D., Pellechia, P.J., and Shimizu, L.S. (2018). Thioureas and squaramides: comparison with ureas as assembly directing motifs for m-xylene macrocycles. Cryst. Growth Des. *18*, 1605–1612.

34. De Angelis, A.A., Capitani, D., and Crescenzi, V. (1998). Synthesis and 13C CP-MAS NMR characterization of a new chitosan-based polymeric network. Macromolecules *31*, 1595–1601.

35. Aime, S., Crich, S.G., Botta, M., Giovenzana, G., Palmisano, G., and Sisti, M. (1999). A macromolecular GD(III) complex as pH-responsive relaxometric probe for MRI applications. Chem. Commun. 1577–1578.

36. Voorhaar, L., and Hoogenboom, R. (2016). Supramolecular polymer networks: hydrogels and bulk materials. Chem. Soc. Rev. *45*, 4013–4031.

37. Tong, C., Liu, T., Saez Talens, V., Noteborn, W.E.M., Sharp, T.H., Hendrix, M.M.R.M., Voets, I.K., Mummery, C.L., Orlova, V.V., and Kieltyka, R.E. (2018). Squaramide-based supramolecular materials for three-dimensional cell culture of human induced pluripotent stem cells and their derivatives. Biomacromolecules *19*, 1091–1099.

38. Schiller, J., Alegre-Requena, J.V., Marqués-López, E., Herrera, R.P., Casanovas, J., Alemán, C., and Díaz Díaz, D. (2016). Self-assembled fibrillar networks of a multifaceted chiral squaramide: supramolecular multistimuli-responsive alcogels. Soft Mater. *12*, 4361–4374.

39. López, C., Ximenis, M., Orvay, F., Rotger, C., and Costa, A. (2017). Supramolecular hydrogels based on minimalist amphiphilic squaramide–squaramates for controlled release of zwitterionic biomolecules. Chem. Eur. J. *23*, 7590–7594.

40. Zhao, B.L., Li, J.H., and Du, D.M. (2017). Squaramide-catalyzed asymmetric reactions. Chem. Rec. *17*, 994–1018.

41. Ahrendt, K.A., Borths, C.J., and MacMillan, D.W.C. (2000). New strategies for organic catalysis: the first highly enantioselective organocatalytic Diels–alder reaction. J. Am. Chem. Soc. *122*, 4243–4244.

42. Connon, S.J. (2006). Organocatalysis mediated by (thio)urea derivatives. Chem. Eur. J. *12*, 5418–5427.

43. Fang, X., and Wang, C.J. (2015). Recent advances in asymmetric organocatalysis mediated by bifunctional amine–thioureas bearing multiple hydrogen-bonding donors. Chem. Commun. *51*, 1185–1197.

44. Malerich, J.P., Hagihara, K., and Rawal, V.H. (2008). Chiral squaramide derivatives are excellent hydrogen bond donor catalysts. J. Am. Chem. Soc. *130*, 14416–14417.

45. Kótai, B., Kardos, G., Hamza, A., Farkas, V., Pápai, I., and Soós, T. (2014). On the mechanism of bifunctional squaramide-catalyzed organocatalytic Michael addition: a protonated catalyst as an oxyanion hole. Chem. Eur. J. *20*, 5631–5639.

46. Bae, H.Y., and Song, C.E. (2015). Unprecedented hydrophobic amplification in noncovalent organocatalysis "on water": hydrophobic chiral squaramide catalyzed Michael addition of malonates to nitroalkenes. ACS Catal. *5*, 3613–3619.

47. Sim, J.H., and Song, C.E. (2017). Water-enabled catalytic asymmetric Michael reactions of unreactive nitroalkenes: one-pot synthesis of chiral GABA-analogs with all-carbon quaternary stereogenic centers. Angew. Chem. Int. Ed. *56*, 1835–1839.

48. Urruzuno, I., Mugica, O., Oiarbide, M., and Palomo, C. (2017). Bifunctional Brønsted base catalyst enables regio-, diastereo-, and enantioselective Cα-alkylation of β-tetralones and related aromatic-ring-fused cycloalkanones. Angew. Chem. Int. Ed. *56*, 2059–2063.

49. Iriarte, I., Olaizola, O., Vera, S., Gamboa, I., Oiarbide, M., and Palomo, C. (2017). Controlling the α/γ-reactivity of vinylogous ketone enolates in organocatalytic enantioselective Michael reactions. Angew. Chem. Int. Ed. *56*, 8860–8864.

50. Roy, T.K., Parhi, B., and Ghorai, P. (2018). Cinchonamine squaramide catalyzed asymmetric aza-Michael reaction: dihydroisoquinolines and tetrahydropyridines. Angew. Chem. Int. Ed. *57*, 9397–9401.

51. Zhao, K., Zhi, Y., Wang, A., and Enders, D. (2016). Asymmetric organocatalytic synthesis of 3-diarylmethine-substituted oxindoles bearing a quaternary stereocenter via 1,6-conjugate addition to para-quinone methides. ACS Catal. *6*, 657–660.

52. Bae, H.Y., Kim, M.J., Sim, J.H., and Song, C.E. (2016). Direct catalytic asymmetric Mannich reaction with dithiomalonates as excellent Mannich donors: organocatalytic synthesis of (R)-sitagliptin. Angew. Chem. Int. Ed. *55*, 10825–10829.

53. Li, B.-Y., and Du, D.-M. (2018). Chiral squaramide-catalyzed asymmetric Mannich reactions for synthesis of fluorinated 3,3′-bisoxindoles. Adv. Synth. Catal. *360*, 3164–3170.

54. Manoni, F., and Connon, S.J. (2014). Catalytic asymmetric Tamura cycloadditions. Angew. Chem. Int. Ed. *53*, 2628–2632.

55. Orue, A., Uria, U., Reyes, E., Carrillo, L., and Vicario, J.L. (2015). Catalytic enantioselective [5+2] cycloaddition between oxidopyrylium ylides and enals under dienamine activation. Angew. Chem. Int. Ed. *54*, 3043–3046.

56. Zhao, H.-W., Yang, Z., Meng, W., Tian, T., Li, B., Song, X.-Q., Chen, X.-Q., and Pang, H.-L. (2015). Diastereo- and enantioselective synthesis of chiral pyrrolidine-fused spirooxindoles via organocatalytic [3+2] 1,3-dipolar cycloaddition of azomethine ylides with maleimides. Adv. Synth. Catal. *357*, 2492–2502.

57. Huang, W.-J., Chen, Q., Lin, N., Long, X.-W., Pan, W.-G., Xiong, Y.-S., Weng, J., and Lu, G. (2017). Asymmetric synthesis of trifluoromethyl-substituted 3,3′-pyrrolidinyl-dispirooxindoles through organocatalytic 1,3-dipolar cycloaddition reactions. Org. Chem. Front. *4*, 472–482.

58. Tallon, S., Manoni, F., and Connon, S.J. (2015). A practical aryl unit for azlactone dynamic kinetic resolution: orthogonally protected products and a ligation-inspired coupling process. Angew. Chem. Int. Ed. *54*, 813–817.

59. Eröksüz, S., Neudörfl, J.M., and Berkessel, A. (2017). Kinetic resolution of 5-substituted oxazinones with bifunctional chiral base/squaramide organocatalysts. Synlett *28*, 1278–1281.

60. Chauhan, P., Mahajan, S., Kaya, U., Hack, D., and Enders, D. (2015). Bifunctional amine-squaramides: powerful hydrogen-bonding organocatalysts for asymmetric domino/cascade reactions. Adv. Synth. Catal. *357*, 253–281.

61. Vetica, F., de Figueiredo, R.M., Orsini, M., Tofani, D., and Gasperi, T. (2015). Recent advances in organocatalytic cascade reactions toward the formation of quaternary stereocenters. Synthesis *47*, 2139–2184.

62. Zhao, B.-L., Liu, L., and Du, D.-M. (2014). Chiral squaramide-catalyzed sulfa-Michael/aldol cascade for the asymmetric synthesis of spirocyclic tetrahydrothiophene chromanone derivatives. Eur. J. Org. Chem. *2014*, 7850–7858.

63. Sun, Q.S., Zhu, H., Chen, Y.J., Yang, X.D., Sun, X.W., and Lin, G.Q. (2015). Squaramide-catalyzed synthesis of enantioenriched spirocyclic oxindoles via ketimine intermediates with multiple active sites. Angew. Chem. Int. Ed. *54*, 13253–13257.

64. Li, J.-H., Wen, H., Liu, L., and Du, D.-M. (2016). Diastereo- and enantioselective synthesis of spiro-pyrrolidine-pyrazolones by squaramide-catalyzed cascade aza-Michael/Michael reactions. Eur. J. Org. Chem. *2016*, 2492–2499.

65. Song, Y.-X., and Du, D.-M. (2018). Squaramide-catalyzed asymmetric Michael/cyclization cascade reaction of unsaturated thiazolidinones and 3-isothiocyanato oxindoles: synthesis of new bispirocyclic heterocycles. Synthesis *50*, 1535–1545.

66. Zhao, Y.L., Lou, Q.X., Wang, L.S., Hu, W.H., and Zhao, J.L. (2017). Organocatalytic Friedel–crafts alkylation/lactonization reaction of naphthols with 3-trifluoroethylidene oxindoles: the asymmetric synthesis of dihydrocoumarins. Angew. Chem. Int. Ed. *56*, 338–342.

67. Kaya, U., Chauhan, P., Mahajan, S., Deckers, K., Valkonen, A., Rissanen, K., and Enders, D. (2017). Squaramide-catalyzed asymmetric aza-Friedel–Crafts/N,O-acetalization domino reactions between 2-naphthols and pyrazolinone ketimines. Angew. Chem. Int. Ed. *56*, 15358–15362.

68. Wang, X.-B., Li, T.-Z., Sha, F., and Wu, X.-Y. (2014). Enantioselective squaramide-catalysed domino Mannich–cyclization reaction of isatin imines. Eur. J. Org. Chem. *2014*, 739–744.

69. Han, J.-L., and Chang, C.-H. (2016). An asymmetric assembly of spirooxindole dihydropyranones through a direct enantioselective organocatalytic vinylogous aldol-cyclization cascade reaction of 3-alkylidene oxindoles with isatins. Chem. Commun. *52*, 2322–2325.

70. Gale, P.A., Howe, E.W., and Wu, X. (2016). Anion receptor chemistry. Chem *1*, 351–422.

71. Aletti, A.B., Gillen, D.M., and Gunnlaugsson, T. (2018). Luminescent/colorimetric probes and (chemo-) sensors for detecting anions based on transition and lanthanide ion receptor/binding complexes. Coord. Chem. Rev. *354*, 98–120.

72. Gale, P.A., and Caltagirone, C. (2018). Fluorescent and colorimetric sensors for anionic species. Coord. Chem. Rev. *354*, 2–27.

73. Gale, P.A., Davis, J.T., and Quesada, R. (2017). Anion transport and supramolecular medicinal chemistry. Chem. Soc. Rev. *46*, 2497–2519.

74. Prohens, R., Martorell, G., Ballester, P., and Costa, A. (2001). A squaramide fluorescent ensemble for monitoring sulfate in water. Chem. Commun. 1456–1457.

75. Prohens, R., Tomàs, S., Morey, J., Deyà, P.M., Ballester, P., and Costa, A. (1998). Squaramido-based receptors: molecular recognition of carboxylate anions in highly competitive media. Tetrahedron Lett. *39*, 1063–1066.

76. Amendola, V., Bergamaschi, G., Boiocchi, M., Fabbrizzi, L., and Milani, M. (2010). The squaramide versus urea contest for anion recognition. Chem. Eur. J. *16*, 4368–4380.

77. Amendola, V., Fabbrizzi, L., Mosca, L., and Schmidtchen, F.P. (2011). Urea-, squaramide-, and sulfonamide-based anion receptors: a thermodynamic study. Chem. Eur. J. *17*, 5972–5981.

78. Li, Y., Yang, G.H., Shen, Y.Y., Xue, X.S., Li, X., and Cheng, J.P. (2017). N-tert-butyl sulfinyl Squaramide Receptors for anion recognition through ssisted tert-butyl C–H hydrogen bonding. J. Org. Chem. *82*, 8662–8667.

79. Elmes, R.B.P., Yuen, K.K.Y., and Jolliffe, K.A. (2014). Sulfate-selective recognition by using neutral dipeptide anion receptors in aqueous solution. Chem. Eur. J. *20*, 7373–7380.

80. Elmes, R.B.P., and Jolliffe, K.A. (2015). Amino acid-based squaramides for anion recognition. Supramol. Chem. *27*, 321–328.

81. Tzioumis, N.A., Yuen, K.K.Y., and Jolliffe, K.A. (2018). Investigating the effects of structure on sulfate recognition by neutral dipeptide receptors. Supramol. Chem. *30*, 667–673.

82. Jin, C., Zhang, M., Deng, C., Guan, Y., Gong, J., Zhu, D., Pan, Y., Jiang, J., and Wang, L. (2013). Novel calix[4] arene-based receptors with bis-squaramide moieties for colorimetric sensing of anions via two different interaction modes. Tetrahedron Lett. *54*, 796–801.

83. Jin, C., Zhang, X., Wu, X., Zhang, M., Jiang, J., Lin, C., and Wang, L. (2015). The recognition of n-alkyl phosphonic or carboxylic acid by mono-squaramide-functionalised pillar[5] arenes. Supramol. Chem. *27*, 329–335.

84. Manesiotis, P., Riley, A., and Bollen, B. (2014). Polymerisable squaramide receptors for anion binding and sensing. J. Mater. Chem. C *2*, 8990–8995.

85. Beswick, J., Blanco, V., De Bo, G., Leigh, D.A., Lewandowska, U., Lewandowski, B., and Mishiro, K. (2015). Selecting reactions and reactants using a switchable rotaxane organocatalyst with two different active sites. Chem. Sci. *6*, 140–143.

86. Tomàs, S., Prohens, R., Vega, M., Rotger, M.C., Deyà, P.M., Ballester, P., and Costa, A. (1996). Squaramido-based receptors: design, synthesis, and application to the recognition of tetraalkylammonium compounds. J. Org. Chem. *61*, 9394–9401.

87. Tomàs, S., Prohens, R., Deslongchamps, G., Ballester, P., and Costa, A. (1999). An effective fluorescent sensor for choline-containing phospholipids. Angew. Chem. Int. Ed. *38*, 2208–2211.

88. López, C., Sanna, E., Carreras, L., Vega, M., Rotger, C., and Costa, A. (2013). Molecular recognition of zwitterions: enhanced binding and selective recognition of miltefosine by a squaramide-based host. Chem. Asian. J. *8*, 84–87.

89. Soberats, B., Martínez, L., Sanna, E., Sampedro, A., Rotger, C., and Costa, A. (2012). Janus-like Squaramide-based hosts: dual mode of binding and conformational transitions driven by ion-pair recognition hosts dual mode of binding and conformational transitions driven by ion-pair recognition. Chem. Eur. J. *18*, 7533–7542.

90. Załubiniak, D., Zakrzewski, M., and Piątek, P. (2016). Highly effective ion-pair receptors based on 2,2-bis(aminomethyl)-propionic acid. Dalton Trans. *45*, 15557–15564.

91. Zdanowski, S., Piątek, P., and Romański, J. (2016). An ion pair receptor facilitating the extraction of chloride salt from the aqueous to the organic phase. New J. Chem. *40*, 7190–7196.

92. Jagleniec, D., Siennicka, S., Dobrzycki, Ł., Karbarz, M., and Romański, J. (2018). Recognition and extraction of sodium chloride by a squaramide-based ion pair receptor. Inorg. Chem. *57*, 12941–12952.

93. Neus Piña, M., Carmen Rotger, M., Costa, A., Ballester, P., and Deyà, P.M. (2004). Evaluation of anion selectivity in protic media by squaramide–cresol red ensembles. Tetrahedron Lett. *45*, 3749–3752.

94. Piña, M.N., Soberats, B., Rotger, C., Ballester, P., Deyà, P.M., and Costa, A. (2008). Selective sensing of competitive anions by non-selective hosts: the case of sulfate and phosphate in water. New J. Chem. *32*, 1919–1923.

95. Elmes, R.B.P., Turner, P., and Jolliffe, K.A. (2013). Colorimetric and luminescent sensors for chloride: hydrogen bonding vs deprotonation. Org. Lett. *15*, 5638–5641.

96. Marchetti, L.A., Mao, N., Krämer, T., Kitchen, J.A., and Elmes, R.B.P. (2018). A long wavelength colourimetric chemosensor for fluoride. Supramol. Chem. *30*, 795–805.

97. Porel, M., Ramalingam, V., Domaradzki, M.E., Young, V.G., Ramamurthy, V., and Muthyala, R.S. (2013). Chloride sensing via suppression of excited state intramolecular proton transfer in squaramides. Chem. Commun. *49*, 1633–1635.

98. Ramalingam, V., Domaradzki, M.E., Jang, S., and Muthyala, R.S. (2008). Carbonyl groups as molecular valves to regulate chloride binding to Squaramides. Org. Lett. *10*, 3315–3318.

99. Danao, A., Ramalingam, V., Ramamurthy, V., and Muthyala, R.S. (2017). On the origin of chloride-induced emission enhancement in ortho substituted squaramides. J. Photochem. Photobiol. A *344*, 108–113.

100. Rostami, A., Wei, C.J., Guérin, G., and Taylor, M.S. (2011). Anion Detection by a Fluorescent Poly(squaramide): Self-Assembly of Anion-Binding Sites by Polymer Aggregation. Angew. Chem. Int. Ed. *50*, 2059–2062.

101. Delgado-Pinar, E., Rotger, C., Costa, A., Piña, M.N., Jiménez, H.R., Alarcón, J., and García-España, E. (2012). Grafted squaramide monoamine nanoparticles as simple systems for sulfate recognition in pure water. Chem. Commun. *48*, 2609–2611.

102. López, K.A., Piña, M.N., and Morey, J. (2013). Squaramide-coated Fe_3O_4 nanoparticles and their selective complexation with carboxylate anions in water. Sens. Actuators B Chem. *181*, 267–273.

103. Busschaert, N., Kirby, I.L., Young, S., Coles, S.J., Horton, P.N., Light, M.E., and Gale, P.A. (2012). Squaramides as potent transmembrane anion transporters. Angew. Chem. Int. Ed. *51*, 4426–4430.

104. Busschaert, N., Elmes, R.B.P., Czech, D.D., Wu, X., Kirby, I.L., Peck, E.M., Hendzel, K.D., Shaw, S.K., Chan, B., Smith, B.D., et al. (2014). Thiosquaramides: pH switchable anion transporters. Chem. Sci. *5*, 3617–3626.

105. Elmes, R.B.P., Busschaert, N., Czech, D.D., Gale, P.A., and Jolliffe, K.A. (2015). pH switchable anion transport by an oxothiosquaramide. Chem. Commun. *51*, 10107–10110.

106. Wu, X., Busschaert, N., Wells, N.J., Jiang, Y.B., and Gale, P.A. (2015). Dynamic covalent transport of amino acids across lipid bilayers. J. Am. Chem. Soc. *137*, 1476–1484.

107. Edwards, S.J., Valkenier, H., Busschaert, N., Gale, P.A., and Davis, A.P. (2015). High-affinity anion binding by steroidal squaramide receptors. Angew. Chem. Int. Ed. *54*, 4592–4596.

108. Dias, C.M., Valkenier, H., and Davis, A.P. (2018). Anthracene bisureas as powerful and accessible anion carriers. Chem. Eur. J. *24*, 6262–6268.

109. Jin, C., Zhang, M., Wu, L., Guan, Y., Pan, Y., Jiang, J., Lin, C., and Wang, L. (2013). Squaramide-based tripodal receptors for selective recognition of sulfate anion. Chem. Commun. *49*, 2025–2027.

110. Liu, Y., Qin, Y., and Jiang, D. (2015). Squaramide-based tripodal ionophores for potentiometric sulfate-selective sensors with high selectivity. Analyst *140*, 5317–5323.

111. Cai, X.J., Li, Z., and Chen, W.H. (2017). Tripodal squaramide conjugates as highly effective transmembrane anion transporters. Bioorg. Med. Chem. Lett. *27*, 1999–2002.

112. Deng, L.Q., Lu, Y.M., Zhou, C.Q., Chen, J.X., Wang, B., and Chen, W.H. (2014). Synthesis and potent ionophoric activity of a squaramide-linked bis(choloyl) conjugate. Bioorg. Med. Chem. Lett. *24*, 2859–2862.

113. Bao, X., Wu, X., Berry, S.N., Howe, E.N.W., Chang, Y.T., and Gale, P.A. (2018). Fluorescent squaramides as anion receptors and transmembrane anion transporters. Chem. Commun. *54*, 1363–1366.

114. Busschaert, N., Park, S.H., Baek, K.H., Choi, Y.P., Park, J., Howe, E.N.W., Hiscock, J.R., Karagiannidis, L.E., Marques, I., Félix, V., et al. (2017). A synthetic ion transporter that disrupts autophagy and induces apoptosis by perturbing cellular chloride concentrations. Nat. Chem. *9*, 667–675.

115. Marques, I., Costa, P.M.R., Q Miranda, M., Busschaert, N., Howe, E.N.W., Clarke, H.J., Haynes, C.J.E., Kirby, I.L., Rodilla, A.M., Pérez-Tomás, R., et al. (2018). Full elucidation of the transmembrane anion transport mechanism of squaramides using in silico investigations. Phys. Chem. Chem. Phys. *20*, 20796–20811.

116. Kinney, W.A., Abou-Gharbia, M., Garrison, D.T., Schmid, J., Kowal, D.M., Bramlett, D.R., Miller, T.L., Tasse, R.P., Zaleska, M.M., and Moyer, J.A. (1998). Design and synthesis of [2-(8,9-dioxo-2,6-diazabicyclo[5.2.0]non-1(7)-en-2-yl)-ethyl]phosphonic acid (EAA-090), a potent N-methyl-d-aspartate antagonist, via the use of 3-cyclobutene-1,2-dione as an achiral α-amino acid bioisostere. J. Med. Chem. *41*, 236–246.

117. ClinicalTrials.gov (2004). Study evaluating EAA-090 in adult outpatients with neuropathic pain associated with diabetic neuropathy. Identifier NCT00073034.

118. ClinicalTrials.gov (2019). Efficacy and safety study of navarixin (MK-7123) in combination with pembrolizumab (MK-3475) in adults with selected advanced/metastatic solid tumors (MK-7123-034). Identifier NCT03473925.

119. ClinicalTrials.gov (2011). Long-term study of the effects of navarixin (SCH 527123, MK-7123) in participants with moderate to severe COPD (MK-7123-019). Identifier NCT01006616.

120. Norman, P. (2013). Evaluation of WO2012080456 and WO2012080457; Boheringer Ingleheim's first CXCR2 antagonists. Expert Opin. Ther. Pat. *23*, 383–388.

121. Martin, B., Lai, X., Baettig, U., Neumann, E., Kuhnle, T., Porter, D., Robinson, R., Hatto, J., D'Souza, A.-M., Steward, O., et al. (2015). Early process development of a squaramide-based CXCR2 receptor antagonist. Org. Process Res. Dev. *19*, 1038–1043.

122. Tantry, S.J., Markad, S.D., Shinde, V., Bhat, J., Balakrishnan, G., Gupta, A.K., Ambady, A., Raichurkar, A., Kedari, C., Sharma, S., et al. (2017). Discovery of imidazo[1,2-a]pyridine ethers and squaramides as selective and potent inhibitors of mycobacterial adenosine triphosphate (ATP) synthesis. J. Med. Chem. *60*, 1379–1399.

123. Kumar, S.P., Glória, P.M.C., Gonçalves, L.M., Gut, J., Rosenthal, P.J., Moreira, R., and Santos, M.M.M. (2012). Squaric acid: a valuable scaffold for developing antimalarials? Med. Chem. Commun. *3*, 489–493.

124. Ribeiro, C.J.A., Kumar, S.P., Gut, J., Gonçalves, L.M., Rosenthal, P.J., Moreira, R., and Santos, M.M.M. (2013). Squaric acid/4-aminoquinoline conjugates: novel potent antiplasmodial agents. Eur. J. Med. Chem. *69*, 365–372.

125. Ribeiro, C.J.A., Espadinha, M., Machado, M., Gut, J., Gonçalves, L.M., Rosenthal, P.J., Prudêncio, M., Moreira, R., and Santos, M.M.M. (2016). Novel squaramides with in vitro liver stage antiplasmodial activity. Bioorg. Med. Chem. *24*, 1786–1792.

126. Olmo, F., Rotger, C., Ramírez-Macías, I., Martínez, L., Marín, C., Carreras, L., Urbanová, K., Vega, M., Chaves-Lemaur, G., Sampedro, A., et al. (2014). Synthesis and biological evaluation of N,N′-squaramides with high in vivo efficacy and low toxicity: toward a low-cost drug against Chagas disease. J. Med. Chem. *57*, 987–999.

127. Buurman, E.T., Foulk, M.A., Gao, N., Laganas, V.A., McKinney, D.C., Moustakas, D.T., Rose, J.A., Shapiro, A.B., and Fleming, P.R. (2012). Novel rapidly diversifiable antimicrobial RNA polymerase switch region inhibitors with confirmed mode of action in Haemophilus influenzae. J. Bacteriol. *194*, 5504–5512.

128. Molodtsov, V., Fleming, P.R., Eyermann, C.J., Ferguson, A.D., Foulk, M.A., McKinney, D.C., Masse, C.E., Buurman, E.T., and Murakami, K.S. (2015). X-ray crystal Structures of *Escherichia coli* RNA polymerase with switch region binding inhibitors enable rational design of squaramides with an improved fraction unbound to human plasma protein. J. Med. Chem. *58*, 3156–3171.

129. Quintana, M., Alegre-Requena, J.V., Marqués-López, E., Herrera, R.P., and Triola, G. (2016). Squaramides with cytotoxic activity against human gastric carcinoma cells HGC-27: synthesis and mechanism of action. Med. Chem. Comm. *7*, 550–561.

130. Zhang, X., Zuo, Z., Tang, J., Wang, K., Wang, C., Chen, W., Li, C., Xu, W., Xiong, X., Yuntai, K., et al. (2013). Design, synthesis and biological evaluation of novel estrogen-derived steroid metal complexes. Bioorg. Med. Chem. Lett. *23*, 3793–3797.

131. Zhang, Z.F., Chen, J., Han, X., Zhang, Y., Liao, H.B., Lei, R.X., Zhuang, Y., Wang, Z.F., Li, Z., Chen, J.C., et al. (2017). (pyridin-2-squaramide) targets both PTEN and ERK1/2 to confer neuroprotection. Br. J. Pharmacol. *174*, 641–656.

132. Glüsenkamp, K.-H., Drosdziok, W., Eberle, G., Jähde, E., and Rajewsky, M.F. (1991). Squaric acid diethylester: a simple and convenient coupling reagent. Zeitschrift für Naturforschung C *46*, 498–501.

133. Fonvielle, M., Sakkas, N., Iannazzo, L., Le Fournis, C.L., Patin, D., Mengin-Lecreulx, D., El-Sagheer, A., Braud, E., Cardon, S., Brown, T., et al. (2016). Electrophilic RNA for peptidyl-RNA synthesis and site-specific cross-linking with tRNA-binding enzymes. Angew. Chem. Int. Ed. *55*, 13553–13557.

134. Dürr, E.-M., Doherty, W., Lee, S.Y., El-Sagheer, A.H., Shivalingam, A., McHugh, P.J., Brown, T., and McGouran, J.F. (2018). Squaramide-based 5′-phosphate replacements bind to the DNA repair exonuclease SNM1A. ChemistrySelect *3*, 12824–12829.

135. Rudd, S.E., Roselt, P., Cullinane, C., Hicks, R.J., and Donnelly, P.S. (2016). A desferrioxamine B squaramide ester for the incorporation of zirconium-89 into antibodies. Chem. Commun. *52*, 11889–11892.

136. Ohara, K., Takeda, Y., Daikoku, S., Hachisu, M., Seko, A., and Ito, Y. (2015). Profiling aglycon-recognizing sites of UDP-glucose:glycoprotein glucosyltransferase by means of squarate-mediated labeling. Biochemistry *54*, 4909–4917.

137. Seio, K., Miyashita, T., Sato, K., and Sekine, M. (2005). Synthesis and properties of new nucleotide analogs possessing squaramide moieties as new phosphate. Isosters. Eur. J. Org. Chem. *2005*, 5163–5170.

138. Lu, M., Lu, Q.B., and Honek, J.F. (2017). Squarate-based carbocyclic nucleosides: syntheses, computational analyses and anticancer/antiviral evaluation. Bioorg. Med. Chem. Lett. *27*, 282–287.

139. Noteborn, W.E.M., Saez Talens, V., and Kieltyka, R.E. (2017). Reversible loading of nanoscale elements on a multicomponent supramolecular polymer system by using DNA strand displacement. Chembiochem. *18*, 1995–1999.

140. Ishida, T., Shinada, T., and Ohfune, Y. (2005). Synthesis of novel amino squaric acids via addition of dianion enolates derived from N-Boc amino acid esters. Tetrahedron Lett. *46*, 311–314.

141. Shinada, T., Ishida, T., Hayashi, K.-i., Yoshida, Y., Shigeri, Y., and Ohfune, Y. (2007). Synthesis of leucine-enkephalin analogs containing α-amino squaric acid. Tetrahedron Lett. *48*, 7614–7617.

142. Maeda, K., Kiniwa, Y.-i., Ohfune, Y., Ishiguro, S., Suzuki, K., Murata, K., Matsuda, H., and Shinada, T. (2014). Solid phase synthesis of α-amino squaric acid-containing peptides. RSC Adv. *4*, 50639–50643.

143. Martínez, L., Sampedro, A., Sanna, E., Costa, A., and Rotger, C. (2012). Synthesis and conformational studies of peptido-squaramide foldable modules: a new class of turn-mimetic compounds. Org. Biomol. Chem. *10*, 1914–1921.

144. Rotger, C., Piña, M.N., Vega, M., Ballester, P., Deyà, P.M., and Costa, A. (2006). Efficient macrocyclization of preorganized palindromic oligosquaramides. Angew. Chem. Int. Ed. *45*, 6844–6848.

145. Martínez-Crespo, L., Escudero-Adán, E.C., Costa, A., and Rotger, C. (2018). The role of N-methyl squaramides in a hydrogen-bonding strategy to fold peptidomimetic compounds. Chem. Eur. J. *24*, 17802–17813.

146. Martínez, L., Martorell, G., Sampedro, Á., Ballester, P., Costa, A., and Rotger, C. (2015). Hydrogen bonded squaramide-based foldable module induces both β- and α-turns in hairpin structures of α-peptides in water. Org. Lett. *17*, 2980–2983.

147. Narasimhan, S.K., Sejwal, P., Zhu, S., and Luk, Y.Y. (2013). Enhanced cell adhesion and mature intracellular structure promoted by squaramide-based RGD mimics on bioinert surfaces. Bioorg. Med. Chem. *21*, 2210–2216.

148. Fernández-Moreira, V., Alegre-Requena, J.V., Herrera, R.P., Marzo, I., and Gimeno, M.C. (2016). Synthesis of luminescent squaramide monoesters: cytotoxicity and cell imaging studies in HeLa cells. RSC Adv. *6*, 14171–14177.